U.PORTO

ICBAS | INSTITUTO DE CIÊNCIAS BIOMÉDICAS ABEL SALAZAR
SCHOOL OF MEDICINE AND BIOMEDICAL SCIENCES

U.PORTO

FACULDADE DE CIÊNCIAS
UNIVERSIDADE DO PORTO

MSc

2.º CICLO

FCUP
ICBAS
2022

U.PORTO

Exploring Axonal Cytoskeleton Defects in Transthyretin Amyloid Polyneuropathy (ATTR-PN)

Guilherme Nóvoa

FC

U.PORTO

ICBAS | INSTITUTO DE CIÊNCIAS BIOMÉDICAS ABEL SALAZAR
SCHOOL OF MEDICINE AND BIOMEDICAL SCIENCES

U.PORTO

FACULDADE DE CIÊNCIAS
UNIVERSIDADE DO PORTO

Exploring Axonal Cytoskeleton Defects in Transthyretin Amyloid Polyneuropathy (ATTR-PN)

Guilherme de Carvalho Sampaio da Nóvoa

Dissertação de Mestrado em Bioquímica apresentada à Faculdade de Ciências da Universidade do Porto e Instituto de Ciências Biomédicas Abel Salazar

2022

MSc

Exploring Axonal Cytoskeleton Defects in Transthyretin Amyloid Polyneuropathy (ATTR-PN)

Guilherme de Carvalho Sampaio da Nóvoa

Mestrado em Bioquímica

Faculdade de Ciências da Universidade do Porto (FCUP) e Instituto de Ciências Biomédicas Abel Salazar (ICBAS)

2022

Supervisor

Márcia Liz, Associate Researcher, Instituto de Investigação e Inovação em Saúde (i3S)

Co-supervisor

Maria Do Rosário Almeida, Associate Professor and Senior Researcher, Instituto de Ciências Biomédicas Abel Salazar (ICBAS) and i3S

U.PORTO
FACULDADE DE CIÊNCIAS
UNIVERSIDADE DO PORTO

U.PORTO
ICBAS | INSTITUTO DE CIÊNCIAS BIOMÉDICAS ABEL SALAZAR
SCHOOL OF MEDICINE AND BIOMEDICAL SCIENCES

INSTITUTO DE INVESTIGAÇÃO E INOVAÇÃO EM SAÚDE
UNIVERSIDADE DO PORTO

Todas as correções determinadas pelo júri, e só essas, foram efetuadas.

O Presidente do Júri,

Porto,_____/_____/_____

Sworn Statement

I, Guilherme de Carvalho Sampaio da Nóvoa, enrolled in the Master Degree in Biochemistry at the Faculty of Sciences of the University of Porto hereby declare, in accordance with the provisions of paragraph a) of Article 14 of the Code of Ethical Conduct of the University of Porto, that the content of this dissertation reflects perspectives, research work and my own interpretations at the time of its submission.

By submitting this dissertation, I also declare that it contains the results of my own research work and contributions that have not been previously submitted to this or any other institution.

I further declare that all references to other authors fully comply with the rules of attribution and are referenced in the text by citation and identified in the bibliographic references section. This dissertation does not include any content whose reproduction is protected by copyright laws.

I am aware that the practice of plagiarism and self-plagiarism constitute a form of academic offense.

Guilherme Nóvoa

14/12/2022

Acknowledgments

Queria agradecer em primeiro lugar à Márcia por me ter dado esta oportunidade e por todo o conhecimento e ajuda que me deu. À Professora Maria do Rosário um obrigado pela sua disponibilidade e pelo apoio que tornou este projeto possível. À Joana Magalhães por me ter transmitido tudo o que conseguiu. Obrigado!

A toda a gente dos grupos *Nerve Regeneration* e *Neurolipid Biology*, nomeadamente, à Dr. Mónica Sousa e ao Dr. Pedro Brites pelo espaço no laboratório e por todo o *input* que deram. À Marina por ser uma companheira de equipa espetacular, à Sara pelas conversas longas na sala das células, à Catarina pelo calor e simpatia, à Joana pelas palavras, e a todos os outros, bem como a estes, a ajuda em tudo e mais alguma coisa, que permitiram que este projeto acontecesse. Obrigado! Um obrigado especial à Maria por ter partilhado o "cargo" de aluno de mestrado do laboratório, e pelos lanches em que muito falávamos.

À minha família, especialmente, à minha mãe que tanto me ensinou e tanto me deu, um enorme obrigado. Aos meus avós, que pelo exemplo ensinaram-me a cumprir a minha palavra e a carregar amor, não ódio. À minha Tia Rosa um especial obrigado pois os meses que passei naquela tua casa serviram de base para este percurso, sempre recebido com amor como de uma "terceira mãe" se tratasse. Aos meus primos, especialmente, à Alice e à Catarina que me demonstraram coisas diversas e sempre me apoiaram um obrigado. Obrigado!

Aos meus amigos que sempre me apoiaram. Ao Pré, à Teresa, ao Tiago, ao Hugo, à Ana e à Mafalda pelo amor incondicional e apoio que me deram ao longo destes cincos anos, sempre fazendo de mim um igual. À Iona pela verdadeira inspiração que é, e pelos mil cafés que tomamos para dar um pouco de apoio mútuo. À Luísa que ao longo deste mestrado me ajudou e me ouviu tantas vezes. Obrigado!

A toda a gente cujas palavras me deram alento para continuar. Agradeço à Professora Laura Oliveira e ao Professor Paulo Correia de Sá, pois num momento em que duvidei da minha permanência neste mestrado poucas palavras fizeram tremendo efeito. Obrigado!

A uma das minhas grandes paixões: a Patinagem Artística. À minha treinadora Raquel que tanto me ensinou e deu. A toda a gente que me fez ver formas e coisas novas, caras e coreografias que nunca vou esquecer. Obrigado!

A toda a gente que contribui para este projeto no *backstage*. À Maria da ALM um gigantesco obrigado pelas palavres sempre de simpatia, pelo conhecimento e apoio incansável. Ao serviço *Cell and Genotyping* por toda a ajuda. À Joana e ao Tiago do grupo *Molecular Neurobiology* um grande obrigado. Obrigado!

Resumo

A Polineuropatia Amiloide da Transtirretina (ATTR-PN), anteriormente conhecida como Polineuropatia Amiloidótica Familiar (PAF), é uma doença autossómica dominante causada por mutações ao nível da transtirretina (TTR). Esta proteína é um homotetrámero com funções essenciais no transporte de tiroxina e retinol, tendo papéis adicionais no crescimento do axónio e regeneração nervosa. Devido à destabilização do tetrâmero causada pela mutação presente, a TTR dissocia-se, os monómeros sofrem *misfolding*, agregam-se e depositam-se no tecido, formando depósitos de amiloide. Na ATTR-PN esta deposição ocorre preferencialmente no sistema nervoso periférico (SNP) levando à degeneração do axónio de neurónios sensitivos, culminando na sua morte.

O citoesqueleto neuronal além de atuar como suporte estrutural, também contribui para a manutenção da homeostasia celular, sendo que, nos neurónios tem sido recentemente associado a várias doenças neurodegenerativas. No entanto, na ATTR-PN o citoesqueleto continua em grande parte ignorado. Resultados já publicados pelo nosso grupo revelam que a TTR *wild type* (WT) solúvel impacta a dinâmica dos microtúbulos, mediando a sua função no crescimento do axónio. Adicionalmente, num modelo de *Drosophila Melanogaster* de ATTR-PN, a TTR amiloidogénica induz disfunção ao nível da actina por intermédio das Rho GTPases. Paralelamente, resultados preliminares para este trabalho indicaram uma disfunção ao nível da actina mediada pela Ras-relacionada ao substrato C3 da Toxina botulínica (Rac1) num modelo de ratinho de ATTR-PN, bem como, uma disrupção no transporte no axónio, numa idade que precedia a neurodegeneração.

Neste trabalho, continuamos a avaliar o impacto da disfunção do citoesqueleto na ATTR-PN utilizando um modelo de ratinho que expressa TTR humana com a mutação A97S ($hTTR^{A97S}$), traduzindo os estádios iniciais da doença. Inicialmente, determinamos em neurónios do gânglio da raiz dorsal de ratinhos $hTTR^{A97S}$ uma redução no número de *actin trails*, estruturas importantes na manutenção da função neuronal, nomeadamente, transporte de vesículas sinápticas. Além disso, os resultados sugeriram que o recetor para produtos avançados de glicolisação (RAGE) e a Rac1 medeiam a disfunção da actina observada em neurónios $hTTR^{A97S}$. Por fim, exploramos efetores da Rac1 e observamos que os níveis do complexo da proteína associada à actina 2/3 (Arp2/3), essencial para ramificação e nucleação da actina, estavam aumentados em neurónios do gânglio da raiz dorsal de ratinhos $hTTR^{A97S}$. A

forma fosforilada e inativa da cofilina, a fosfo-cofilina, estava por sua vez diminuída, sugerindo que esta proteína está também envolvida na disfunção de actina mediada pela Rac1.

Tendo em conta os nossos resultados preliminares em transporte no axónio, determinamos que os defeitos observados no transporte de mitocôndrias iniciavam-se aos 9 meses de idade em raízes periféricas do gânglio da raiz dorsal (contem axónios de neurónios sensitivos e motores) de ratinhos $hTTR^{A97S}$, estando relacionados com níveis reduzidos de acetilação da α-tubulina. Adicionalmente, queríamos determinar se os defeitos no transporte no axónio e, possivelmente, dinâmica de microtúbulos (essencial para o transporte no axónio), eram recapitulados num nervo puramente sensitivo implicado nos estádios iniciais da ATTR-PN, o nervo sural. Deste modo, otimizamos com sucesso um protocolo de *live imaging* de mitocôndrias e dinâmica de microtúbulos em explantes deste nervo.

A disfunção no citoesqueleto é um participante ativo na progressão da ATTR-PN. A continuação da investigação neste tópico trará uma melhor compreensão da neurodegeneração bem como, poderá permitir a identificação de novos alvos terapêuticos em ATTR-PN.

Palavras-chave: [Polineuropatia Amiloide da Transtirretina, transtirretina, sistema nervoso periférico, citoesqueleto, neurónios do gânglio da raiz dorsal, actina, microtúbulos, transporte no axónio, Ras-relacionada ao substrato C3 da Toxina botulínica]

Abstract

Transthyretin Amyloidosis Polyneuropathy (ATTR-PN), formerly known as Familial Amyloidosis Polyneuropathy (FAP), is an autosomal dominant disease associated with mutations in transthyretin (TTR). TTR is an homotetrameric protein essential for the transport of thyroxine and retinol and was also shown to play a role on axonal growth and nerve regeneration. Due to destabilization, the TTR tetramer dissociates into monomers that misfold, aggregate and deposit in tissue, forming amyloid deposits. In ATTR-PN the deposition of mutant TTR occurs preferentially in the peripheral nervous system (PNS), leading to a sensory axonal degeneration culminating in neuronal death.

The neuronal cytoskeleton besides acting as structural support, also contributes to cell homeostasis, being recently associated to multiple neurodegenerative diseases but remaining heavily unaddressed in the context of ATTR-PN. Published data from our group established that wild type (WT) soluble TTR impacts microtubule dynamics underlying its function in axonal growth. Additionally, in a *Drosophila Melanogaster* model of ATTR-PN, amyloidogenic TTR induced actin dysfunction mediated by the Rho GTPase family. Importantly, preliminary data to this thesis indicated neuronal actin dysfunction mediated by Ras-related C3 botulinum toxin substrate 1 (Rac1) in a mouse model of ATTR-PN, as well a disruption in axonal transport, at an age preceding neurodegeneration.

In this work we further analysed the impact of cytoskeleton dysfunction on ATTR-PN by using a mouse model carrying the A97S mutation in human TTR ($hTTR^{A97S}$), translating the early stages of ATTR-PN. We determined that dorsal root ganglia (DRG) neurons from $hTTR^{A97S}$ mice presented a reduction in the number of axonal actin trails, structures which are important for neuronal function namely the transport of synaptic vesicles. Additionally, our results suggested that a pathway involving the receptor for advanced glycation products (RAGE) and Rac1 mediates the observed actin dysfunction in $hTTR^{A97S}$ neurons. Finally, we explored downstream effectors of Rac1 and observed that the levels of the complex of actin related protein 2/3 (Arp2/3), essential for branching and nucleation of actin, were augmented in extracts from $hTTR^{A97S}$ DRG neurons. Moreover, the inactive phosphorylated form of cofilin, phospho-cofilin, was reduced suggesting that this actin binding protein is also involved in the Rac-1 mediated actin dysfunction.

Concerning previous data on axonal transport, we determined that defects on the transport of mitochondria were initiated at 9 months of age in DRG peripheral roots (which contain both sensory and motor axons) from $hTTR^{A97S}$ mice, and they were related with decreased levels of α-tubulin acetylation. Additionally, we aimed to determine whether defects on mitochondrial transport, and possibly on microtubule dynamics (essential for axonal transport), were recapitulated in a purely sensory nerve implicated in early stages of ATTR-PN, the sural nerve. For that, we successfully of implemented a protocol for live imaging of mitochondria and MTs dynamics in sural nerve explants.

Cytoskeleton dysfunction has an active role in the progression of ATTR-PN. More research in this topic is, therefore, essential to further our understanding of neurodegeneration and allow for the identification of new therapeutical targets on ATTR-PN.

Key words: [Transthyretin Amyloidosis Polyneuropathy, transthyretin, peripheral nervous system, cytoskeleton, dorsal root ganglia neurons, actin, microtubules, axonal transport, Ras-related C3 botulinum toxin substrate 1]

Table of contents

Acknowledgments ... ii
Resumo ... iv
Abstract ... vi
List of abbreviations ... 4
List of figures ... 10
List of tables ... 12
Introduction ... 13
1. Transthyretin Amyloidosis ... 13
1.1. Amyloidosis: a general introduction ... 13
1.2. Transthyretin: a protein with amyloidogenic potential ... 14
1.2.1. TTR gene and structure ... 14
1.2.2. Production and metabolism ... 15
1.2.3. TTR physiological functions ... 16
1.2.4. TTR aggregation potential ... 16
1.3. Transthyretin Amyloidosis ... 17
2. Transthyretin Amyloid Polyneuropathy (ATTR-PN) ... 18
2.1. Discovery and epidemiology ... 18
2.2. Pathophysiology and symptomatology ... 18
2.3. Molecular mechanisms of TTR neurotoxicity ... 19
2.4. Diagnostic and Current Therapeutic Approaches ... 20
2.5. Mouse models of ATTR-PN ... 22
3. Cytoskeleton disruption and neurodegeneration ... 23
3.1. The cytoskeleton components: function and regulation ... 23
3.1.1. Actin ... 23
3.1.2. Microtubules ... 25
3.1.3. Neurofilaments ... 29
3.2. Neuronal cytoskeleton organization: structure leads to function ... 30

3.3. Neuronal cytoskeleton: major regulators 33
3.4. Cytoskeleton dysfunction in neurodegenerative diseases 37
4. Cytoskeleton dysfunction in ATTR-PN: preliminary data 40
4.1. Rac1 mediates actin dysfunction and neurodegeneration in ATTR-PN 40
4.2. Axonal transport defects in an ATTR-PN mouse model 41
Objectives 43
Methods 44
1. Animals 44
2. DRG neuronal cultures and transfection 44
3. Plasmid production: pIRESneo3+GFP-UTR_CH and EGFP-actin+pEGFP-C1 45
4. Actin trails: transfection and cell culture conditions 45
5. Human TTR Enzyme-linked immunosorbent assay (ELISA) 46
6. Immunocytochemistry (ICC) 46
6.1. Growth cone morphology experiments 46
6.2. Phospho-cofilin 47
7. Immunoblotting 47
8. Acetylated α-tubulin immunohistochemistry (IHC) 48
9. Imaging and data analysis 50
9.1. Actin trails live imaging 50
9.2. Growth cone morphology 51
9.3. Phospho-cofilin ICC 52
9.4. Mitochondrial transport in DRG peripheral root from 6-months old mice 53
9.5. Acetylated α-tubulin immunohistochemistry 53
10. Statistics 53
Results 54
1. Impact of amyloidogenic TTR on the actin cytoskeleton 54
1.1. DRG neurons from an ATTR-PN mouse model present axonal actin alterations 54

1.2. Axonal actin alterations are mediated by Rac1 in hTTR^{A97S} DRG neurons 56

1.3. Dissecting the molecular mechanism underlying TTR-induced actin dysfunction 58

1.3.1. A RAGE-Rac1 pathway mediates TTR-induced actin cytoskeleton alterations 58

1.3.2. Dissecting Rac1 downstream effectors on TTR-induced actin defects 59

1.3.3. TTR is present extracellularly in DRG neurons *in vitro* 61

2. Evaluation of microtubule and axonal transport alteration in hTTR^{A97S} mice.. 62

2.1. Evaluation of mitochondrial transport in hTTR^{A97S} DRG peripheral roots ... 62

2.2. Tubulin acetylation is decreased in hTTR^{A97S} DRG peripheral roots 63

2.3. Microtubule and axonal transport alterations in sural nerves from hTTR^{A97S} mice 65

Discussion 69

Conclusion 74

References 75

Supplementary information 89

Sural mitochondrial transport live imaging optimization 89

FRAP EGFP-actin optimization 89

Polymerase chain reaction 90

TTR ICC 91

List of abbreviations

AAA+ ATPases ATPases Associated with diverse cellular Activities

ABP Actin binding protein

AD Alzheimer's Disease

ADF Actin depolymerizing factor

ADP Adenosine Diphosphate

AIS Axon initial segment

ALS Amyotrophic lateral sclerosis

ApoA-1 Apolipoprotein A-1

Arp2/3 Actin-related protein 2/3

ASO Antisense oligonucleotide

ATAT1/α-TAT1 Alpha tubulin N-acetyltransferase 1

ATP Adenosine triphosphate

ATTR Transthyretin Amyloidosis

ATTR-CM Transthyretin Amyloid Cardiomyopathy

ATTR-PN Transthyretin Amyloid Polyneuropathy

Aβ Amyloid beta

BSA Bovine serum albumin

CAP-Gly domain Cytoskeleton-Associated Proteins-glycine rich domain

CCP Carboxypeptidase

Cdc42 Cell division control protein 42 homolog

C-domain Central domain

CFP Cyan fluorescent protein

CH Calponin homology

CLASP Cytoplasmatic linker protein associating proteins

CMT1/2 Charcot-Marie Tooth disease type 1/2

CMT4H Charcot-Marie-Tooth neuropathy type 4H

CNS Central nervous system

COX-1 Cyclooxigenase-1

CP Capping protein

CRMP-2 Collapsin response mediator protein 2

CSF Cerebrospinal fluid

CyD Cyclodextrin

DAPI 4′,6-diamidino-2-phenylindole

DIV Day *in vitro*

DMEM:F12 Dulbecco's modified eagle medium

DNA Deoxyribonucleic acid

DRG Dorsal root ganglia

EB3 End-binding protein 3

EBs End-binding proteins

EGTA Ethylene glycol-bis(β-aminoethyl ether)-N,N,N′,N′-tetraacetic acid

ELISA Enzyme-linked immunosorbent assay

ER Endoplasmic Reticulum

F-actin Filamentous actin

FAP Familial Amyloidotic Polyneuropathy

FBS Foetal bovine serum

FDA Food and Drug Administration

FHOD1 FH1/FH2 domain-containing protein 1

FRL1 Formin-like protein 1

G-actin Globular actin

GAP GTPase-activating protein

GDI Guanosine dissociation inhibitor

GDP Guanosine diphosphate

GEF Guanine exchange factor

GFP Green fluorescent protein

GSK3β Glycogen synthase kinase-3 beta

GTP Guanosine triphosphate

HD Huntington's disease

HDAC6 Histone deacetylase 6

HRP Horseradish peroxidase

HSPB1 Heat shock protein beta 1

hTTR Human transthyretin

ICC Immunocytochemistry

IDOX 4′-iodo-4′-deoxydoxorubicin

IHC Immunohistochemistry

IL-1β Interleukin-1 beta

KO Knockout

LB Luria broth

L-Glu L-Glutamine

LRP2 LDL Receptor Related Protein 2

MAP Microtubule-associated protein

MAP2 Microtubule-associated protein 2

MAP4 Microtubule-associated protein 4

mDia1/2 Diaphanous-related formin-1/2

MES 2-(N-morpholino) ethanesulfonic acid

MFN2 Mitofusin 2

MGV Mean grey value

moTTR Mouse transthyretin

MT Microtubule

MTOC Microtubule organizing centre

NDS Normal donkey serum

NF Neurofilament

NF-H Neurofilament-heavy

NF-L Neurofilament-light

NF-M Neurofilament-medium

NMII Non-muscle myosin II

N-WASp Neural Wiskott Aldrich Syndrome Protein

O/N Overnight

OCT Optimal cutting temperature

P/S Penicillin/Streptomycin

PBS Phosphate-buffered saline

P-domain Peripheral-domain

PFA Paraformaldehyde

PI Protease inhibitor

PLL Poly-L-Lysine

PNS Peripheral nervous system

PTM Post-translational modification

Rac1 Ras-related C3 botulinum toxin substrate 1

RAGE Receptor for advanced glycation products

RAP Receptor-associated protein

RhoA Ras homolog family member A

Rho1 Ras-like GTP-binding protein

RNA Ribonucleic acid

RNS Reactive nitrogen species

Rock Rho-associated protein kinase

Rok Rho kinase

ROS Reactive oxygen species

RT Room temperature

SAP Serum amyloid P

Scar/WAVE Suppressor of cAR/WASP-family verprolin homologous protein

SDS Sodium dodecyl sulphate

siRNA Small interfering RNA

SIRT2 NAD-dependent deacetylase sirtuin 2

SSA Systemic Senile Amyloidosis

STORM Stochastic optical reconstruction microscopy

SVBP Small vasohibin-binding protein

T_4 thyroxine

TBS Tris-buffered saline

T-domain Transitional domain

TIP+ Plus-end tracking protein

TNF-α Tumour necrosis factor alfa

TTL Tubulin tyrosine ligase

TTLL Tubulin tyrosine ligase like

TTR Transthyretin

TUDCA Tauroursodeoxycholic acid

Tβ4 Thymosin beta-4

UTR Utrophin

VASH1/2 Vasohibins 1/2

WASp Wiskott Aldrich Syndrome Protein

WT Wild type

XMAP215 Xenopus microtubule-associated protein 215

YFP Yellow Fluorescent Protein

γ-TuRC Gama-tubulin ring complex

List of figures

Figure 1. Overview of the process for aggregation of an unspecific amyloidogenic protein. 13
Figure 2. TTR molecular structure..... 14
Figure 3. Synthesis, transport, and uptake/degradation of TTR. 15
Figure 4. Process of TTR tetramer dissociation, monomer misfolding and formation of aggregates..... 17
Figure 5. World distribution of ATTR-PN. 18
Figure 6. Overview of the possible ways aggregates of TTR lead to cytotoxicity. 19
Figure 7. Overview of F-actin formation. 24
Figure 8. Overview of the myriad of processes regulated by ABPs. 25
Figure 9. Overview of MTs dynamics. 27
Figure 10. Overview of the possible PTMs that MTs can suffer and its localization in α- and β-tubulin structures. 28
Figure 11. Overview of an expanding growth cone morphology and organization of cytoskeletal components. 31
Figure 12. Overview of actin structures identified in the axon shaft. 32
Figure 13. Cytoskeleton organization of a developing neuron. 33
Figure 14. Distribution of MTs PTMs in a developing neuron. 34
Figure 15. Overview of a Rho GTPase mechanism of regulation. 35
Figure 16. Overview of RhoA, Cdc42 and Rac1 interplay and signalling cascades regarding cytoskeletal components. 36
Figure 17. Impact of Rac1 on growth cone morphology and neurodegeneration (ND) index in $hTTR^{A97S}$ DRG neurons. 41
Figure 18. Axonal transport of mitochondria in impaired in DRG peripheral root of 9-months old $hTTR^{A97S}$ mice. 42
Figure 19. pIRESneo3+GFP-Utr_CH plasmid construct used. 46
Figure 20. Overview of a kymograph. 51
Figure 21. Latrunculin causes a reduction in the number of actin trails in DRG neurons. 55
Figure 22. $hTTR^{A97S}$ DRG neurites presented reduced number of actin trails. 56
Figure 23. Rac1 mediates axonal actin dysfunction in $hTTR^{A97S}$ DRG neurons. 57
Figure 24. A RAGE-Rac1 pathway mediates actin dysfuntion in the growth cone of $hTTR^{A97S}$ DRG neurons. 59

Figure 25. Both Arp2/3 and cofilin downstream effectors of Rac1 are dysregulated in hTTR^{A97S} neurons. 60
Figure 26. Axonal transport defects were not present in DRG peripheral root explants from 6-months old hTTR^{A97S}. 62
Figure 27. Tubulin isoforms and PTMs are not altered in hTTR^{A97S} DRG peripheral root via Western Blot. 64
Figure 28. Levels of α-tubulin acetylation are reduced in DRG peripheral roots of hTTR^{A97S} mice. 65
Figure 29. Representative still images of live-imaging of mitochondria in sural nerve axons from hTTR^{A97S}-Thy1-MitoCFP mouse. Black arrows and red arrows indicate anterograde and retrograde moving mitochondria, respectively. 66
Figure 30. Representative still image of live-imaging of EB3 comets in sural nerve axons from hTTR^{A97S}-Thy1:EB3-YFP mouse. 67
Figure 31. MT density in the sural nerve of hTTR^{A97S} is not altered. 68
Figure 32. Scissors plus dashed lines denote the zone where incisions were made to obtain the explant. 89
Figure 33. EGFP-Actin + pEGFP-C1 plasmid construct used in FRAP. 90

List of tables

Table 1. Antibodies and probe-conjugated dyes used all throughout this work. 49
Table 2. Overview of growth cone classification. 52
Table 3. Mean length and mean rate of polymerization of all the registered actin trails in control DRG neurons ($hTTR^{WT}$) 54
Table 4. List of the primers used for PCR and respective sequences 91

Introduction

1. Transthyretin Amyloidosis

1.1. Amyloidosis: a general introduction

Amyloidosis are a large group of pathologies characterized by the deposition of 7-13nm cross β-sheet conformation fibrillar proteins in tissues, forming amyloid deposits, which occur due to the misfolding and aggregation of small proteins. A proneness to misfolding, high serum levels, hereditary mutations or an abnormal proteolytic remodulation of the amyloidogenic protein are the underlying causes of amyloidosis (Merlini and Bellotti 2003, Hazenberg 2013). Normally, proteins misfold and aggregate into oligomers creating a critical nucleus for the formation of fibrillar aggregates which form amyloid. In this process of amyloid formation, there is a lag phase observed before fibril assembly, which corresponds to the necessity of the formation of this critical nucleus. Additionally, fibrils act as "harbours" for further aggregation, leading to a feed forward type of mechanism, where the pre-existence of amyloid leads to formation of more amyloid, justifying the reduction of the prementioned lag phase when fibrils are already present (Merlini and Bellotti 2003) (Figure 1).

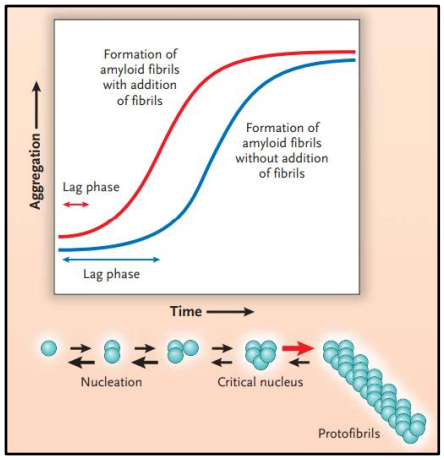


Figure 1. Overview of the process for aggregation of an unspecific amyloidogenic protein. Before the formation of amyloid fibrils, the lag phase for occurrence of aggregation is much larger reinforcing the idea of establishment of a "feed forward mechanism" where more fibrils lead to more aggregation. Adapted from (Merlini and Bellotti 2003).

Amyloidosis may be sporadic or acquired, with aging being a risk factor for their development (Johnson, Connelly et al. 2012). Generically, deposition of amyloid fibrils causes dysfunction in organs either by simply altering organ structure or through the activation of inflammatory cascades and interaction with specific receptors (Merlini and Bellotti 2003). Additionally, several studies report that oligomers can also induce stress,

namely changes in oxidative state and activation of apoptosis, and that fibrils act as reservoirs of such “toxic particles” (Merlini and Bellotti 2003, Wechalekar, Gillmore et al. 2016).

More than 30 proteins have been identified has being able to lead to amyloidosis through misfolding. Transthyretin (TTR) is included in that group of proteins and gives rise to a small group of rare diseases denominated Transthyretin Amyloidosis (ATTR) (Sipe, Benson et al. 2012).

1.2. Transthyretin: a protein with amyloidogenic potential

1.2.1. TTR gene and structure

Transthyretin (TTR) is an homotetrameric protein first identified in 1942, being initially called pre-albumin due to its ability to migrate ahead of albumin in electrophoresis (Seibert and Nelson 1942). Later, it was uncovered that TTR subunits are encoded by a single-copy gene, containing 4 exons, located in the long arm (q) of the chromosome 18 with a variable length of 6.9kb to 7.0kb (Sasaki, Yoshioka et al. 1985, Wallace, Naylor et al. 1985).

Structure wise, TTR, in its tetrameric form, has a molecular weight of 55kDa being that each subunit has 127 amino acids and a molecular weight of 14kDa (Kanda, Goodman et al. 1974). TTR has an extensive secondary structure with each monomer composed by eight antiparallel β-strands, forming two four-stranded β-sheets, and an α-helix (EF-helix) (Blake, Geisow et al. 1978) (Figure 2). To form dimers each monomer interacts through hydrogen bounds, and tetramer formation occurs through interactions of residues in the loops that join β-strands G to H and A to B. (Yokoyama, Mizuguchi et al. 2012) (Figure 2). Interestingly, TTR enrichment in β-structure attributes a high amyloidogenic potential to this protein (Costa et al., 1978).

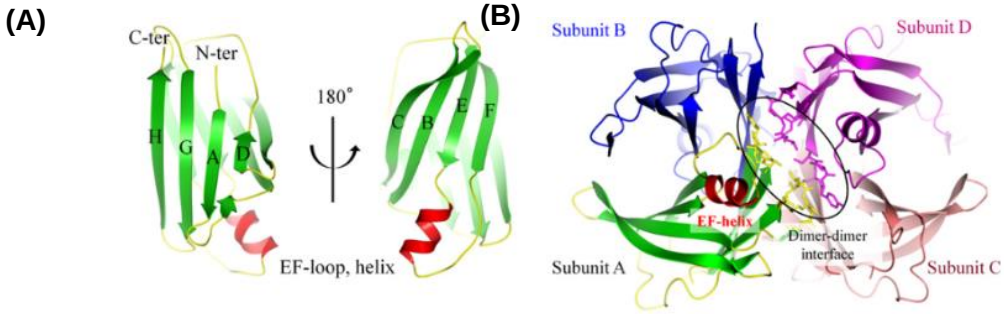


Figure 2. TTR molecular structure. (A) Structure of a monomer of TTR. TTR has eight antiparallel β-strands (green arrows) and one α-helix (red ribbon). (B) Structure of the assembled tetramer. Adapted from (Yokoyama, Mizuguchi et al. 2012).

1.2.2. Production and metabolism

TTR is mainly synthesized in the liver (Felding and Fex 1982) and the choroid plexus of the brain (Aleshire, Bradley et al. 1983) which are the sources for its circulation in serum (Seibert and Nelson 1942) and cerebrospinal fluid (CSF), respectively (Figure 3). TTR circulates in the serum at a concentration in the range of 170-420 mg/L, and in the CSF at 5-20 mg/L (Vatassery, Quach et al. 1991). Besides these main locations of synthesis TTR has also been reported to be synthesized in: endothelial cells of Islets of Langerhans, ciliary pigment epithelia, retinal pigment epithelium, intestine, visceral yolk sack, stomach, heart, skeletal muscle, spleen, meninges and human placenta (Magalhães, Eira et al. 2021).

TTR has an half-life in humans of 2-3 days (Socolow, Woeber et al. 1965) being mainly degraded in the liver (36-38%), muscle (12-15%) and skin (8-10%). Other organs such as kidneys, testis, adipose tissues and the gastrointestinal tract contribute less to TTR degradation (1-8%) (Makover, Moriwaki et al. 1988) (Figure 3). TTR uptake occurs in the liver in a receptor-associated protein (RAP)-sensitive manner, a protein that binds to all members of the low density lipoproteins receptors (LDLr) family, so identification of the specific receptor that mediates this uptake has still not been achieved (Sousa and Saraiva 2001) (Figure 3). In the kidney TTR uptake is megalin-mediated (Sousa, Norden et al. 2000). Interestingly, the megalin receptor, also called low density lipoprotein receptor-related protein-2 (LRP2), is expressed in multiple cell types of the nervous system, namely, astrocytes (Bento-Abreu, Velasco et al. 2008), oligodendrocytes (Wicher, Larsson et al. 2006), and dorsal root ganglion (DRG) neurons (Fleming, Mar et al. 2009).

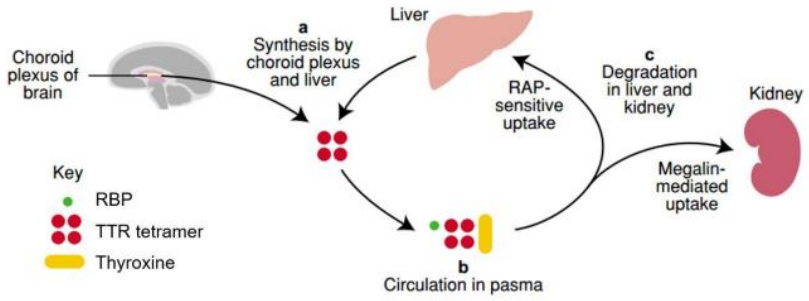


Figure 3. Synthesis, transport, and uptake/degradation of TTR. (a) TTR (red circles) is synthesized in the liver and choroid plexus and (b) binds its physiological ligands: thyroxine (yellow bar) and RBP (green dot). (c) TTR uptake and consequent degradation in the liver and kidney. Adapted from (Saraiva 2002).

1.2.3. TTR physiological functions

The most well-known physiological function of TTR is its ability to transport thyroxine (T_4) and retinol (vitamin A) (Raz and Goodman 1969), garnering its current name of transthyretin ("**T**ransport of **T**hyroxine and **R**etinol"). TTR transports vitamin A by binding to the retinol-binding protein (RBP), being able to transport a maximum of two of these molecules *in vitro*, however, *in vivo* the isolation of these complex always reveals a stoichiometry of 1:1 (Naylor and Newcomer 1999). TTR can bind two molecules of T_4. Interestingly, both the binding of T_4 and RBP have been proven to stabilize TTR tetrameric structure (Hyung, Deroo et al. 2010, Johnson, Connelly et al. 2012). In the serum TTR only transport about 15% of T_4 while in the CFS is responsible for the transport of about 80% of this hormone. Contrarily, TTR transports almost all RBP in the serum, binding to almost 95% of this protein (Magalhães, Eira et al. 2021).

Alternatively, other roles for TTR have been reported. For example, TTR can act as a metalloprotease, and is able to process proteolytically apolipoprotein A1 (apoA-1) and reduce cholesterol efflux (Vieira and Saraiva 2014, Magalhães, Eira et al. 2021). Besides this substrate, TTR can proteolytically cleave both neuropeptide Y and amyloid β peptides (Aβ) and probably other unidentified substrates that were suggested to mediate its observed neuritogenic activity (Magalhães, Eira et al. 2021). Aβ is the main component of amyloid deposits in Alzheimer's disease (AD), when cleaved by TTR Aβ amyloidogenic potential is reduced, revealing a neuroprotective activity of TTR (Silva, Eira et al. 2017). Additionally, TTR has been implicated in the regulation of nerve regeneration and neurite outgrowth *in vitro*, as in TTR knockout (KO) mice both these parameters where impaired (Fleming, Saraiva et al. 2007, Fleming, Mar et al. 2009). Moreover, TTR has a direct link to the neuronal cytoskeleton as it was shown using TTR KO mice that it remodels MTs (Eira, Magalhaes et al. 2021).

1.2.4. TTR aggregation potential

Amyloidogenic proteins may undergo misfolding and aggregation via different processes. In the case of proteins with amyloidogenic potential due to lack of well-defined tertiary structure, normally, amyloidosis develops associated with gene duplications or abnormal post-translational processing or modifications. Other amyloidogenic proteins, such as TTR, in turn, need to suffer a partial unfolding before completely misfolding and aggregating (Johnson, Connelly et al. 2012). Mutations with an amyloidogenic potential lead to TTR tetramer destabilization and dissociation into monomers, however, wild-type (WT) TTR may also undergo the amyloidogenic pathway and originate amyloid deposits. TTR tetramer dissociation is the rate limiting

step of TTR amyloidosis (Yang, Yordanov et al. 2006, Johnson, Connelly et al. 2012). After TTR dissociation into monomers, these unfold and assemble soluble oligomers which, finally, associate to form insoluble fibrils that deposit in organs leading to formation of amyloid deposits (Johnson, Connelly et al. 2012) (Figure 4).

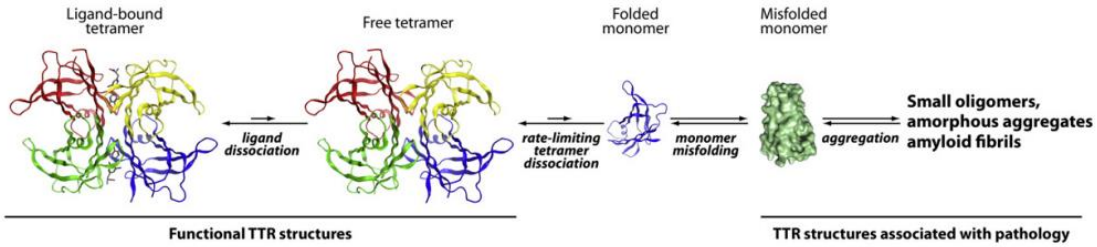


Figure 4. Process of TTR tetramer dissociation, monomer misfolding and formation of aggregates. Adapted from (Johnson, Connelly et al. 2012).

1.3. Transthyretin Amyloidosis

TTR dissociation, misfolding and deposition leads to multiple pathologies, either sporadic or acquired, commonly referred to as transthyretin amyloidosis (ATTR). The sporadic form of transthyretin amyloidosis is known as Senile Systemic Amyloidosis (SSA), and is associated with the aggregation and deposition of WT TTR mainly in the myocardium, leading to cardiac failure (Cornwell, Sletten et al. 1988). SSA is a prevalent disease in people over 80 years of age, remarkedly, it has been reported that one quarter of these individuals have cardiac deposits of WT TTR (Westermark, Sletten et al. 1990, Tanskanen, Peuralinna et al. 2008). Additionally, ATTR may be acquired, as referred early, being characterized by amyloidogenic mutations in the TTR gene leading to a primarily cardiomyopathic phenotype or to a primarily neuropathic one. Transthyretin Amyloid Cardiomyopathy (ATTR-CM) is associated with the accumulation of mutant TTR in the cardiac tissue, being an underdiagnosed pathology (Ruberg, Grogan et al. 2019, Rozenbaum, Large et al. 2021). The most common mutation leading to this ATTR form is Val122Ile (Ruberg, Grogan et al. 2019), but over 100 mutations have been already identified for all acquired forms of ATTR (Connors, Lim et al. 2003), being that the pathology that ensues is dependent on the specific mutation that occurs. These mutations may also lead to ATTR with a neuropathic phenotype that we shall dissect further.

2. Transthyretin Amyloid Polyneuropathy (ATTR-PN)

2.1. Discovery and epidemiology

Our focus, Transthyretin Amyloid Polyneuropathy (ATTR-PN), another form of acquired TTR amyloidosis, formerly known as Familial Amyloid Polyneuropathy (FAP), was first identified in 1952 in Portugal (Andrade 1952). Later, the most common amyloidogenic mutation in TTR was identified, a substitution of valine in the 30th residue by a methionine (V30M) (Saraiva, Birken et al. 1984). ATTR-PN is an autosomal dominant disease with endemic focus in Japan, Portugal, and Sweden, but several thousand cases are reported each year all around the world (Planté-Bordeneuve and Said 2011) (Figure 5).

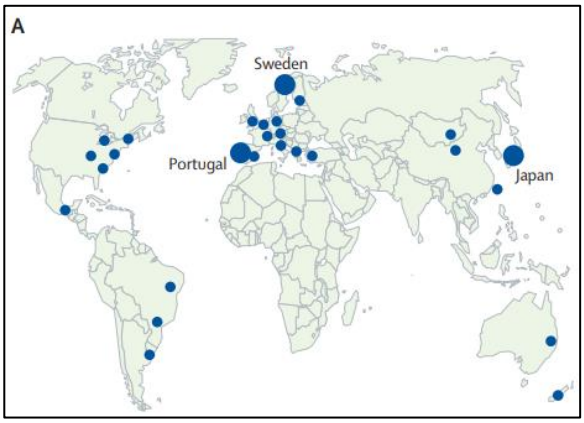


Figure 5. World distribution of ATTR-PN. Special focus on the endemic focus in Portugal, Sweden, and Japan. Adapted from (Planté-Bordeneuve and Said 2011).

2.2. Pathophysiology and symptomatology

In ATTR-PN, deposition of mutant TTR is systemic but preferably occurs in the peripheral nervous system (PNS) including the nerve trunks, plexuses, and sensory and autonomic ganglia (Coimbra and Andrade 1971), leading to a length-dependent polyneuropathy which leads to neurodegeneration. Interestingly, Schwann cells are especially susceptible to the “toxic activity” of mutant TTR, as aggregates accumulate in the endoneurium close to these cells and also collagen fibrils (Sousa, Cardoso et al. 2001), and relate to the early loss of sensory unmyelinated fibres, as these fibres depend nutritionally on Schwann cells (Planté-Bordeneuve and Said 2011). The degeneration of sensory fibres justifies the appearance of the first symptoms of ATTR-PN, namely the loss of pain and temperature sensation in the feet. Evolution of the disease determines extension of loss of sensation to the lower and, eventually, upper limbs, accompanied by a progressive loss of locomotor function. Finally, in the later stages of ATTR-PN dysautonomia sets in leading to death. The first symptoms may

appear in an early onset fashion, 30 to 40 years of age, or a late onset one, 70 to 80 years of age, typical to endemic and non-endemic areas, respectively, (Planté-Bordeneuve and Said 2011) and after diagnosis death occurs approximately in six to twelve years (Adams, Ando et al. 2021). In addition to the typical neuropathic manifestation of ATTR-PN, other manifestations may occur parallelly such as cardiac manifestations, ocular manifestations, and renal manifestations (Planté-Bordeneuve and Said 2011).

2.3. Molecular mechanisms of TTR neurotoxicity

How aggregates trigger neurodegeneration is still not fully understood but intermediate species, oligomers and unfolded monomers, were shown to present significant cytotoxicity (Reixach, Deechongkit et al. 2004). Several mechanisms for TTR cytotoxicity have been described: (i) TTR interactions with the Fas receptor leading to apoptosis through the activation of pro-caspase 8 and subsequently pro-caspase 3 (Macedo, Batista et al. 2007); (ii) TTR disruption of cell homeostasis by causing an abnormal calcium influx. Aggregates induce endoplasmic reticulum (ER) stress which promotes calcium dysregulation and activation of the apoptosis pathway (Saraiva, Magalhaes et al. 2012); (iii) TTR interacts with the Receptor for Advanced Glycation End products (RAGE) inducing the nuclear factor kappa β (Nf-kB) pathway which leads to the release of pro-inflammatory cytokines interleukin-1β (IL-1β) and tumour necrosis factor TNF-α). RAGE also has been reported to lead to caspase-3 activation (Sousa, Du Yan et al. 2001); (iv) TTR induced formation of reactive oxygen species (ROS) and reactive nitrogen species (RNS) leading to the destabilization of the oxidative status of the cell relating to increased DNA damage and lipid peroxidation (Saraiva, Magalhaes et al. 2012) (Figure 6).

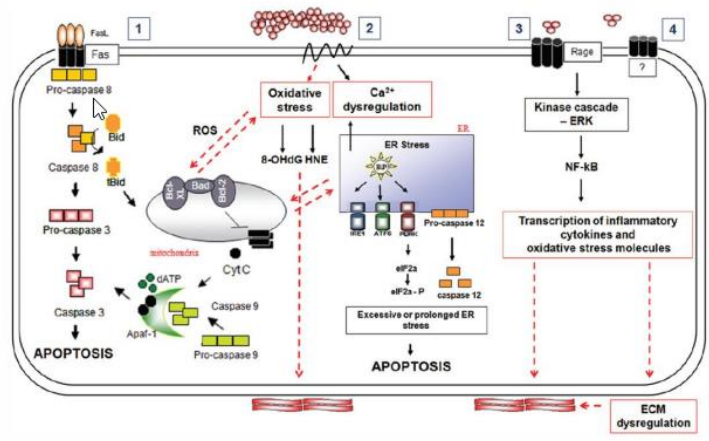


Figure 6. Overview of the possible ways aggregates of TTR lead to cytotoxicity. (1) Activation of FAS receptor leads to apoptosis. (2) Interaction with aggregates with the cell membranes leads to calcium disruption and ER

stress. (3) RAGE interacts with aggregates and triggers NF-kB leading to an inflammatory response. (4) Unidentified players in causing cytotoxicity by TTR aggregates. Adapted from (Saraiva, Magalhaes et al. 2012).

Alternatively, it was recently reported that in a model of *Drosophila Melanogaster* expressing TTR with the mutation V30M in the retina, the Rho GTPase family is involved in inducing cytoskeletal dysfunction at the level of actin leading to neurodegeneration (I. Oliveira da Silva, Lopes et al. 2020). This will be further explored in future sections.

2.4. Diagnostic and Current Therapeutic Approaches

Current approaches in the diagnosis of TTR amyloidosis are divided in TTR gene sequencing and tools for detection of amyloid deposits (Adams, Ando et al. 2021). Furthermore, family history is also considered and accelerates diagnosis in endemic areas. Regarding genetic approaches: discovering the mutation carried is essential as it allows to predict severity of the disease and which organs may be more affected. However, the presence of a TTR amyloidogenic mutation does not mean that the patient will develop symptoms so confirmation through biopsy is needed to evaluate amyloid deposition. Nowadays, the most used approaches of biopsy are labial salivary gland biopsy, skin biopsy, and abdominal fat biopsy, being preferred over nerve and cardiac biopsies due to being less invasive (Adams, Ando et al. 2021). Unfortunately, misdiagnosis and consequent accurate diagnosis delay is still a common problem, being especially relevant in non-endemic areas and patients without family history as only in 26-38% of initial evaluations suspect ATTR-PN (Ando and Ueda 2012, Adams, Ando et al. 2021).

Regarding treatment for ATTR-PN, the most well-established approach is liver transplantation as this is the major site for the synthesis of TTR. This approach leads to reduced serum levels of mutant TTR (Holmgren, Steen et al. 1991) and effective prolongation of life expectancy in most patients (Benson 2013). However, this therapeutic approach is extremely invasive and expensive. Besides this, it also presents some other major drawbacks: liver transplantation cannot be performed in older patients or in later stages of the disease; is not as effective in patients that do not carry the most common mutation V30M (Wilczek, Larsson et al. 2011); and in some patients deposition of amyloid continues either through the “capture” of WT TTR in previously established amyloid deposits (Liepnieks and Benson 2007) or through the continued production of mutant TTR in other sites of synthesis such as the choroid plexus (Planté-Bordeneuve and Said 2011).

Another more recent therapeutic approach is the stabilization of the TTR tetramer to impair amyloid formation using specific drugs such as, tafamidis and diflunisal. Tafamidis , Vydaqel®, has already been approved in over 40 countries for the treatment of ATTR-PN leading to slowed deterioration of the PNS and maintenance of health-related life quality in early stages of the disease in patients carrying the V30M mutation (Lamb and Deeks 2019). Tafamidis stabilizes the quaternary structure of TTR by binding to the T_4 site, halting dissociation into monomers and consequent aggregation and deposition (Connelly, Choi et al. 2010). Diflunisal, a member of the anti-inflammatories non-steroidal (AINEs) family, was also shown to improve quality of life in patients carrying V30M mutation when tested in repurposing clinical trials for the treatment of ATTR-PN. Nevertheless, the adverse diflunisal activity associated with cyclooxygenase 1 (COX-1) inhibition leads to gastric mucose injury and renal dysfunction (and other undesirable effects) demanding careful monitoring and further trials to understand this therapy's limitations (Ueda and Ando 2014, Sekijima 2015).

Genetic therapeutic approaches were also developed for ATTR-PN. Two examples of this are: antisense oligonucleotides (ASO) and small interfering RNAs (siRNAs) which lead to RNA enzymatic degradation and gene silencing, respectively (Ueda and Ando 2014). Inortesen, a type of ASO, slowed neuropathy progression and ameliorated quality of life in patients, independently of the carried mutation, in phase 3 clinical trials. This gene silencing agent presented some major drawbacks, namely, thrombocytopenia and glomerulonephritis, so, besides careful monitoring of patients receiving such therapy, further trials and studies are needed (Benson, Waddington-Cruz et al. 2018). Another gene silencing agent that showed promise was Patisiran, a siRNA encapsulated in lipid-nanoparticles which improved neuropathy, and quality of life without showing significant side effects in phase 3 clinical trials (Adams, Gonzalez-Duarte et al. 2018). In the United States of America the Food and Drug Administration (FDA) approved the use of Patisiran for the treatment of TTR amyloidosis in 2018 (Ledford 2018).

Additionally, other therapeutic approaches such as 4′-iodo-4′-deoxydoxorubicin (IDOX), doxycycline, tauroursodeoxycholic acid (TUDCA), and cyclodextrin (CyD) also show some promise but further study is required. Alternatively, immunotherapy using anti-Serum amyloid P (SAP) antibodies also showed some interesting prospects in preclinical assays, leading to AA amyloid removal in mice (Ueda and Ando 2014).

Even though the recent advances in therapeutics seemingly bridge the limitations of liver transplantation, not adequate for late onset and advanced cases of ATTR-PN, none of them target neurodegeneration, which to this day remains irreversible.

2.5. Mouse models of ATTR-PN

To study ATTR-PN the generation of animal models that replicate what happens in humans is capital. The first mouse models developed for ATTR-PN carried the most common mutation, V30M. Early mouse models, still carrying the mouse gene for TTR besides the mutated inserted gene, revealed low concentration of mutated TTR in the serum and lacked deposition of amyloid in the PNS, a hallmark of ATTR-PN (Sasaki, Tone et al. 1986, Shimada, Maeda et al. 1989, Yi, Takahashi et al. 1991). Further attempts were made inserting the human gene of TTR in TTR-null background mice but, equally, failed to translate the human pathophysiology of ATTR-PN (Kohno, Palha et al. 1997). Finally, the generation of a model with TTR V30M mutation in a heat shock transcription factor 1 (HSF1) null background proved fruitful presenting as extensive TTR deposition in the PNS, accompanied by a progressive loss of unmyelinated fibres (Santos, Fernandes et al. 2010).

Recently, the generation of a mouse model carrying the A97S mutation in human TTR, the most common mutation in patients in Taiwan, created by replacing the TTR mouse gene without altering promotor and enhancer sequences proved fruitful, as this model mimicked the early signs of ATTR-PN. Importantly, deposition of amyloid in the PNS was observed. Additionally, neuropathic pain behaviours, small nerve fibre neuropathy and large sensory fibre neuropathy, characterized by reduced sural sensory nerve action potential amplitudes and myelinated fibres density, were observed in this mouse model (Kan, Chiang et al. 2018). Therefore, this model presents itself as a valuable tool to further our understanding of ATTR-PN.

3. Cytoskeleton disruption and neurodegeneration

3.1. The cytoskeleton components: function and regulation

The neuronal cytoskeleton is essential to maintain cell polarity and to maintain cell homeostasis, being that dysfunction at this level has been reported to be a hallmark of neurodegeneration (Eira, Silva et al. 2016). The cytoskeleton is composed of microtubules (MTs), actin and intermediate filaments, in neurons the so called neurofilaments, all which we shall explore next.

3.1.1. Actin

Actin is a vital component of eukaryotic cells being a highly conserved and expressed protein. This importance is highlighted by the fact that actin is the protein which has most known protein-protein interactions. Vertebrates express 3 isoforms actin, α-actin and β- and γ- actin. Actin undergoes polymerization, going from monomeric actin (G-actin) to filamentous actin (F-actin), forming a two-chained helix (Dominguez and Holmes 2011) (Figure 7). Additionally, filaments of actin exhibit polarization, having a pointed end and a barbed end. Barbed ends grow much faster than pointed ends, these last ones are relatively stable having a lack of addition or removal of actin monomers (Pollard 2016). To form F-actin, first, nucleation is needed. This process occurs when small oligomers are formed by the association of G-actin, which are suitable for elongation. After F-actin formation, ATP-actin is added to the polymer in the barbed end while ADP-actin is removed from the pointed end. *In vitro,* this generates a steady state known as treadmilling (Dominguez and Holmes 2011) (Figure 7). This way, the conversion of ATP into ADP that occurs in the filament almost acts as a timer for the cycles of elongation/depolymerization of F-actin (Pollard 2016). It is important to note that although actin monomers associate freely *in vitro* this process has a high kinetic barrier (Coles and Bradke 2015).

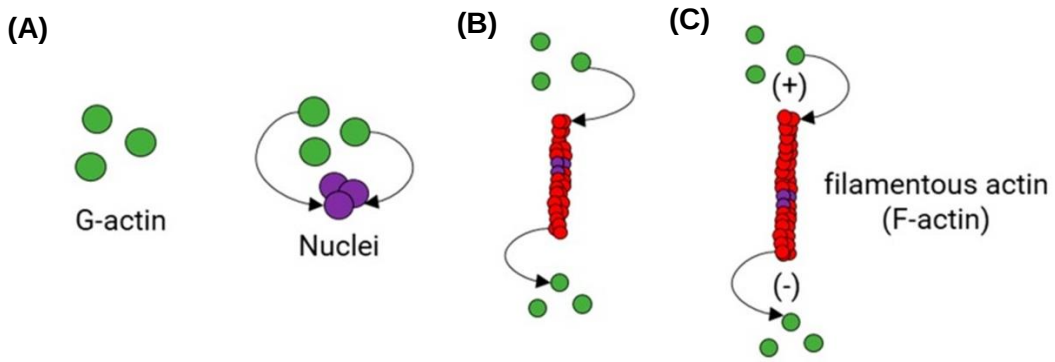


Figure 7. Overview of F-actin formation. (A) G-actin associate and forms a nucleus suitable for elongation (B) The proper formation of a nucleus elicits elongation of the filament (C) A steady state is achieved, actin treadmilling, where new subunits of G-actin are added to the barbed end (+) and others are removed from the pointed end (-). G-actin, nuclei, and F-actin in green, purple and red respectively. Barbed end (+) and pointed end (-). Adapted from (Muñoz-Lasso, Romá-Mateo et al. 2020).

As previously mentioned, the formation of F-actin can occur *in vitro* with proper conditions and without the presence of any specific proteins. *In vivo*, actin behaviour (nucleation, elongation/branching, depolymerization) is tightly regulated by several actin binding proteins (ABPs) which include: (i) actin-monomer binding proteins, such as profilin and thymosin β4 which determine the pool of G-actin available for polymerization in a localized manner, by sequestering monomers and inhibiting spontaneous F-actin polymerization *in vivo*. G-actin bound to profilin may be used in polymerization, contrarily, Tβ4 blocks polymerization (Dominguez and Holmes 2011, Coles and Bradke 2015, Pollard 2016); (ii) severing proteins, such as the ADF/cofilin family and gelsolin, bind strongly to ADP-actin ensuring its removal. This severing activity, often, leads to more polymerization as more barbed ends become available (Pollard 2016, Møller, Klip et al. 2019); (iii) nucleation proteins break the unfavourable conditions for F-actin *de novo* formation, exacerbated by the activity of profilin and Tβ4. Examples of such nucleators are actin-related protein 2/3 (Arp2/3), which nucleates new filaments by binding to the lattice of a pre-existing one, and formins, which promote linear polymerization of F-actin; (iv) actin filament polymerases elongate filaments. The Ena/Vasp homology proteins are important elongators of F-actin. Interestingly, formins may also exhibit this activity; (v) capping proteins interact with the ends of F-actin, namely the barbed end, halting monomer addition. Capping protein (CP) and gelsolin bind strongly to barbed ends and block polymerization forcing the addition of monomers in the pointed end, eliciting a non-canonical actin behaviour. Conversely, tropomodulin and Arp2/3 cap pointed ends and allow for filament stabilization; (vi) cross-linking proteins normally possess two calponin homology (CH)

domains and stabilize important structures such as filopodia. Examples of cross-linking proteins are fascin, which originates disorganized bundles of F-actin, and fimbrin, which originates well-organized actin networks; (vii) filament-binding proteins give stability to filaments or limit the possible protein interactions of F-actin. An example is tropomyosin which binds to F-actin and controls myosin binding (Dominguez and Holmes 2011, Pollard 2016). Besides the myriad of ABPs other proteins can associate and allow for contractability of actin arrangements, such as myosins, which over 17 classes have been identified. Interestingly, these proteins produce movement via the hydrolysis of ATP using actin as a track for the transport of multiple cargos (Winder and Ayscough 2005) (Figure 8).

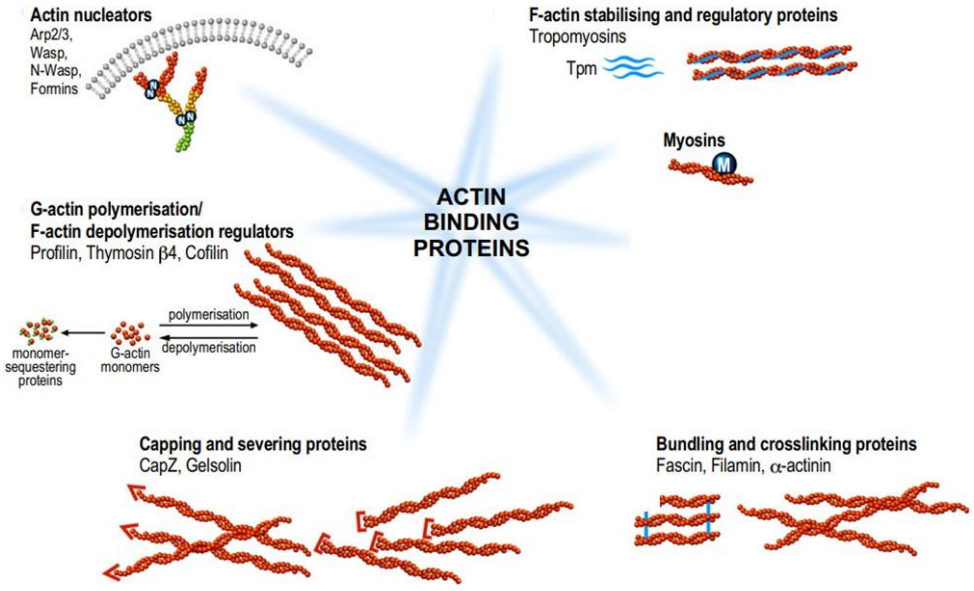


Figure 8. Overview of the myriad of processes regulated by ABPs. F-actin may be severed, cross-linked, branched, capped, or elongated. Monomer binding proteins control availability of G-actin. Adapted from (Ruggiero and Lalli 2021).

3.1.2. Microtubules

Microtubules (MTs) are tubular structures composed of 13 protofilaments, in most mammalian cells, with each protofilament being composed by heterodimers of α- and β- tubulin organized in a linear arrangement. These structures have an essential role being found in all known eukaryotes. Multiple isoforms of tubulin exist: α- and β-tubulins, essential to form cytoplasmatic MTs, γ-tubulin, essential for nucleation and thus the generation of new MTS, and δ-, ε- and ζ-tubulins, present in organisms with cilia, flagella, and basal bodies. MTs exhibit polarity having a fast-growing end, the

plus-end, and a slow growing end, the minus-end (Conde and Cáceres 2009, Goodson and Jonasson 2018).

MTs are generated through nucleation: however, this process does not occur easily *in vitro*, even with high concentrations of α- and β-tubulins. Spontaneous formation of MTs is thus extremely improbable and other players are important to start this process *in vivo*, such as the γ-Tubulin Ring Complex (γ-TuRC). This ring complex functions both as a template for a new MT, and as a cap for the minus end. Augmin is also relevant in this context, being able to generate MTs using the lattice of a pre-existing MT (Goodson and Jonasson 2018). After being formed, MTs undergo cycles of polymerization/depolymerization, going from growth to shrinkage, called catastrophe, and from shrinkage to growth, called rescue. This erratic behaviour is often referred to as dynamic instability (Horio and Hotani 1986) (Figure 9). This process is controlled by the GTP state of β-tubulin, as α-tubulin also binds GTP, but it is not available for hydrolysis along the course of MT polymerization (Goodson and Jonasson 2018). Tubulin dimers bound to GTP are continuously added to the plus end of MTs, GTP gets hydrolysed to GDP and, if no more GTP bound tubulin is added, removal of tubulin begins. GTP hydrolysis happens after the last α-tubulin subunit is added, its catalytic domain interacting with the nucleotide exchangeable site, the E site, of the previous β-tubulin subunit, promoting the hydrolysis of its bound GTP to GDP. Parallelly, in the minus end contact is done directly between the last added α-subunit and the newly added β-tubulin subunit determining direct GTP hydrolysis (Conde and Cáceres 2009, Goodson and Jonasson 2018). Generally, MTs are nucleated around centrosomes which act as a microtubule organizing centre (MTOC), allowing for organization and nucleation of this cytoskeleton component (Goodson and Jonasson 2018). However, in neurons and other cell types, the centrosome loses the ability to function as a MTOC, and to this day, what structure act as a harbour for nucleation or, even, how molecular players lead to MT nucleation is poorly understood (Sanchez and Feldman 2017).

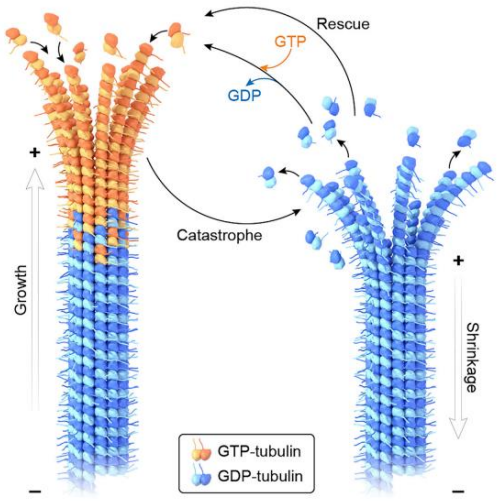


Figure 9. Overview of MTs dynamics. GDP bound tubulin in blue and GTP bound tubulin in orange. The loss of the GTP cap in the plus-end (lack of addition of GTP-tubulin) leads to catastrophe while addition of GTP-tubulin rescues this accelerated shrinkage. Adapted from (Roll-Mecak 2020).

MTs fate and function is not left in the hand of probability but it is, as all biological processes, tightly regulated by multiples proteins. These proteins are often referred to as microtubules associated proteins (MAPs) and include: (i) growing plus-end tracking proteins, TIPs+, associate to the plus-end of MTs following their growth. Examples of TIPs+ are Xenopus microtubule-associated protein 215 (XMAP215), end-binding (Ebs) proteins, cytoplasmic linker associated proteins (CLASPs) and the CAP-Gly domain containing families, often, promoting polymerization of MT by altering the structure of the plus-end. However, some TIPs+ promote depolymerization spending ATP, such as the kinesin-8, -13 and -14 families (Akhmanova and Steinmetz 2015); (ii) lattice-binding proteins, cross-link and stabilize MTs. The classical MAPs, Tau, microtubule associated protein 2 (MAP2) and microtubule associated protein 4 (MAP4), stabilize MTs. Aditionally, the classical MAPs can crosslink actin and MTs and, even, recruit signalling components (Dehmelt and Halpain 2005); (iii) nucleating proteins and severing enzymes, lead to the augment of the number of MTs, by generating new MTs or by severing pre-existing ones, respectively. Augmin and γ-TuRC were already explored as important nucleators. Additionally, fidgetin, spastin and katanin are AAA+ ATPases which spend ATP to sever MTs (Roll-Mecak and McNally 2010); (iv) motor proteins elicit movement of cargoes using MTs as “tracks”. Dynein and kinesin spend ATP to produce kinetic energy, moving towards the minus-end and the plus-end, respectively; (v) tubulin folding cofactors are chaperones that induce proper folding of tubulin subunits, and (vi) enzymes that post translationally modify tubulin and generate a complex “tubulin code” (Janke and Kneussel 2010, Goodson and Jonasson 2018).

As stated, some MAPs can alter tubulin post-translationally creating a special code, subject of a lot of discussion as its richness and impact is tremendous in MT behaviour. Functionally, this “tubulin code” arises contributing to the fate of multiple cell processes. Post-translational modifications (PTMs) range from acetylation (α- and β-tubulin), methylation (α-tubulin), phosphorylation (α- and β-tubulin), palmitoylation (α-tubulin), polyamination (α- and β-tubulin), tyrosination/detryrosination (α-tubulin), generation of Δ2-tubulin (removal of two C-terminal glutamates in α-tubulin), glutamylation (α- and β-tubulin) and glycylation (α-tubulin) (Roll-Mecak 2020) (Figure 10).

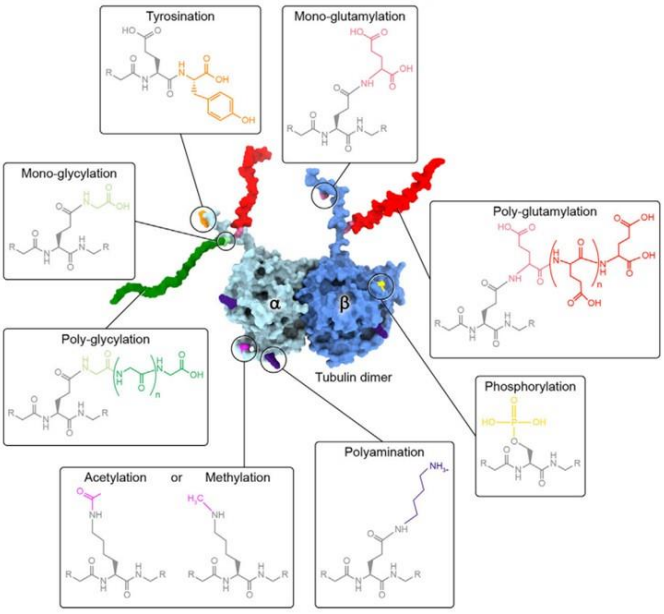


Figure 10. Overview of the possible PTMs that MTs can suffer and its localization in α- and β-tubulin structures. α-tubulin in light blue and β-tubulin in dark blue. (Roll-Mecak 2020).

Acetylation occurs in Lys40 of α-tubulin and in Lys252 of β-tubulin and it is associated with stable MTs. This modification is mainly catalysed by α-tubulin N-acetyltransferase 1 (α-TAT1/ATAT1) (Kalebic, Martinez et al. 2013) and the reverse process, deacetylation, by histone deacetylase 6 (HDAC6) and NAD-dependent protein deacetylase sirtuin-2 (SIRT2). Most α-tubulin is expressed with a tyrosine in the C-terminal which can be removed and, eventually, readded. Removal of tyrosine is catalysed by the vasohibins (VASH1/2)/small vasohibin-binding protein (SVBP) complex (Aillaud, Bosc et al. 2017) and readdiction is catalysed by tubulin tyrosine ligase (TTL). Tyrosinated microtubules are highly dynamic and detyrosinated ones very stable. Glutamylation and glycylation are catalysed by tubulin tyrosine ligase like

(TTLLs). TTLL1, 2, 4, 5, 6, 7, 9, 11, and 13 have glutamylase activity and TTLL3, 8 and 10 have glycalase activity. Cytosolic carboxypeptidase (CCP) 1, 2, 3, 4 and 6 shorten glutamate chains, reverting glutamylation, and, in some cases, generating Δ2-tubulin, an apparently irreversible PTM, which is characterised by the remotion of carboxy-terminal glutamyl-tyrosine group on its αlpha-subunit. Interestingly, Δ2-tubulin is impervious to tyrosination and is abundant in neurons, being associated with stable MTs. Other truncated forms have been also identified, Δ3- and Δ4-tubulin, but their relevance is poorly understood (Fukushima, Furuta et al. 2009, Aillaud, Bosc et al. 2016). CCP5 removes branching point glutamates and, to this day, no enzyme with deglycilating activity has been identified. Functionally, glutamylation seems to mediate the severing of MTs, it has been reported that this PTM can promote spastin mediated MT-severing (Lacroix, van Dijk et al. 2010), and regulates axonal transport in neurons (Yu, Garnham et al. 2015, Roll-Mecak 2020). This “tubulin code” is not “jury and judge” and in fact coexists with MAPs and interacts with a lot of other players generating one more layer of complexity in MT behaviour.

3.1.3. Neurofilaments

Neurofilaments (NFs) are members of the family of intermediate filaments (IFs), encoded by more than 70 genes, characterized normally by bundles with approximately 10μm in diameter which are extremely abundant in neurons. Five types of subunits that compose NFs have been identified: neurofilament light protein (NF-L), neurofilament medium protein (NF-M), neurofilament heavy protein (NF-H), α-internexin, only present in the central nervous system (CNS), and peripherin, only present in the PNS. Association of this subunits is not stoichiometrically constant all throughout neuron populations. Interestingly, this cytoskeletal component lacks an intense dynamic behaviour as it is seen in MTs and actin.

NFs are essential for radial growth through the development of the nervous system, nerve conduction velocity and synapse function. Besides these functions, and ensuring structural support, NFs bridge actin and MTs via proteins such as: spectrin, bullous pemphigoid antigen (BPAG), plectin and some MAPS such as Tau, MAP1 and MAP2. The importance of NFs is exacerbated by the fact that abnormalities in the proteins that compose them are associated with multiple neurodegenerative pathologies (Herrmann, Strelkov et al. 2009, Yuan, Rao et al. 2017).

3.2. Neuronal cytoskeleton organization: structure leads to function

Neurons are among the most polar cells known being that the maintenance of their structure is essential for cell homeostasis and function. Neurons are divided into two main compartments: i) the somatodendritic one, which normally emits dendrites that may receive signals that the cell body will integrate, and ii) the axon, typically a slender process that extends forming synapses, neuromuscular junctions or, in axonal growth conditions, such as human development, *in vitro* neuron culture, or peripheral axon lesion, a growth cone (Stiess and Bradke 2011, Murillo and Mendes Sousa 2018). The growth cone has a highly specific cytoskeletal organization which allows it to rapidly organize depending on specific cues, leading to extension or retraction of the axon. The growth cone is divided into three domains from a proximal to a distal perspective: the central (C-) domain, the transitional (T-) domain and the peripheral (P-) domain. The C-domain, the boundary between axon tip and growth cone, has unbundled MTs with their plus-end facing the periphery. A subset of highly dynamic MTs “escape” the C-domain and penetrate the T- and P-domains. The T-domain, located between the C- and P-domains, possesses actomyosin arcs bound to non-muscle myosin II (NMII) being able to contract. The P-domain, the most distal growth cone portion, is highly enriched in actin organized in lamellipodia, actin networks, and filopodia, finger-like actin bundles. Actin retrograde flow, actin polymerization from the leading edge to the centre of the growth cone, in close association with the actomyosin arcs and continuous F-actin polymerization in the edge, actin treadmilling, makeup the engine for growth cone advancements in response to extracellular direction growth cues (Lowery and Van Vactor 2009, Leite, Pinto-Costa et al. 2021) (Figures 11 and 13).

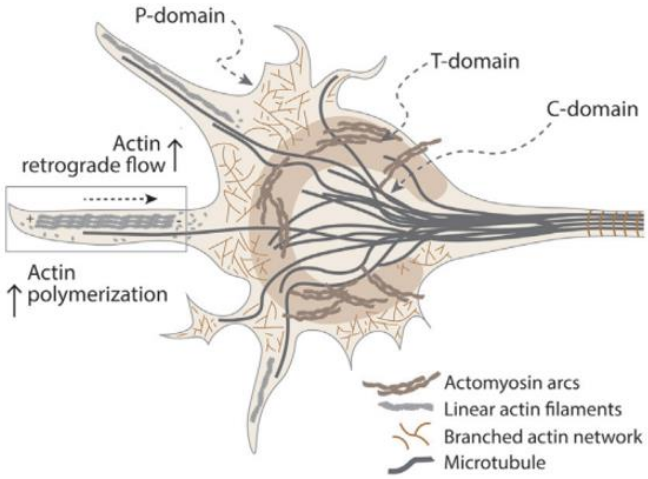


Figure 11. Overview of an expanding growth cone morphology and organization of cytoskeletal components. Identification of C-, T-, and P- domains. The C-domain contains dynamic unbundled MTs that come from the axon shaft. The T, domain contains the actomyosin arcs that allow for contractility. The P-domain contains a branched actin network and filaments that undergo continuous polymerization and retrograde flow. Adapted from (Leite, Pinto-Costa et al. 2021).

The axon also presents a highly organized cytoskeleton. For many years the axonal organization of F-actin was a mystery that in recent years has been partially unveiled. F-actin in the axon, besides being present in the borders, apparently static, presents itself as highly specific forms namely waves (Ruthel and Banker 1998), rings (Xu, Zhong et al. 2013), actin patches (Loudon, Silver et al. 2006), and actin trails (Ganguly, Tang et al. 2015) (figure 11). Actin waves are slow moving (2-3μm/min) growth-cone like structures that appear periodically starting in the axonal initial segment (AIS) and moving towards the tip of the axon. These structures cause membrane flaring and have been described has being composed by actin filaments fanning out in acute angles towards the membrane and suffering continuous directional treadmilling (Bretschneider, Anderson et al. 2009, Roy 2016). These structures are both sensitive to drugs that affect actin and MTs dynamics, indicating an interesting interplay between two cytoskeletal components. Biological relevance of waves is poorly understood although recent studies associate them with being important for MT dynamics (Huang, Hsu et al. 2020), axon growth (Woo, Seo et al. 2019) and actin transport in neurons. Actin rings are F-actin structures that wrap underneath the axonal plasma membrane at regular intervals of about 190nm. Although seemingly stable structures the use of depolymerizing agents disrupts them (Leite and Sousa 2016). Their function is still not well-established, but actin rings seem to have more than a structural purpose, elucidated by the observed interplay with MTs (Leite and Sousa

2016, Roy 2016). Actin patches are a type of meshwork of actin associated with the genesis of filopodia in the distal axon. These structures are also present in the AIS arresting cargoes being able to limit their advance and act as possible filters of non-axonal cargoes versus axonal cargoes (Watanabe, Al-Bassam et al. 2012, Arnold and Gallo 2014). Actin trails are extremely dynamic forms of F-actin that undergo rapid linear polymerization at an average velocity of 1μm/s. This form of actin dynamics seems to arise from F-actin hotspots, high concentration of bundles of actin along the axon which seemingly colocalize with stationary endosomes, probably serving as harbours for initiation of polymerization. Actin trails are formin-dependent and extremely sensitive to depolymerizing actin agents. Physiological relevance of actin trails can be associated with the transport of actin along the axon or even, as it was already shown, the transport of pre-synaptic vesicles (Ganguly, Tang et al. 2015, Roy 2016, Chenouard, Xuan et al. 2020) (Figure 12).

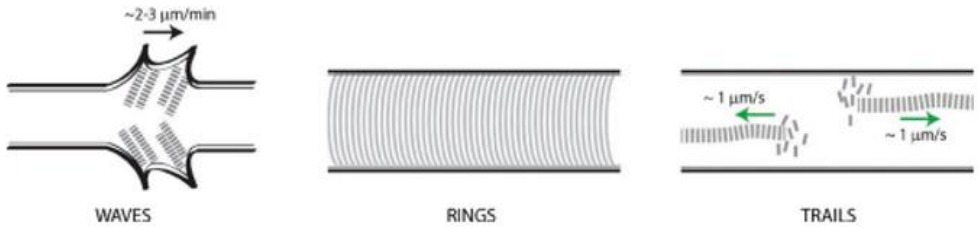


Figure 12. Overview of actin structures identified in the axon shaft. From left to right: the slow-moving growth cone-like waves; actin rings, the seemingly stable ring-like structures; actin trails, the fast-polymerizing filaments of actin that seem to have a role in the transport of some cargoes. Adapted from (Roy 2016).

MTs in the axon exhibit a much more uniform behaviour, being present as long linear stable bundles that provide structural support and function as “highways” for axonal transport of cargoes. Most axonal MTs have their plus-end facing the axon tip and their minus-end point to the somatodendritic compartment, being that this organization is capital for the correct transport of cargoes in neurons. Additionally, this transport may happen anterogradely (towards the axon tip) or retrogradely (towards the cell body), being controlled by kinesin and dynein, respectively (Kapitein and Hoogenraad 2011) (Figure 13).

In dendrites, MTs have mixed orientations (Kapitein and Hoogenraad 2011) and are limited to the shaft, although some penetrate into dendritic spines, essential structures for neurons to properly receive input (Hu, Viesselmann et al. 2008). Actin is important for the formation and maintenance of dendritic spines, being extensively present in these structures (Okabe 2020) (Figure 13).

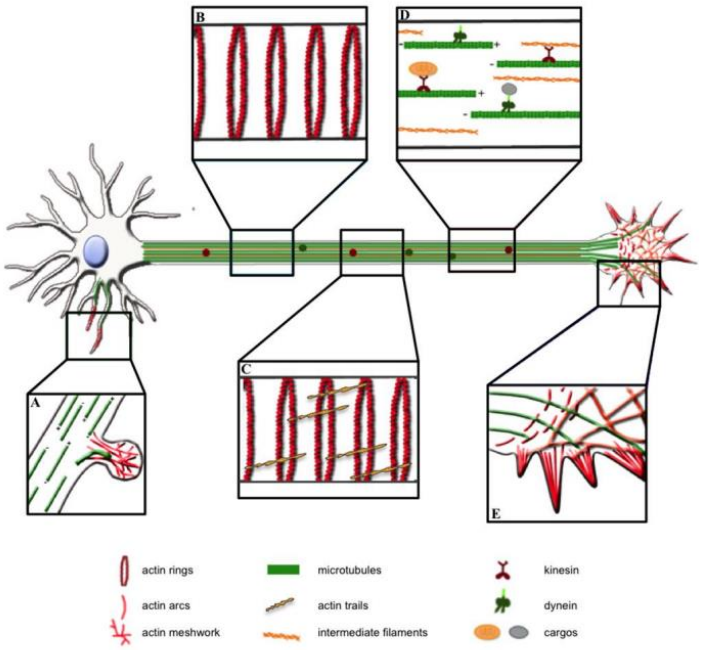


Figure 13. Cytoskeleton organization of a developing neuron. (A) Actin (in red) is present in dendritic spines as actin patches. (B) and (C) actin forms both rings (B) and leads to rapid spurs of polymerization, the actin trails, in the axon shaft. (D) Along the axon MTs (in green) run like “tracks” for the transport of cargoes with their minus-ends pointing to the cell body and the plus-ends pointing to the axon tip. MTs also penetrate the growth cone (E) and are present in dendrites with mixed orientations (A). (E) Actin organizes as bundles in filopodia and as a meshwork in lamellipodia. Adapted from (Eira, Silva et al. 2016).

3.3. Neuronal cytoskeleton: major regulators

As previously mentioned, PTMs play a major role in MTs regulation. In neurons, growth cones accumulate tyrosinated tubulin compatible with dynamic MTs, which are needed to respond readily to extracellular cues. Additionally, the growth cone also accumulates short-chained tubulin polyglutamylation in MTs. This modification has a function that is not fully understood, but it is known that contributes to fine tuning of cargos that MTs transport, as previously described (Roll-Mecak 2020). Contrarily, in the axon detyrosination, acetylation and Δ2-tubulin, PTMs associated with stability, accumulate in MTs. Moreover, long chained polyglutamylation is preferred. In the axon, MTs need to support the overall structure and be able to transport cargoes, justifying promotion of stability (Janke and Kneussel 2010) (Figure 14).

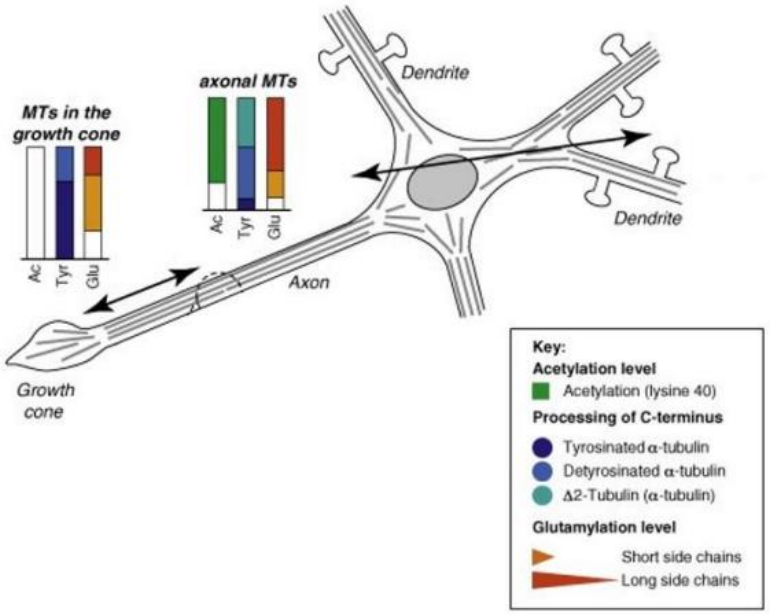


Figure 14. Distribution of MTs PTMs in a developing neuron. Acetylation, tyrosination, delta2-tubulin and long-chained polyglutamylation are preferred in the axon shaft, while reduced levels of acetylation and high levels of tyrosination and of short-chained glutamylation are present in the growth cone. Adapted from (Janke and Kneussel 2010).

Additionally, to tubulin PTMs, the Rho GTPase family is a well-known regulator of the cytoskeleton, namely, the actin component. This family is divided into 2 classes typical [more importantly, Rac1, Ras homolog family member A (RhoA), Cell division control protein 42 homolog (Cdc42)] and atypical. RhoA, Rac1 and Cdc42 are the most well studied ones. Typical Rho GTPases are active when bound to GTP and inactive when bound to GDP. This ties them functionally to guanine nucleotide exchange factors (GEFs) and GTPase-activating proteins (GAPs) (Kalpachidou, Spiecker et al. 2019). GEFs exchange GDP to GTP and activate these proteins while GAPs do the opposite and determine inactivation. The human genome encodes more than 60 GEFs and more than 70 GAPs (Etienne-Manneville and Hall 2002), proving the fine tuning that these signalling molecules can attribute to cell processes. Guanosine dissociation inhibitors (GDIs) also contribute to this complex signalling by blocking these small GTPases of trading GDP for GTP inhibiting them (Heasman and Ridley 2008) (Figure 15).

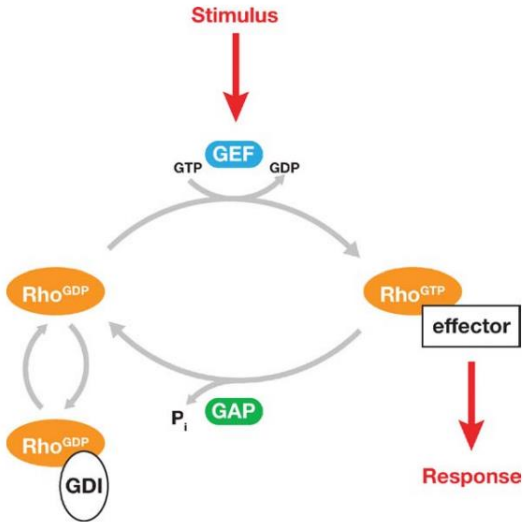


Figure 15. Overview of a Rho GTPase mechanism of regulation. An extracellular cue activates a receptor that in turn activates a GEF. This GEF trades GDP for GTP and leads to activation of Rho GTPase leading to a cellular response. A GAP determines inactivation. Note that, a GDI controls the ability of the GEF to activate the Rho GTPase by blocking the trade of GDP for GTP. Adapted from (Jaffe and Hall 2005).

It has been reported that RhoA promotes the formation of stress fibres, contractile actin structures in non-muscle cells, and focal adhesion sites (Ridley and Hall 1992); Rac1 leads to protrusion of lamellipodia and membrane ruffling (Ridley, Paterson et al. 1992); and Cdc42 leads to extension of filopodia (Nobes and Hall 1995). Rho GTPases regulate actin via downstream effectors that act upon ABPs. Such an example of this is Rac1, which activates the Suppressor of cAR (Scar)/WASP-family verprolin homologous protein (WAVE) complex family, in turn, activating the Arp2/3 complex promoting actin polymerization (Eden, Rohatgi et al. 2002, Tahirovic, Hellal et al. 2010). Parallelly, Arp2/3 is activated by Cdc42 but via the Wiskott–Aldrich Syndrome protein (WASp) or neural-WASp (N-WASP) families, generating different types of actin alterations (Jaffe and Hall 2005). As previously mentioned, cofilin is an important regulator of the actin cytoskeleton being an important depolymerizer of actin filaments essential for growth cone dynamics and axon extension (Heasman and Ridley 2008). LIMK promotes inactivation of cofilin, by phosphorylation of its Ser3 residue, being activated through p21-activated kinase (PAK) or RhoA kinase (ROCK), downstream effector of Cdc42/Rac1 and RhoA, respectively. Slingshot phosphatases, SSHs, namely, SSH1 (mammalians encode 3 forms, SSH1, SSH2 and SSH3) alleviates cofilin inhibition by dephosphorylation (Namme, Bepari et al. 2021). This inter play between the Rho GTPases family translates guidance: Rac1/Cdc42 seem to respond to attractive cues while Rho seems to induce growth cone collapse when associated with repulsive cues (Dickson 2001, Caron 2003), being, equally, essential to axon growth

and specification (Heasman and Ridley 2008).This important role in axon biology of Rho GTPases, is further reinforced by the fact that Rac1 and Cdc42 have been implicated in axon sorting and myelinization (Feltri, Suter et al. 2008) (Figure 16).

Parallelly, Rho and Rac1 also seem to act at the MT level as it has been reported that Rho activates Diaphanous-related formin-1 (mDia1), which can lead to accumulation of detyrosinated MTs, a hallmark of stable MTs, and to the promotion of F-actin nucleation and polymerization (Kühn and Geyer 2014) (Figure 16). Additionally, Rac1 can inactivate the MT destabilizing protein, stathmin, through p65PAK (Etienne-Manneville and Hall 2002, Jaffe and Hall 2005). Furthermore, Collapsing response mediator protein 2 (CRMP-2) , a protein that when active leads to MTs assembly, is inactivated by Rho leading to growth cone collapse (Jaffe and Hall 2005).

The complex roles of Rac1, Cdc42 and Rho are further justified by the important interactions they share (Nimnual, Taylor et al. 2003, Diebold, Fowler et al. 2004, Zenke, Krendel et al. 2004). This crosstalk is not fully understood but, for example, some reports suggest that Rac1 and Cdc42 inhibit indirectly Rho (Alberts, Qin et al. 2005) (Figure 16).

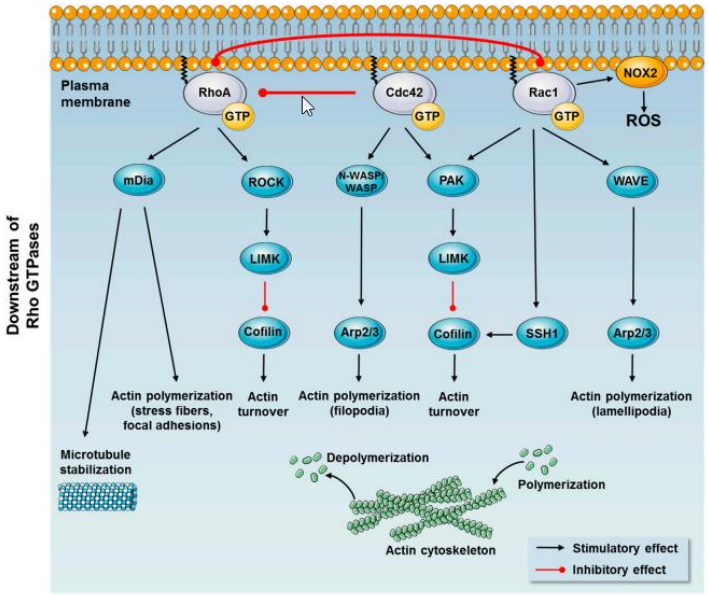


Figure 16. Overview of RhoA, Cdc42 and Rac1 interplay and signalling cascades regarding cytoskeletal components. RhoA leads to activation of mDia1 which alter MTs dynamics and leads to actin polymerization. Cdc42 activates N-WASP and PAK leading to actin polymerization and actin turnover, respectively. Rac1 activates both PAK and SSH1 leading to contrary activities in actin turnover. Rac1 also activates WAVE leading to actin polymerization. Note that, Rac1 can also interact with NOX2 which leads to production of ROS. Adapted from (Møller, Klip et al. 2019).

3.4. Cytoskeleton dysfunction in neurodegenerative diseases

The cytoskeleton is not only the structural backbone of neurons, but as it was clarified, it also presents major functions in the maintenance of neuronal homeostasis. Neurogenerative diseases such as Alzheimer's disease (AD), Parkinson's disease (PD), Amyotrophic lateral sclerosis (ALS), Huntington's disease (HD), Charcot-Marie-Tooth disease (CMT), among others, have been related to neuronal cytoskeletal dysfunction, pinpointing this cell component as a promising therapeutic target (Eira, Silva et al. 2016).

The main cytoskeletal alterations seen in neurodegenerative diseases include: (i) altered microtubule dynamics and axonal transport defects. In AD, HD and CMT decreased level of acetylated α-tubulin have been reported. Additionally, in AD Tau hyperphosphorylation and glycogen synthase kinase-3 β (GSK3β) hyperactivation, a protein with involvement in the neuronal cytoskeleton regulation, mainly, neurodevelopment (Hur and Zhou 2010), have been reported. In PD increased levels of βIII-tubulin and in ALS mutations in superoxide dismutase 1 (SOD1), an enzyme that act as an antioxidant and it decreased activity relates to oxidative stress and cytoskeletal dysfunction (Tu, Raju et al. 1996), were also observed; (ii) MT excessive severing observed in AD associated with increased polyglutamylation and more recruitment of severing enzymes; (iii) axonal transport defects, independent of MTs, such as mutations in molecular motors, in ALS and CMT, increased kinesin phosphorylation by GSKβ3, in AD, mutated huntingtin, in HD and protein aggregation in AD, PD and HD; (iv) actin cytoskeleton dysregulation associated with the formation of cofilin-actin rods, stable structures composed of active cofilin and actin induced by oxidative stress among other factors (Bamburg, Bernstein et al. 2010), in AD and HD, Hirano bodies, structures composed of actin, ABPs and other proteins, deleterious to neuronal homeostasis (Hirano 1994), in AD, cofilin inactivation, in PD, profilin 1 mutation, in ALS and dysregulation in the Rho GTPases families, in PD, CMT, HD and AD (Eira, Silva et al. 2016). Unfortunately, most of these pathologies, except CMT, affect extensively the CNS, being that we shall further dissect what happens in peripheral neuropathies.

CMT is the most prevalent inherited peripheral neuropathy being characterized, like ATTR-PN, by a progressive length dependent nerve loss of function. CMT is highly heterogenous, and several mutations can lead to two main phenotypes: CMT type 1 (CMT1) and CMT type 2 (CMT2). CMT1 is characterized by demyelination, while CMT2 relates to axon loss. Mutations can occur in multiple proteins with functions in

maintenance of myelin and the cytoskeleton, axonal transport, and mitochondrial transport (Pareyson and Marchesi 2009, d'Ydewalle, Benoy et al. 2012). In CMT2 impairment at the level of neurofilaments was observed when a neurofilament light (NEFL) mutation was present, leading to their aggregation and disruption of the network. Another mutation present in mitofusin 2 (MFN2), a protein essential for the maintenance of mitochondrial dynamics such as fusion and fission, leads to severe axonal transport impairment and axonopathy (d'Ydewalle, Benoy et al. 2012). Also, it has been reported that in a mouse model of CMT2 carrying a mutation in heat shock protein family B member 1 (HSPB1), a chaperone that induces correct protein folding under stress conditions, acetylated α-tubulin levels were reduced and defects in axonal transport were observed. Interestingly, HDAC6 inhibition reverted this phenotype (d'Ydewalle, Krishnan et al. 2011). Additionally, in autosomal recessive demyelinating Charcot-Marie-Tooth neuropathy type 4H (CMT4H) mutation in the FGD4 gene were observed. This gene encodes frabin, a GEF specific to Cdc42, which may relate to dysregulation of different levels of the cytoskeleton like actin (Delague, Jacquier et al. 2007, Fabrizi, Taioli et al. 2009). This evidence further reinforces the major role that cytoskeleton dysfunction plays in neurodegeneration, in this case regarding peripheral neuropathies.

On the other hand, acquired peripheral neuropathies may also provide clarity regarding this link between the cytoskeleton and neurodegeneration. Acquired peripheral neuropathies may be caused by physical injury, diabetes, inflammation, chemotherapy, or toxins (Prior, Van Helleputte et al. 2017). One of the most interesting examples is chemotherapy-induced polyneuropathy (CIPN) where the use of certain drugs, namely, platinum compounds, taxanes, vinca alkaloids, thalidomide and proteasome inhibitors leads to a dose-dependent peripheral neuropathy. This is interesting because some of these drugs have a direct impact in the cytoskeleton and their application leads to neurodegeneration. For example, agents that stabilize microtubules, taxanes and others, have been implicated in axonopathy. Application of paclitaxel to DRG neurons inhibited anterograde axonal transport and in mice causes impairment of fast axonal transport. However, the mechanism through which taxanes trigger neurodegeneration remains unclear (Lee and Swain 2006). Another stabilizing agent seems to have a more deleterious effect, iscabepilone, as it has been reported that it heavily disrupts fast axonal transport either retrogradely or anterogradely. Interestingly, vincristine, a vinca alkaloid that destabilizes MTs had a similar effect on axonal MTs in squid axons (LaPointe, Morfini et al. 2013). The other drugs referred do

not have a direct effect on cytoskeleton components but seem to induce neuropathy through general alterations in cell homeostasis, which eventually lead to cytoskeleton defects (Zajączkowska, Kocot-Kępska et al. 2019). The link of taxanes and vinca alkaloids with neurodegeneration induced by alterations in the cytoskeleton, namely, MTs dynamics is reinforced by the fact that coadministration of these drugs with a HDAC6, which deacetylates MTS, inhibitor prevented axonal defects (Krukowski, Ma et al. 2017, Van Helleputte, Kater et al. 2018).

All this evidence strongly suggests that cytoskeleton dysfunction plays a major role in neurodegeneration, preceding it. So, targeting of this cell component would most probably allow for avoidance of neurodegeneration. In ATTR-PN this link is even less established than in previously referred pathologies, supporting the need for this work.

4. Cytoskeleton dysfunction in ATTR-PN: preliminary data

In our group a link between cytoskeleton dysregulation and ATTR-PN has been previously explored. In a work using a *Drosophila melanogaster* model expressing the mutant TTR V30M in the retina, a severe rough-eye phenotype, reduced lifespan and climbing activity were observed (I. Oliveira da Silva, Lopes et al. 2020). Besides this, larvae exhibited impaired axonal projections in photoreceptor axons, presenting an actin dysfunction as the number of normal growth cones, with a spread distribution of filopodia and lamellipodia, from projecting axons, was reduced. Interestingly, the Rho GTPase family was implicated in the inducement of the observed actin dysfunction in TTRV30M expressing flies, as Ras-like GTP-binding protein (Rho1) and Rho kinase (Rok) downregulation enhanced the rough eye phenotype, while the downregulation of Rac1 and Cdc42 reduced the severity of this phenotype. Due to the high homology between flies and vertebrates regarding the neuronal cytoskeleton, this results point to an actin dysfunction mediated by the Rho GTPase family of protein in ATTR-PN (I. Oliveira da Silva, Lopes et al. 2020). Moreover, a physiologic relation between TTR and MTs has also been reported, as the reported TTR function on axonal growth was related with its ability to modulate MT dynamics via regulation of α-tubulin acetylation (Eira, Magalhaes et al. 2021). This means that TTR modulates the MT cytoskeleton in its physiological form, being that a loss of function of the amyloidogenic protein could occur in ATTR-PN. Additionally, preliminary data to this thesis, further implicated cytoskeleton dysfunction in ATTR-PN.

4.1. Rac1 mediates actin dysfunction and neurodegeneration in ATTR-PN

Based on the results obtained with *D. melanogaster* ATTR-PN model, actin cytoskeleton alterations and the respective role of Rho GTPases were investigated in a mouse model of the disease. The mouse model used carries mutant human TTR A97S ($hTTR^{A97S}$). As controls, mice carrying the WT human TTR ($hTTR^{WT}$) were used. Results obtained showed an alteration of the actin organization on the growth cone from $hTTR^{A97S}$ DRG neurons, as determined by a decreased percentage of neurons with spread growth cones, growth cones containing regular organization of lamellipodia and filopodia. Moreover, Rac1 mediated the actin dysfunction, as its activity was increased in $hTTR^{A97S}$ DRG neurons, and its inhibition rescued the actin phenotype (unpublished data, Figure 17). Furthermore, neurodegeneration of $hTTR^{A97S}$ DRG neurons was observed after the timepoint of actin dysfunction, and it was equally reverted by the inhibition of Rac1, suggesting that the cytoskeletal defect observed

preceded neurodegeneration (unpublished data, Figure 17). These results were further reinforced by a pull-down assay using sciatic nerves from both 9-months old $hTTR^{WT}$ and $hTTR^{A97S}$ mice, an age where neurodegeneration was not observed (Kan, Chiang et al. 2018), which revealed that Rac1 activity is increased in $hTTR^{A97S}$ mice. To summarize, this data pinpoints an actin dysfunction in a mouse model of ATTR-PN mediated by Rac1 preceding and leading to neurodegeneration, prompting further exploration of this cytoskeletal defect.

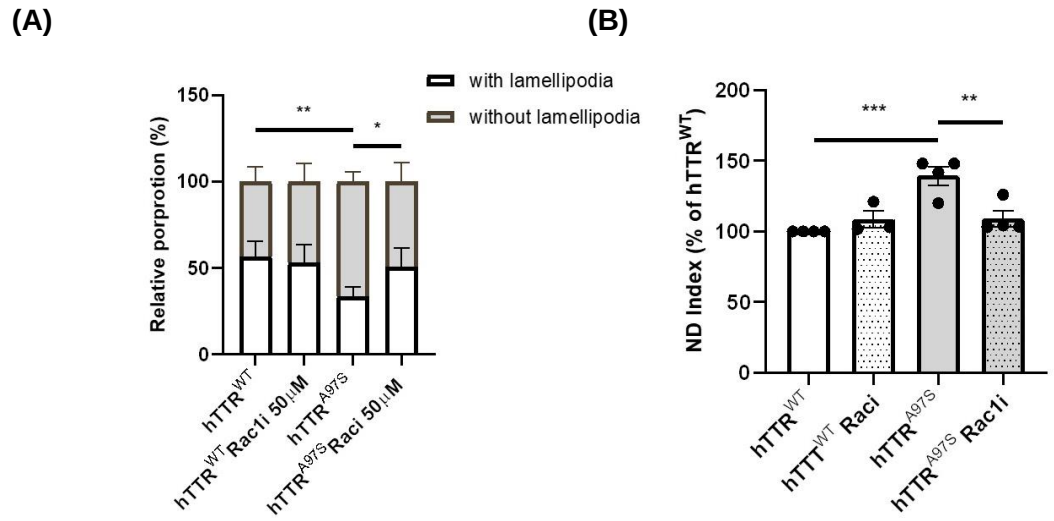


Figure 17. Impact of Rac1 on growth cone morphology and neurodegeneration (ND) index in $hTTR^{A97S}$ DRG neurons. (A) Quantification of growth cone with and without lamellipodia. n=3 independent experiments performed with technical duplicates. (B) Quantification of the neurodegeneration (ND) index. n=4 independent experiments. (A) and (B) data presented as mean ± SEM. *p<0.05 **p<0.01 ***p<0.001.

4.2. Axonal transport defects in an ATTR-PN mouse model

Previous data did not only support the involvement of actin dysfunction in ATTR-PN, but also of axonal transport, a process which is highly dependent on MTs, being that impaired axonal transport in neurons has been related to neurodegeneration and multiple neurodegenerative disorders (Jellinger 2010, Eira, Silva et al. 2016). Results obtained revealed an impairment in mitochondrial axonal transport in DRG peripheral roots of 9-months old $hTTR^{A97S}$ mice when compared with $hTTR^{WT}$ control mice (unpublished data, Figure 18). Alterations at the level of mitochondrial axonal transport do not mean direct alterations in MTs, demanding further dissection of this data.

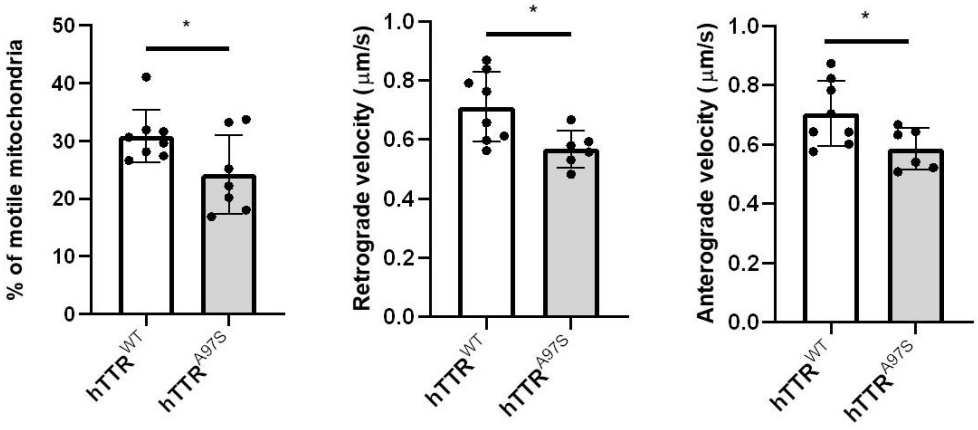


Figure 18. Axonal transport of mitochondria in impaired in DRG peripheral root of 9-months old hTTR^{A97S} mice. Quantification of % of motile mitochondria, retrograde velocity, and anterograde velocity in hTTR^{A97S} and hTTR^{WT} DRG peripheral root explants of 9-months old mice. n=7-8 animals/conditions. Data presented as mean ± SEM. *p<0.05.

Overall, the previous data from our group suggested a generalized dysfunction of the neuronal cytoskeleton in peripheral neurons preceding neurodegeneration in an ATTR-PN mouse model, which we aimed to further dissect in this master thesis.

Objectives

The following work aimed at further characterizing neuronal cytoskeleton alterations in an ATTR-PN mouse model ($hTTR^{A97S}$).

The following objectives were delineated at the actin cytoskeleton level:

i) To evaluate actin dysfunction of $hTTR^{A97S}$ DRG neurons axons via live imaging of actin trails and the respective involvement of Rac1.
ii) To clarify the Rac1 regulated molecular mechanism of actin dysfunction in $hTTR^{A97S}$ DRG neurons.

The following objective were delineated at the microtubule cytoskeleton level:

i) To further evaluate axonal transport alterations, and the involvement of MT defects, in DRG peripheral roots from $hTTR^{A97S}$ mice.
ii) To validate axonal transport and MT alterations in the sural nerve (a pure sensory nerve which is mainly affected in ATTR-PN) of $hTTR^{A97S}$ mice.

Methods

1. Animals

Mice were handled according to European Union and National laws. $hTTR^{WT}$ mice (controls) and $hTTR^{A97S}$ mice on the C57BL/6 background were kindly provided by Doctor S.-T. Hsieh. Knock-in mice were generated by replacing the gene for mouse TTR (moTTR) with the gene of human TTR (hTTR), either WT ($hTTR^{WT}$ mice) or with the mutation A97S ($hTTR^{A97S}$ mice), without altering the promotor and enhancer sequences. Both homozygous, $hTTR^{WT}/hTTR^{WT}$ and $hTTR^{A97S}/hTTR^{A97S}$, and heterozygous, $hTTR^{WT}$/moTTR and $hTTR^{A97S}$/moTTR, animals were generated and used conversely. For mitochondria and MT live imaging, hTTR mice were crossed with to Thy1-MitoCFP mice (Misgeld, Kerschensteiner et al. 2007) and Th1-EB3-YFP mice (Kleele, Marinković et al. 2014), generating hTTR.Thy1-MitoCFP and hTTR.Thy1-EB3-YFP, respectively. All animals were maintained under a 12-hour light/dark cycle and fed with hard pellets and distilled water, *ad libitum*.

2. DRG neuronal cultures and transfection

Animals between 4-12 weeks were humanely euthanized in a CO_2 chamber. After removal and opening of the vertebral column all dorsal root ganglia (DRG) were collected in DMEM:F12 (Dulbecco's Modified Eagle Medium: Nutrient Mixture F-12, Pan-Biotech GmbH, Germany) supplemented with 1% P/S (penicillin/streptomycin, Thermo Fisher Scientific, EUA) and preserved on ice. Collagenase type IV-S (Sigma-Aldrich, EUA) was added at a final concentration of 0,125% and DRG were incubated for 1 hour and 30 minutes in a cell incubator (37ºC and 5% CO_2). After digestion and enzyme wash DMEM: F12 supplemented with 1%P/S+10% FBS (fetal bovine serum, Sigma-Aldrich, EUA) was added to DRG and they were mechanically dissociated by passing through glass pipettes achieving a cell suspension. This suspension was then pipetted carefully on top of a 15% BSA (bovine serum albumin, Sigma-Aldrich, EUA) in DMEM:F12 solution. The resulting phase gradients were centrifuged at 200g for 10 minutes. Interphase and all supernatant were discarded and the pellet (containing DRG) was resuspended in 1mL of complete DRG growth medium: DMEM:F12 supplemented with 1%P/S, 50ng/mL NGF (nerve growth factor, Merck Millipore, EUA), B27 (Thermo Fisher Scientific, EUA) and 2mM L-Glu (L-glutamine, Thermo Fisher Scientific, EUA). DRG neurons were counted and platted at desired densities in multi-well plates (with or without glass coverslips) or in glass bottom µ-dishes, all properly

coated with 20µg/mL PLL (poly-L-lysine, Sigma-Aldrich, EUA) and 5µg/mL laminin (Sigma-Aldrich, EUA).

When neuronal transfection was required, cells from 2 animals were pooled, as minimum of 200000 total cells per condition for transfection was required. A 4D Nucleofector Amaxa system (Lonza, Barcelona, Spain), CM#137 program (appropriated for primary mouse DRG) was used to ensure nucleofection of DRG neurons with the desired plasmids. Transfected cells were resuspended in complete DRG growth medium and plated at desired density.

3. Plasmid production: pIRESneo3+GFP-UTR_CH and EGFP-actin+pEGFP-C1

All plasmid production was done using NZYStar Competent cells and the NZYMaxiPrep (NZYTech, Portugal). After thawing the bacteria, 50-100ng of plasmid was added to 100µL of cells and incubated in ice for 15 minutes. After this incubation the tube was heat-pulsed in a water bath at 45ºC for 45 seconds. Cells were again incubated in ice for 2 minutes. At this point transformation has occurred with the desired plasmid. To the volume of cells 900µL of LB (Luria Broth, NZYTech, Portugal) was added and incubated at 37ºC for 1 hour with shaking (225-250rpm). This tube was centrifuged at 4000rpm for 5 minutes and 850µL were discarded. The remaining content was then platted in a Petri dish containing agar (NZYTech, Portugal) mixed with LB plus the resistance antibiotic of the given plasmid and incubated at 37ºC O/N (overnight). One colony was then isolated and added to 100mL of LB supplemented with resistance antibiotic and left to grow at 37ºC overnight (O/N) with continuous shaking (190rpm). Grown bacteria where then used in the NZYMaxiPrep kit and the provided protocol was followed.

4. Actin trails: transfection and cell culture conditions

DRG neurons were transfected has previously described with 0,5µg of pIRESneo3+GFP-UTR_CH which expresses the calponin homology (CH) domain of utrophin (UTR) which binds specifically to F-actin (Figure 19). pIRESneo3+GFP-UTR_CH was kindly provided by Dr Jorge Ferreira, i3S. Cells were then platted in glass bottom µ-dishes (35mm) at a density of 20000 cells/dish. After 24 hours, medium was changed to fully supplemented (1%P/S, 50ng/mL NGF, B27 and 2mM L-Glu) DMEM:F12 without phenol red (Sigma-Aldrich, EUA). For experiments using Rac1 inhibitor NSC23766 (Sigma-Aldrich, EUA) was added at DIV1 at a final concentration of 50µM. All live imaging was performed at DIV2.

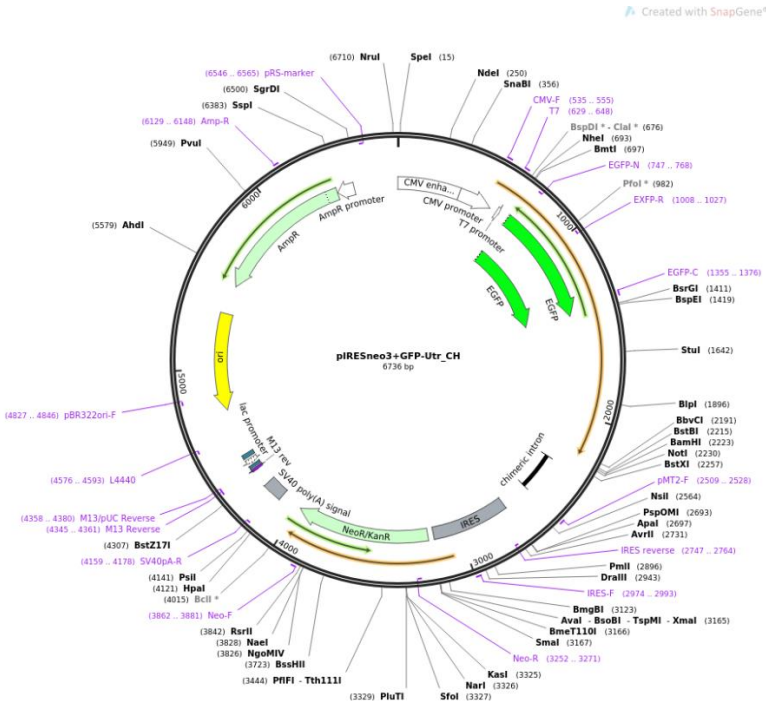


Figure 19. pIRESneo3+GFP-Utr_CH plasmid construct used.

5. Human TTR Enzyme-linked immunosorbent assay (ELISA)

Medium of DIV2 DRG neurons was collected and centrifuged at top speed at 4ºC for 10 minutes to remove cell debris. Supernatant was recovered and concentrated to a volume of about 100µL using a Vivaspin 500 centrifugal concentrators (Sartorius, Germany) with a cut-off of 3kDa. This medium was then used for ELISA using the commercially available Human PreAlbumin ELISA Kit (Transthyretin) (ab108895) (Abcam, UK). This kit uses the method of indirect sandwich ELISA: after transthyretin is bound to the antibody coating the wells (capture antibody), another antibody (detection antibody) that recognizes the protein is added. The conjugated antibody with peroxidase recognizes this last antibody binding strongly to it. By adding a substrate that when degraded by peroxidase generates colour, absorbance can be correlated to concentration of transthyretin. This method ensures a better sensitivity and specificity than direct ELISA. The provided protocol was followed.

6. Immunocytochemistry (ICC)

6.1. Growth cone morphology experiments

DRG neurons were obtained has previously described. Cells were platted at a density of 5000cells/well in a 24well-plate containing properly coated glass coverslips (20µg/mL PLL and 5µg/mL laminin). All drugs were added after platting. Rac1 inhibitor

NSC23766 was added at a concentration of 50µM and RAGE antagonist FPS-ZM1 (Sigma-Aldrich, EUA) was added at a concentration of 10µM.

For the ICC: cells were washed once with PBS (phosphate-buffered saline) and fixed with a cytoskeleton preservation fixative [4% PFA (paraformaldehyde, Sigma-Aldrich), 4% sucrose (VWR), 0,25% Glutaraldehyde (Polysciences), 0,1% Triton X-100 (Sigma-Aldrich), 300mM PIPES (piperazine-N,N′-bis(2-ethanesulfonic acid), VWR)] for 30 minutes at room temperature (RT). After washing with PBS cell were permeabilized with 0,5% Triton X-100 (Sigma-Aldrich, EUA) in PBS for 10 minutes at RT. Washing with PBS was repeated and autofluorescence was quenched using NH_4Cl 200mM (Merck Millipore, EUA) for 5 minutes at RT. Washing was repeated and coverslips were transferred to a humid chamber and blocking was performed with 2% BSA plus 0,2% fish gelatine (Sigma-Aldrich, EUA) in PBS for 1 hour at RT. Primary antibody was added in diluted blocking buffer and incubated at 4ºC O/N. Coverslips were washed 3x with PBS and secondary antibodies and rhodamine-phalloidin (Thermo Fisher Scientific, EUA) were added in diluted blocking buffer. Coverslips were mounted using Fluromount (Southern Biotech, USA) (Table 1).

6.2. Phospho-cofilin

DRG neurons were platted at a density of 5000cells/well in a 24well-plate. Cells were fixed with 4% PFA in cytoskeleton preservation buffer [10mM MES pH6,1 (2-(N-morpholino) ethanesulfonic acid, Sigma-Aldrich, EUA), 138mM KCl (Merck Millipore, EUA), 3mM $MgCl_2$ (Merck Millipore, EUA), 10mM EGTA (ethylene glycol-bis(β-aminoethyl ether)-N,N,N′,N′-tetraacetic acid, Sigma-Aldrich, EUA), and 0,32M sucrose (Merck Millipore, EUA)] for 20 minutes. Cells were permeabilized using ice cold methanol for 3 minutes at RT. After washing with tris-buffered saline (TBS). Coverslips were transferred to a humid chamber and were blocked using 2,5% normal donkey serum (NDS, Sigma-Aldrich, EUA) in 1% BSA in TBS for 1 hour at RT. Coverslips were then incubated with primary antibodies: anti-phospho-cofilin and anti-β3-tubulin, at 4ºC O/N in 1% BSA in TBS. Subsequently, coverslips were washed and incubated with secondary antibodies in 1% BSA in TBS for 1 hour at RT (Table 1). Cells were then incubated with DAPI (4′,6-diamidino-2-phenylindole, Bio-Rad, EUA) for 10 minutes at RT and finally mounted using Fluromount.

7. Immunoblotting

Either tissues or cells were lysed using RIPA buffer [1% Triton X-100, 0,1% SDS (NZYTech, Portugal), 140mM NaCl (Thermo Fisher Scientific, EUA), PI (Thermo Fisher

Scientific, EUA), 1mM orthovanadate (Sigma-Aldrich, EUA) in TE ph8]. Protein extracts were sonicated (2 × 10 cycles, output power 50 Watts, Branson sonifier 250). Extracts were centrifuged at 15000g at 4ºC for 10 minutes to remove debris. Protein was quantified using DC Protein Assay (Bio-Rad, EUA) and samples were prepared with SDS sample buffer. For tissues 1,25µg of protein were run while for cells 12,5µg of protein were run. All samples were run in 12% acrylamide SDS-gels and then transferred via wet system to a nitrocellulose membrane 0,45µm (Amersham Biosciences, UK). To ensure protein transfer membranes were incubated with 0,1% Ponceau S (Sigma-Aldrich, EUA) in 5% glacial acetic acid (Merck Millipore, EUA) in water for 10 minutes. Membranes were blocked for 1 hour at RT in 5% skim milk (Sigma-Aldrich, EUA) in TBS-T [TBS with 0,1% Tween 20 (Sigma-Aldrich, EUA)]. Membranes were then incubated at 4ºC O/N with respective primary antibodies. After primary antibody incubation membranes were washed 3 times for 10 minutes using TBS-T and secondary antibodies were added in 5% skim milk in TBS-T for 1 hour at RT (Table 1). Blots were then imaged in a Chemidoc™ system (Bio-Rad, EUA) system following incubation of the membrane with Immobilon Crescendo Western HRP substrate (Merck Millipore, EUA) or Pierce™ ECL Western Blotting Substrate (Thermo Fisher Scientific, EUA).

8. Acetylated α-tubulin immunohistochemistry (IHC)

DRG peripheral roots were collected from perfused animals and PFA fixed. Tissues were embedded in OCT (optimal cutting temperature compound, Thermo Fisher Scientific, EUA) and then cut at 10µm thickness in a cryostat. Before starting the protocol, slides were thawed for 1 hour at RT. After washing with PBS, allowing full removal of OCT and hydration of tissues, tissues were permeabilized using 0,5% Triton X-100 in PBS for 30 minutes at RT. After washing in PBS, autofluorescence was quenched with 200Mm NH_4Cl in PBS for 30 minutes at RT. Slides were then transferred to a humid chamber and using a PAP-pen (Delta Microscopies, France) area probed was limited to each cut. Blocking was performed using 5% NDS in PBS for 1 hour at RT. Tissues were incubated with respective primary antibodies in blocking buffer at 4ºC O/N. After washing tissues were incubated with secondary antibodies in blocking buffer for 1 hour at RT (Table 1). After washing with PBS tissues were incubated with DAPI for 10 minutes at RT. Sections were mounted using Ibidi Mounting Medium (Ibidi, Germany).

Table 1. Antibodies and probe-conjugated dyes used all throughout this work. Host, dilution, application, and source of each antibody/probe-conjugated dyes.

Antibody	Host	Dilution and application	Source
Primary			
βIII-tubulin	Mo	1:2000, ICC 1:500, IHC 1:2000, WB	Promega
βIII-tubulin	Rb	1:1000, ICC 1:500, IHC	Synaptic Systems
βIII-tubulin	Rb	1:10000, WB	BioLegend
Total cofilin	Rb	1:10000 WB	Cell Signalling
Phospho-cofilin	Rb	1:500, ICC 1:1000, WB	
Acetylated α-tubulin	Mo	1:500, IHC 1:40000, WB	Sigma-Aldrich
GT335	Mo	1:10000, WB	
PolyE	Rb	1:2000, WB	AdipoGen
Detyr	Rb	1:5000, WB	Milipore
Δ2-tubulin	Rb	1:2000, WB	Milipore
α-tubulin	Mo	1:400, WB	DSHB
ERK	Rb	1:3000, WB	Cell Signalling
hTTR	Rb	1:1000, ICC	Dako
Secondary			
488 anti-mouse	D	1:1000, ICC	Life Technologies
568 anti-rabbit	D	1:1000, ICC	Life Technologies
488 anti-rabbit	D	1:500, IHC	Life Technologies
568 anti-mouse	D	1:500, IHC	Life Technologies
HRP mouse	Go	1:10000, WB	Santa-Cruz
HRP rabbit	Go	1:10000, WB	Santa-Cruz
HRP mouse light chain	Go	1:5000, WB	Santa-Cruz

Conjugated dyes	Dilution and application	Source
Rhodamine-conjugated phalloidin	1:50, ICC	Life Technologies

9. Imaging and data analysis

For all image analysis Fiji software was used.

9.1. Actin trails live imaging

Videos with 2 minutes and 300ms interval between each frame were captured of well distinguishable neurites. Neurons were identified by general morphology. The following settings in a Nikon Eclipse Ti (Nikon, Japan) inverted epifluorescence microscope equipped with an IRIS 9 camera (Teledyne Photometrics, USA) were used: PL APO LAMBDA 60x/1,4 Oil DIC WD 0,13mm objective, 12% LED power and ND4 filter.

To analyse the videos a line with a certain width (remained constant throughout the analysis) was drawn in each neurite after using the function of subtracting background provided by Fiji. Using the plug-in *KymoResliceWide*, a kymograph considering the maximum intensity values of each pixel was generated. A kymograph is a plot of distance through time allowing for the identification of static or moving structures. Actin trails appear in these kymographs as faint fluorescent lines, also referred to as “fluorescent plumes” (Ganguly, Tang et al. 2015) (Figure 20). By simply determining the coordinates of the initial and final point of such phenomena we could determine the rate and the length as well as the number of times it occurs in a specific period.

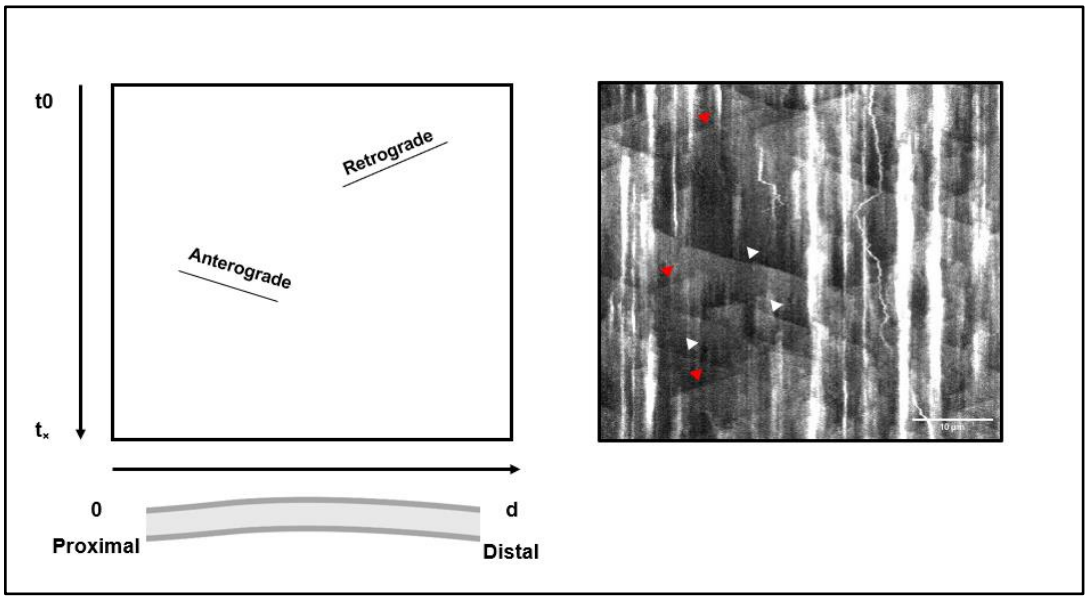


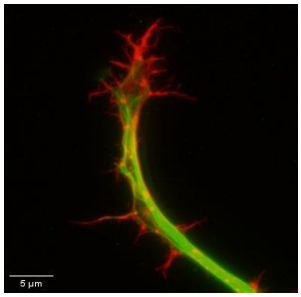
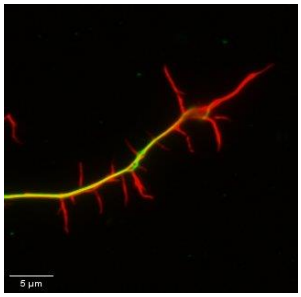
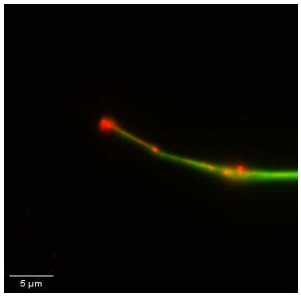
Figure 20. Overview of a kymograph. In the left, a simplified view of a kymograph and in the right, a real kymograph from one neurite from on experience. Red arrows and white arrows denote retrograde and anterograde actin trails, respectively.

9.2. Growth cone morphology

DRG neurons were imaged using an upright epifluorescence microscope (Zeiss Axio Imager Z1, Carl Zeiss) using a 63x magnification (Plan-Apochromat 63x/1.40 Oil DIC) objective. β3-tubulin staining allowed for identification of neurons as this isoform of tubulin is only present in neuronal cells and F-actin staining allowed for evaluation of the actin cytoskeleton. Images of the distal portion containing the growth cone of neurites were captured randomly. About 30 images of each technical replicate were captured giving a total of about 60 images captured per condition.

Analysis of this data set was done qualitatively: growth cones with lamellipodia and filopodia were considered normal/spread and growth cones with lack or total absence of lamellipodia and filopodia were considered abnormal (Table 2). Abnormal GCs are associated with actin dysfunction, being a well stablished read-out of such phenomenon.

Table 2. Overview of growth cone classification. β3-tubulin staining in green and F-actin staining in red. Scales bar in the lower left corner.

Type of growth cone	Representative image	Notes
Spread/Normal growth cone		Abundant lamellipodia and filopodia
Abnormal growth cone		Lack of lamellipodia
Abnormal growth cone		Complete lack of lamellipodia and filopodia

9.3. Phospho-cofilin ICC

DRG neurons were imaged using an upright epifluorescence microscope (Zeiss Axio Imager Z1, Carl Zeiss) using a 40x magnification objective (EC-Plan-Neofluar 40x/1.30 Oil Ph3). Images of well identifiable neurites prioritizing a medial zone were captured. About 15 images of each technical replicate were taken giving rise to a total of about 30 images per condition. To analyse these images a line of certain width was drawn in each neurite and mean grey value (MGV) was measured in the green channel (β3-tubulin staining) and in the red channel (phospho-cofilin staining). A value of MGV from the background was subtracted by drawing the same line in an area without any

staining. Values of MGV for the interest proteins were normalized using the MGV of B3 tubulin staining.

9.4. Mitochondrial transport in DRG peripheral root from 6-months old mice

Videos acquired, via the live imaging of DRG peripheral root explants from 6-months old animals stained with Mito Tracker, were quantified using the plug-in MTrackJ. Trajectories of moving mitochondria were recorded as well as their direction of movement. Stationary mitochondria were counted in the end of the video. Velocities and number of mitochondria were recorded allowing for anterograde and retrograde velocity determination and percentage (%) of motile mitochondria.

9.5. Acetylated α-tubulin immunohistochemistry

DRG peripheral roots were imaged using a fluorescence confocal microscope SP5 Leica (Leica, Germany) and a 40x objective (HC PL APO CS 40x /1.10 CORR Water) without any digital zoom. A medial zone of each sections trying to capture the entire width of the DRG peripheral root was captured. Enough Z-stacks were obtained to ensure complete imaging of stained tissue (Z-step remained constant all throughout the imaging).

To analyse this data set all images were collapsed using the option “Sum” of Fiji, which sums the fluorescence intensity of all pixels from all planes. After this, a region of interest (ROI) was established in only β3-tubulin^{+}/acetylated α-tubulin^{+} axons. The maximum number possible of axons were analysed avoiding the quantification of the same axon. MGVs regarding acetylated-α-tubulin staining were normalized with the MGVs regarding β3-tubulin staining. To all values a MGV of the background was subtracted by drawing a ROI in an area without staining proximal to each axon.

10. Statistics

Results are presented as mean ± standard error of the mean (SEM). Data comparison between groups was performed using One-Way ANOVA or Two-Way ANOVA, followed by Tukey’s multiple comparison test, or Student’s t-test. All statistical analyses were performed using GraphPad Prism 6 software: *$p<0.05$; **$p<0.01$; ***$p<0.001$; ****$p<0.0001$.

Results

1. Impact of amyloidogenic TTR on the actin cytoskeleton

1.1. DRG neurons from an ATTR-PN mouse model present axonal actin alterations

Supported by the preliminary data of this thesis and to further dissect the impact of actin dysfunction in ATTR-PN we assessed whether, besides a disruption of actin organization, $hTTR^{A97S}$ DRG neurons presented axonal actin alterations. As it was previously stated, the growth cone is a structure that *in vivo* is only present throughout nervous system development or in a situation of axonal injury in the PNS. Given the fact that in ATTR-PN there is axonal degeneration of mature neurons, we explored whether actin dysfunction was observed in DRG neurite shafts, an analogous structure to the axon, being that DRG neurons *in vivo* do not differentiate into pseudo unipolar neurons but emit multiple processes. We focused on actin trails, fast linear events of polymerization that occur all throughout the axon and seemingly contribute for the transport of presynaptic vesicles (Roy 2016, Chenouard, Xuan et al. 2020).

To search for actin trails we used live imaging of DRG neurons transfected with a reporter expressing GFP fused the calponin homology domain of utrophin (GFP-UTR_CH) which binds specifically to F-actin and does not affect its dynamics considerably (Burkel, Von Dassow et al. 2007).

The nature of the observed actin trails in control DRG neurons, derived from $hTTR^{WT}$ mice, had common parameters with the ones previously observed in hippocampal neurons (Ganguly, Tang et al. 2015) such as rate of polymerization, although the length of the trails was reduced (Table 3).

Table 3. Mean length and mean rate of polymerization of all the registered actin trails in control DRG neurons ($hTTR^{WT}$). Values are presented as mean ± SEM. Data from hippocampal neurons comes from (Ganguly, Tang et al. 2015).

	DRG neurons		Hippocampal neurons	
Direction	**Retrograde**	**Anterograde**	**Retrograde**	**Anterograde**
Mean length/μm	5.889±0.4283	6.088±0.3203	8.87 ± 0.22	8.85 ± 0.18
Rate of polymerization/$\mu m.s^{-1}$	1.146±0.05337	1.070±0.05937	0.99 ± 0.01	0.99 ± 0.01

To further confirm actin trails presence in DRG neurons we used the drug latrunculin which promotes depolymerization of F-actin and was previously show to reduce the frequency of actin trails in hippocampal neurons (Ganguly, Tang et al. 2015). Similarly, we observed a reduction in the number of actin trails in latrunculin-treated DRG neurons (Figure 21). These observations support the presence of actin trails in DRG neurons.

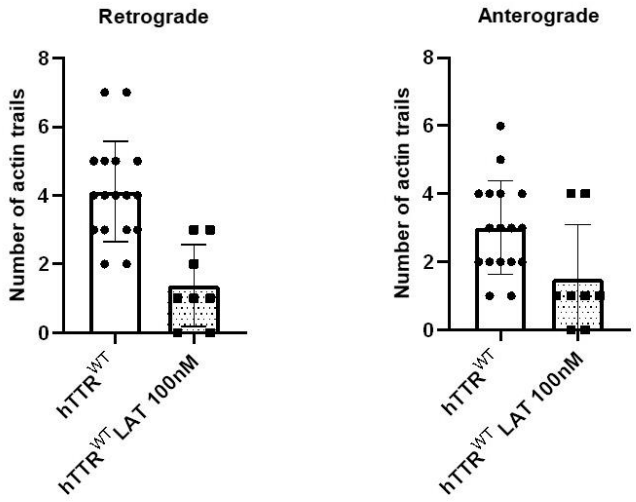


Figure 21. Latrunculin causes a reduction in the number of actin trails in DRG neurons. Quantification of number of actin trails in in hTTR^{WT} DRG neurons untreated (hTTR^{WT}) or treated with latruculin (hTTR^{WT} LAT 100 nM) both retrogradely and anterogradely. Data presented as mean ± SEM. n=8-17 neurites/condition, representative experiment.

We followed by analysing the differences in the dynamics of actin trails between hTTR^{WT} and hTTR^{A97S} DRG neurites. While we did not find any difference regarding length or rate of polymerization comparing the two genotypes (Figure 22), we observed a reduction in the number of actin trails running both retrogradely and anterogradely in hTTR^{A97S} DRG neurites, supporting an actin dysfunction in the axon shaft (Figure 22). This way, the actin dysfunction is generalized, as it is observed both at the level of growth cones and neurites/axons.

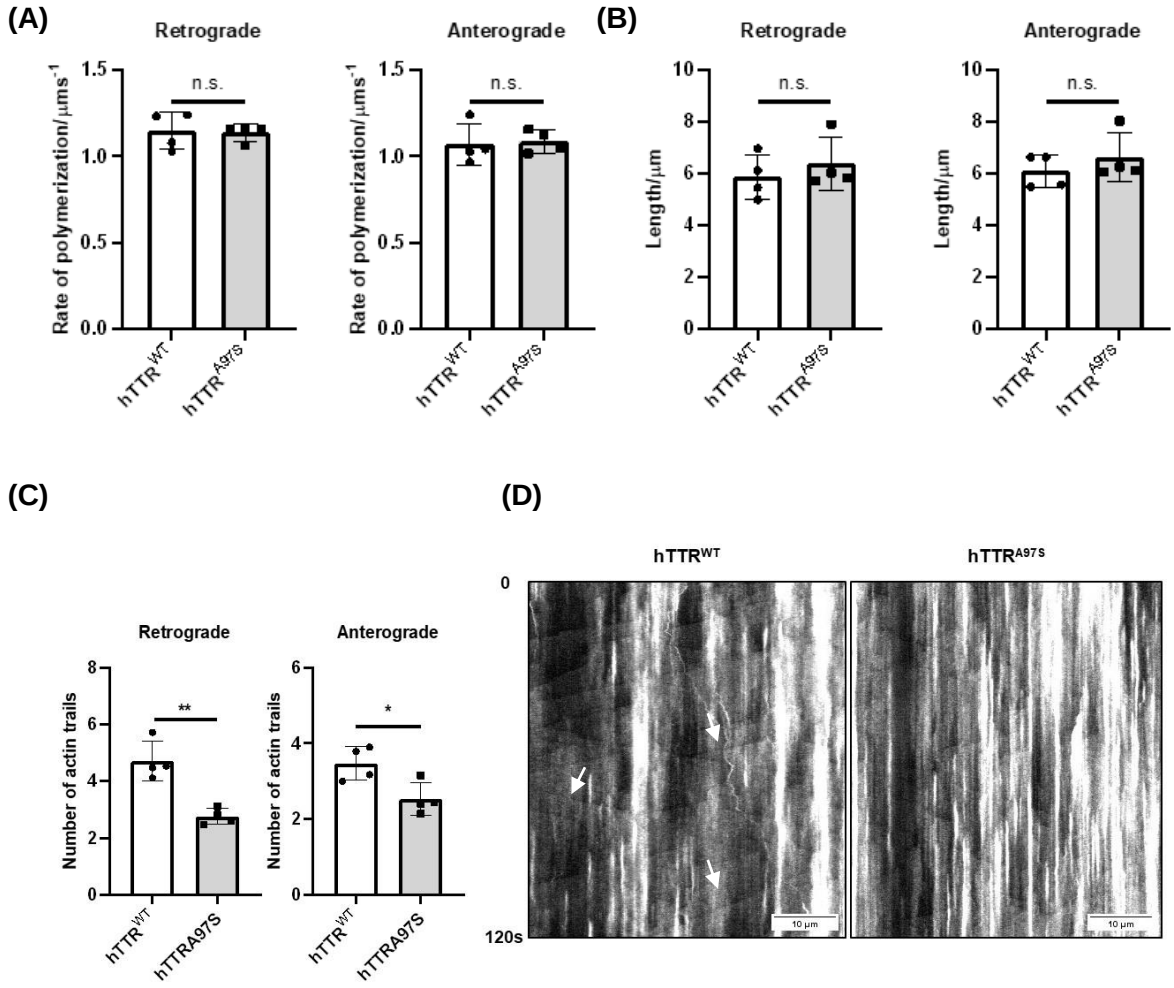


Figure 22. hTTR^{A97S} DRG neurites presented reduced number of actin trails. (A-C) Quantification of rate of polymerization (A), length (B) and number of actin trials (C) in, hTTR^{WT} and hTTR^{A97S} DGR neurons, retrograde and anterograde directions. Data presented as mean ± SEM. n= 4 independent experiments, a total of 67-68 neurites shafts/genotype. Statistical significance was determined by Student's t-test: *p<0.05 **p<0.01. (D) Representative kymographs of analysed neurites from hTTR^{WT} and hTTR^{A97S} DRG neurons. Note the abundance of "faints lines", marked with white arrows, representing actin tails in hTTR^{WT} kymograph when compared with hTTR^{A97S} kymograph.

1.2. Axonal actin alterations are mediated by Rac1 in hTTR^{A97S} DRG neurons

To evaluate if the reduction of actin trails was compatible with previous results in growth cone morphology analysis, i.e. mediated by Rac1, we used the inhibitor NSC23766, which hinders specifically the interaction between Rac1 and GEFs not interacting with Cdc42 or RhoA (Gao, Dickerson et al. 2004). Interestingly, Rac1 inhibition recovered the observed phenotype of reduction of actin trails running retrogradely in hTTR^{A97S} DRG neurons. Anterogradely only a strong tendency of

recovery was observed. Rac1 inhibition did not affect the number of events in hTTR^{WT} control DRG neurons (Figure 23).

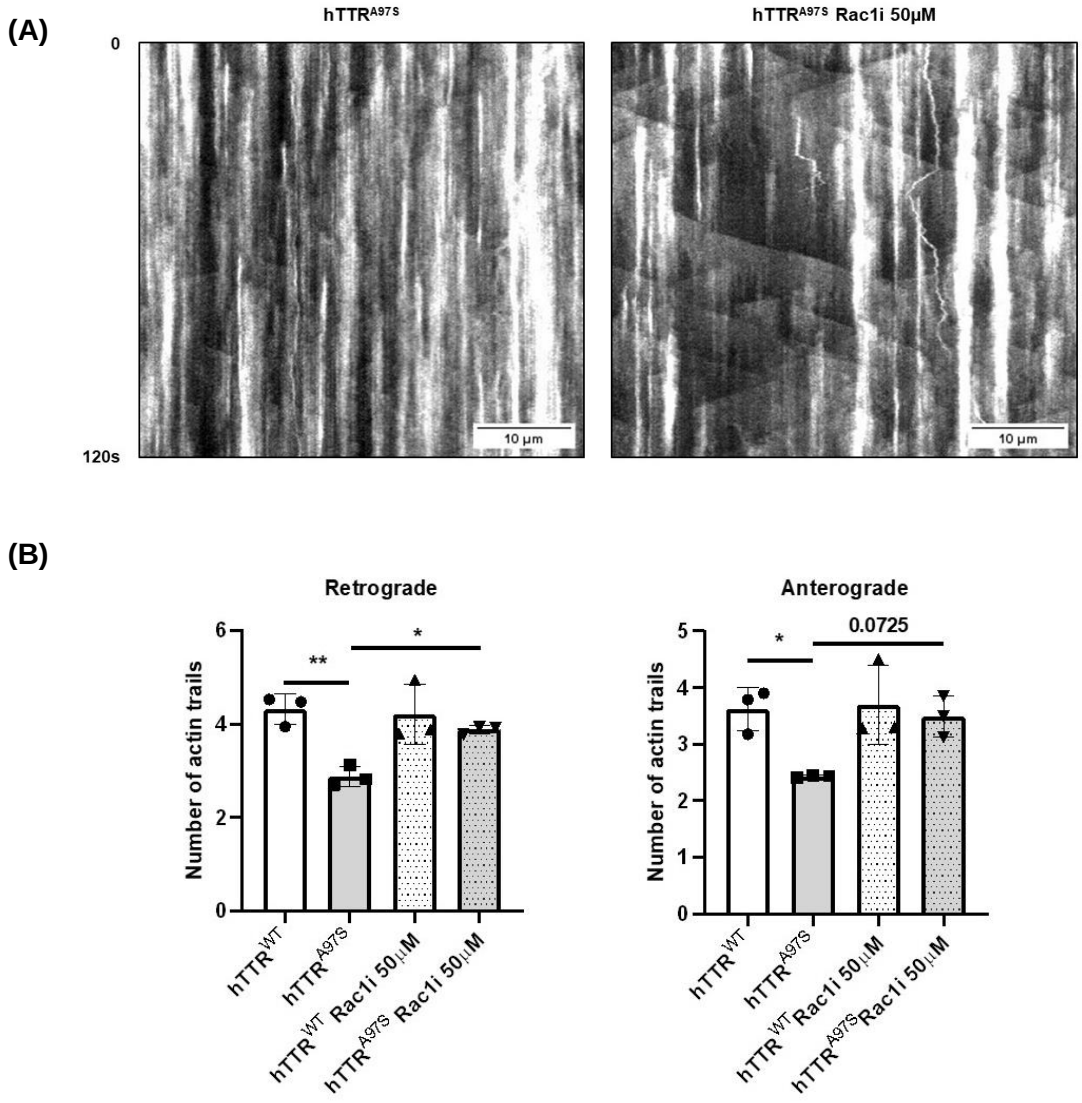


Figure 23. Rac1 mediates axonal actin dysfunction in hTTR^{A97S} DRG neurons. (A) Representative kymographs of probed neurites in hTTR^{A97S} versus Rac1 inhibitor treated-hTTR^{A97S} neurons (hTTR^{A97S} Rac1i 50 uM). (B) Quantification of the number of actin trails observed in Raci inhibitor treated- and untreated- hTTR^{WT} and hTTR^{A97S} DRG neurons. Data presented as mean ± SEM. n=3 independent experiments, a total of 50-56 neurites/condition. Statistical significance determined by one-way ANOVA: n.s. p>0.05 *p<0.05 **p<0.01.

These results suggest that actin dysfunction observed in neurites of hTTR^{A97S} DRG neurons is mediated by Rac1 (Figure 23). Coupled with the previous data obtained regarding growth cone morphology and neurodegeneration, these results reinforce the important role that Rac1 overactivation plays in cytoskeletal dysregulation in hTTR^{A97S} DRG neurons.

1.3. Dissecting the molecular mechanism underlying TTR-induced actin dysfunction

1.3.1. A RAGE-Rac1 pathway mediates TTR-induced actin cytoskeleton alterations

RAGE is broadly implicated in neurodegeneration (Ramasamy, Vannucci et al. 2005) and it has been reported that its activation leads to activation of Rac1 (Hudson, Kalea et al. 2008). As described in the introduction section, in ATTR-PN, RAGE was shown to act as a receptor for amyloidogenic TTR mediating its neurotoxicity (Sousa, Yan et al. 2000).

To evaluate whether RAGE was implicated in the mechanism of TTR-induced Rac1 activation and subsequent actin dysfunction, we evaluated the effect of a RAGE antagonist, FPS-ZM1 (Deane, Singh et al. 2012), on the disruption of actin organization on the growth cone of $hTTR^{A97S}$ DRG neurons. We observed that the decreased in the percentage of spread growth cones in $hTTR^{A97S}$ neurons, when compared to $hTTR^{WT}$ DRG neurons, was rescued by the RAGE antagonist, implicating the receptor in the mechanism of TTR-induced actin dysfunction. To access whether RAGE and Rac1 were linked in this molecular mechanism we combined the addition of the RAGE inhibitor with the one of Rac1 inhibitor in our experiments. Initially, we confirmed previous data demonstrating by showing that the Rac1 inhibition reverts growth cone defects of $hTTR^{A97S}$ DRG neurons. Interestingly, treatment with both the RAGE inhibitor and the Rac1 inhibitor presented a similar effect to the on seen when the compounds were added separately. These results suggest that RAGE and Rac1 are linked in the TTR-induced molecular pathway which results on disruption of the actin cytoskeleton (Figure 24).

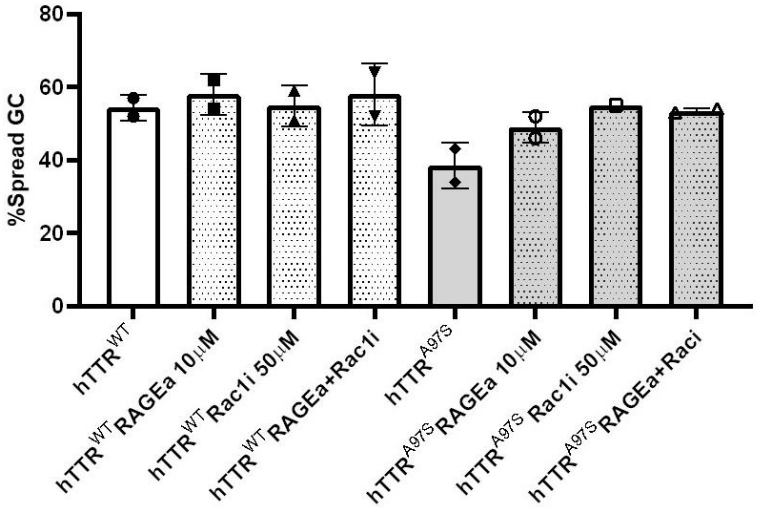


Figure 24. A RAGE-Rac1 pathway mediates actin dysfuntion in the growth cone of hTTR^{A97S} DRG neurons. Quantification of the percentage of spread growth cones in hTTR^{WT} or hTTR^{A97S} DRG neurons untreated (hTTR^{WT} and hTTR^{A97S}) or treated with Rac1 inhibitor (hTTR^{WT} and hTTR^{A97S} Raci50uM) RAGE antagonist (hTTR^{WT} and hTTR^{A97S} RAGEa 10uM) or both (hTTR^{WT}/hTTR^{A97S} Raci+RAGEa). Data presented as mean ± SEM. Representative experiment with technical duplicates.

1.3.2. Dissecting Rac1 downstream effectors on TTR-induced actin defects

To further dissect which signalling players were involved in the observed actin dysfunction of hTTR^{A97S} DRG neurons, we evaluated the levels of Rac1 downstream effectors. Rac1 activates directly WAVE, SSH1 and PAK being the most rational approach to analyse the levels and activation status of these proteins, but the correspondent antibodies proved ineffective. WAVE activates the Arp2/3 complex, which is essential for actin polymerization, namely, branching of pre-existing filaments. Parallelly, PAK activates LIMK which inhibits cofilin depolymerizing activity, by promoting its phosphorylation, a reaction which is reverted by the SSH1 phosphatase. As such, we decided to analyse the levels of the ABPS Arp2/3 and cofilin, downstream effectors of Rac1, which directly regulate actin dynamics.

Western blot analysis of protein extracts from DRG neuronal cultures revealed that the levels of Arp2/3, analysed with an antibody that recognizes the ARP3 subunit, were increased in hTTR^{A97S} DRG neurons (Figure 25). This increase in Arp2/3 levels is in accordance with the increased Rac1 activity and might underly the alteration of actin dynamics in hTTR^{A97S} neurons by dysregulating actin polymerization. To understand the cellular localization of Arp2/3 in our settings we also performed immunocytochemistry, however, the antibody did not work in this methodology.

Concerning cofilin, western blot analysis revealed no differences regarding p-cofilin, the inactive form of cofilin, when normalized with total cofilin (Figure 25). Alternatively, via immunocytochemistry we were able to probe for p-cofilin, although not for total cofilin, and results showed a reduction of its levels in hTTR^{A97S} DRG neurons, suggesting an augmented severing activity of this enzyme (Figure 25).

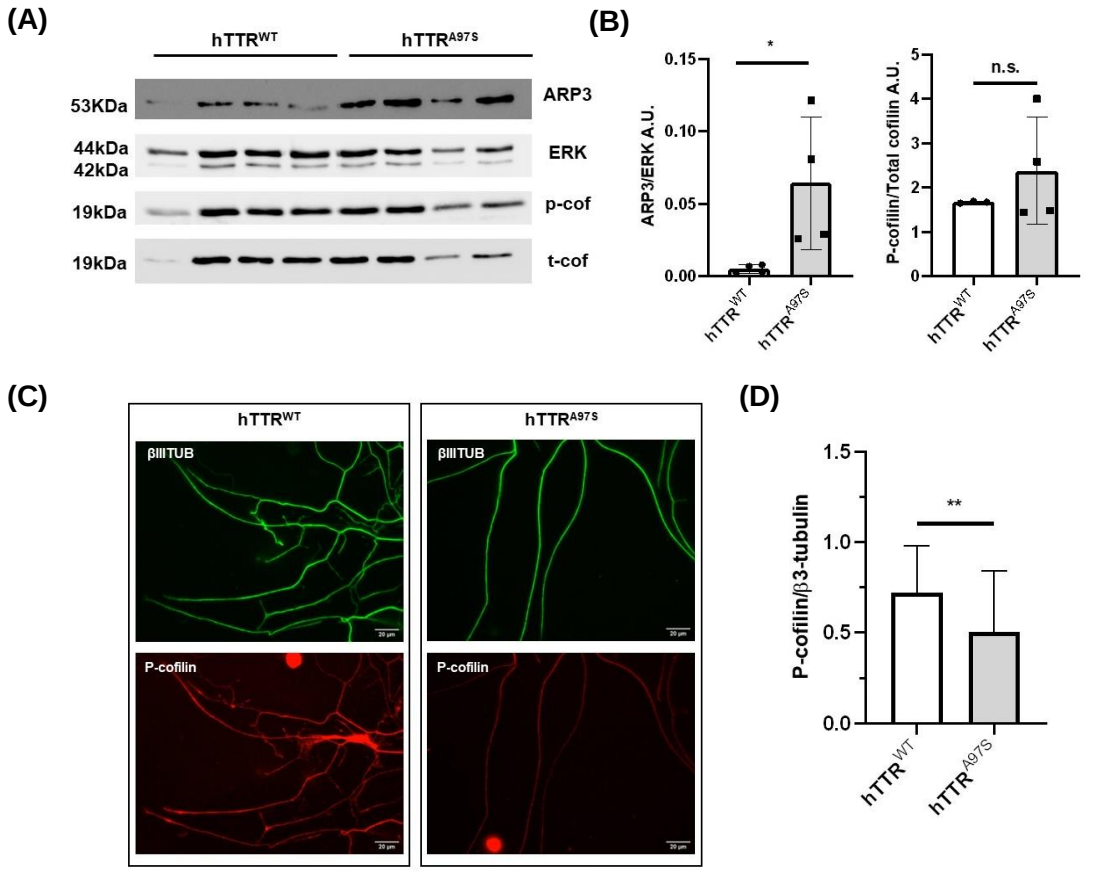


Figure 25. Both Arp2/3 and cofilin downstream effectors of Rac1 are dysregulated in hTTR^{A97S} neurons. (A-B) Western blot analysis (A) and respective quantification (B) showing levels of ARP3 and p-cofilin in DRG neurons lysates. ERK and total cofilin were used as loading controls. Data presented as mean ± SEM. Statistical significance determined by Student's t-test: n.s. non-significant **p<0.01 (C) Representative images of p-cofilin in hTTR^{A97S} and hTTR^{WT}.DRG neurons. (D) Quantification of p-cofilin in DRG neurites. Data presented as mean ± SEM. One representative experiment. Statistical significance determined by Student's t-tes: *p<0.05.

1.3.3. TTR is present extracellularly in DRG neurons *in vitro*

At this point, a phenotype of actin dysfunction was clearly established but one question remained: how TTR induced actin dysfunction *in vitro*? Initially, we aimed to explore the source of TTR in out established neuronal cultures of $hTTR^{A97S}$ and $hTTR^{WT}$ to confirm TTR presence and if it was having an intracellular or extracellular effect. It has been reported that Schwan cells express TTR (Murakami, Sango et al. 2015), so we hypothesize that glia present in our neuronal cultures could produce TTR.

To determine expression levels in culture we performed qPCR for the human TTR gene, but no expression was detected (data not shown), probably due to the difficulty in isolating enough genetic material from primary cultures of DRG neurons. Note that all the primers were tested in positive controls, RNA extracted from livers from both $hTTR^{WT}$ and $hTTR^{A97S}$ mice. We also assessed protein expression by TTR immunocytochemistry, but we were not able to detect a specific signal, as determined by using TTR KO DRG neurons (data not shown). Being that TTR is an extracellular protein we performed human TTR quantitative ELISA of culture media collected and subsequently concentrated with a Vivaspin 500 centrifugal concentrator from both $hTTR^{WT}$ and $hTTR^{A97S}$ DRG neurons cultures. We determined a concentration of 0.432 ng/mL in the media from $hTTR^{WT}$ neurons, suggesting the extracellular presence of TTR. Nevertheless, in $hTTR^{A97S}$ neuronal media no TTR was detected. The fact that no signal was detected in media from $hTTR^{A97S}$ DRG neurons may relate to the fact that, due to the dissociation and misfolding of mutant TTR, the protein “escapes” the concentration step. This way, further experiments to confirm the presence in $hTTR^{A97S}$ DRG neurons are essential.

Our results suggest an actin dysfunction mediated by a RAGE-Rac1 pathway and elicited by Rac1 downstream effectors, Arp2/3 and p-cofilin, in $hTTR^{A97S}$ DRG neurons.

2. Evaluation of microtubule and axonal transport alteration in hTTR^{A97S} mice

2.1. Evaluation of mitochondrial transport in hTTR^{A97S} DRG peripheral roots

Besides a general actin dysfunction, in our group, were previously observed defects in the axonal transport of mitochondria in peripheral root axons of DRG explants from 9-months old hTTR^{A97S} mice labelled with Mito Tracker (Figure 18, Introduction chapter 3). Axonal transport impairment has been identified has being an hallmark of several peripheral neuropathies (Jellinger 2010). Aiming at understanding at which age mitochondrial transport defects were initiated in hTTR^{A97S} mice, we performed the quantification of these parameters in 6-months old hTTR^{A97S} (from which live imaging of DRG peripheral roots stained with Mito Tracker was previously performed in the laboratory). At 6 months of age no impairment in axonal transport was observed in hTTR^{A97S} DRG peripheral roots (Figure 26).

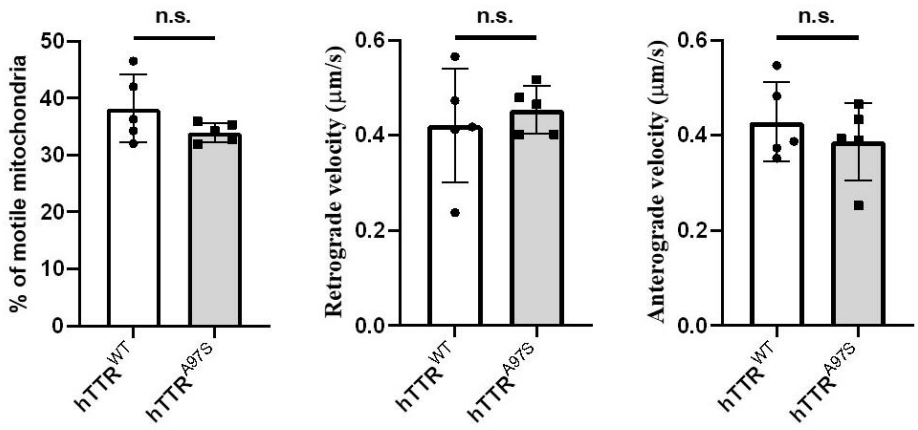


Figure 26. Axonal transport defects were not present in DRG peripheral root explants from 6-months old hTTR^{A97S}. Quantification of the percentage (%) of motile mitochondria, retrograde and anterograde velocities. Data presented as mean ± SEM. n=5 animals/genotype. Statistical significance determined by Students t-test. n.s., not significant.

These results suggest that axonal transport alterations in hTTR^{A97S} mice are initiated around 9 months of age, and that this time point is the ideal to further dissect cytoskeleton alterations in the mouse model. hTTR^{A97S} mice showed sensory peripheral neuropathy at approximately 24 months of age suggesting that this cytoskeletal alteration precedes neurodegeneration in ATTR-PN before the first symptoms would develop (Kan, Chiang et al. 2018).

2.2. Tubulin acetylation is decreased in hTTR^{A97S} DRG peripheral roots

Axonal transport is tightly related to MT organization and dynamics, as these present as “tracks” for cargo transport. As previously referred (Introduction, chapter 2.1.2) MTs are regulated by PTMs (Roll-Mecak 2020), being that a dysregulation at this level has been related to axonal transport defects and neurodegeneration (Eira, Silva et al. 2016).

As such, based on the axonal transport in hTTR^{A97S} DRG peripheral root explants, we aimed to determine whether these findings were related with alterations on the levels of tubulin PTMs. We started by determining whether the total levels of α- and β3-tubulin, this last one is neuron specific, were altered, which could suggest an alteration on MT mass. No differences were found regarding the isoforms of tubulin comparing hTTR^{WT} and hTTR^{A97S} protein extracts of DRG peripheral roots (Figure 27). Having no differences on the total levels of tubulins, we investigated the levels of their PTMs. No differences were observed regarding: Δ2-tubulin, acetylated α-tubulin, detyrosinated tubulin and polyglutamylated tubulin (Figure 27). Concerning polyglutamylation no differences were found either regarding longer chains, the PolyE antibody recognizes linear chains of 4 or more glutamates, or total levels of this PTM, the GT335 antibody recognizes all polyglutamylation.

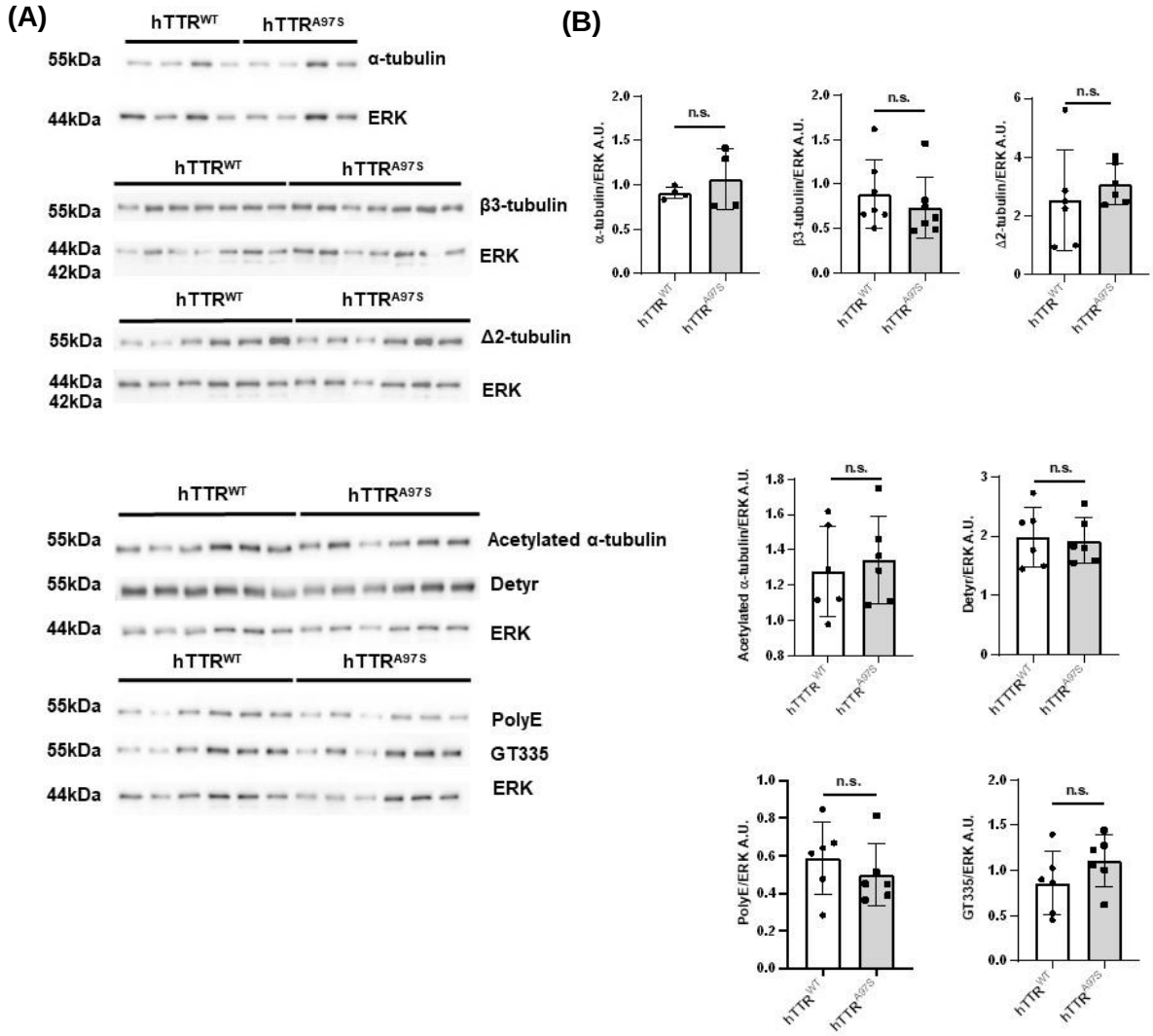


Figure 27. Tubulin isoforms and PTMs are not altered in hTTR^{A97S} DRG peripheral root via Western Blot. (A-B) Western blot analysis (A) and respective quantification showing levels of α-tubulin, β3-tubulin and probed PTMs. ERK was used as a loading control. Data represented as mean ± SEM. n=4-7 animals/conditions. Statistical significance determined by Student's t-test: n.s. non-significant.

The lack of success in finding tubulin PTMs alterations by western blot could be due to a "dilution effect" in peripheral roots axons by glial cells and other cell types, or simply because this alterations in fact do not occur. As such we rationalized the search of PTMs in an axonal specific manner, recurring to immunohistochemistry of section of DRG. We focused on tubulin acetylation as it had already been observed in our group that TTR remodels the MT cytoskeleton by inducing acetylation of α-tubulin (Eira, Magalhaes et al. 2021). Only positive axons for β3-tubulin staining and acetylated α-tubulin were quantified to assure axonal assessment. We observed in hTTR^{A97S} DRG peripheral root from 9-months old mice reduced levels of acetylated α-tubulin (Figure 28). This alteration might reflect a decrease in MT stability on hTTR^{A97S} peripheral root

axons and underlie axonal transport defects previously observed. Reduced levels of acetylation have been observed in HD, AD and CMT and related with axonal transport defects (Eira, Silva et al. 2016).

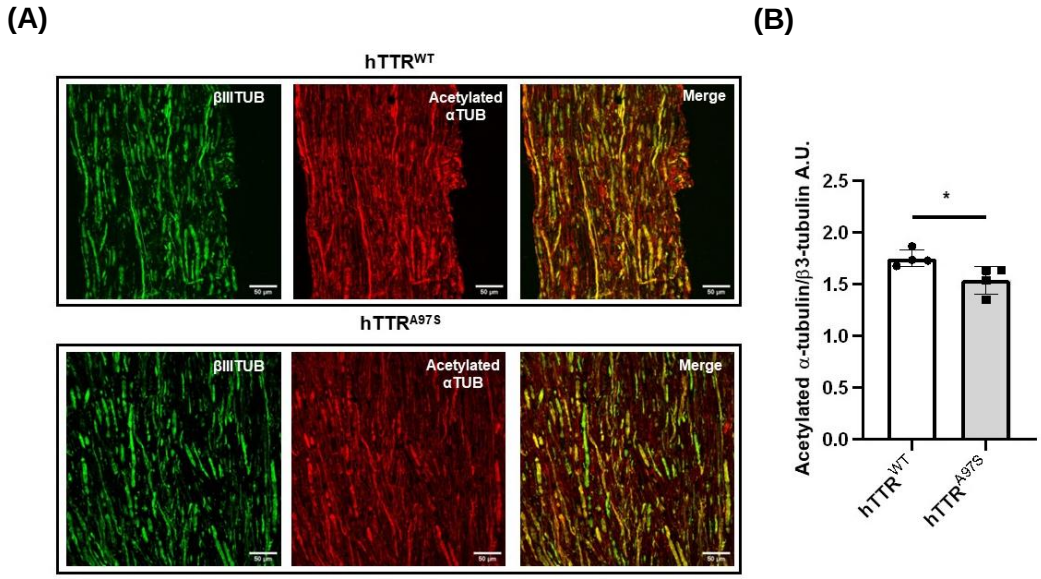


Figure 28. Levels of α-tubulin acetylation are reduced in DRG peripheral roots of hTTR^{A97S} mice. (A-B) Immunohistochemistry analysis: representative images (A) and respective quantification (B) showing levels of acetylated α-tubulin. Normalization was done with β3-tubulin signal. Data presented as mean ± SEM. n=4 animals/condition. Statistical significance determined by Student's t-test: *p<0.05.

2.3. Microtubule and axonal transport alterations in sural nerves from hTTR^{A97S} mice

The sural nerve was used for many years as a "biopsy target" for the diagnostic of ATTR-PN, as deposition of TTR aggregates in that tissue occurred early in the course of the disease and gave reliable and quantifiable morphometric data (Planté-Bordeneuve and Said 2011, Fernandes, Coelho et al. 2019). Additionally, the sural nerve is a purely sensory nerve and innervates targets such as feet, ankle and heel (Miniato and Nedeff 2021), so loss of fibres in this nerve leads to loss of sensation in its targets relating to the early symptomatology of ATTR-PN.

Additionally, in the hTTR^{A97S} mouse model a reduction of myelinated fibres and abnormal myelin sheath profiles were observed in the sural nerve, when compared with the control group hTTR^{WT} (Kan, Chiang et al. 2018). Previously in our group, the assessment of the axonal transport of mitochondria was done in DRG peripheral root which contains both motor and sensory neurons. The fact that only the last ones are involved in the earliest pathology of ATTR-PN, justifies our goal to image axonal transport

of mitochondria in the sural nerve. However, experiments in sural nerve explants stained with Mito Tracker were unsuccessful. As such, we decided to use hTTR^{A97S}-Thy1-MitoCFP mice, hTTR^{A97S} mice crossed with mice expressing a mitochondrial sequence fused to cyan fluorescent protein (CFP) under the neuronal Thy1 promoter (Thy1-MitoCFP) (Misgeld, Kerschensteiner et al. 2007), to evaluate axonal transport. Additionally, to access MT dynamics, as an alteration in this parameter could underly alterations in axonal transport, we used hTTR^{A97S} mice crossed with transgenic mice that express the plus-end binding protein EB3, which labels microtubule growing, fused to yellow fluorescent protein (YFP) controlled by the neuron-specific Thy1 promoter (Thy1:EB3-YFP) (Kleele, Marinković et al. 2014), hTTR^{A97S}-Thy1:EB3-YFP.

The original objective was to image mice *in vivo* using a multiphoton microscope but that was not available. This way, we started by optimizing the imaging of sural nerve explants. The sural nerve is very thin and fragile, so dissection was challenging, especially when considering that tissue integrity should be maximally maintained to allow for live imaging of mitochondrial transport and MT dynamics. To achieve the necessary conditions for live imaging the dissection protocol was optimized (Supplementary information). With the established optimizations we were able to image both mitochondrial transport and EB3 dynamics in in hTTR^{A97S}-Thy1-MitoCFP and hTTR^{A97S}-Thy1:EB3-YFPmice (Figures 29 and 30).

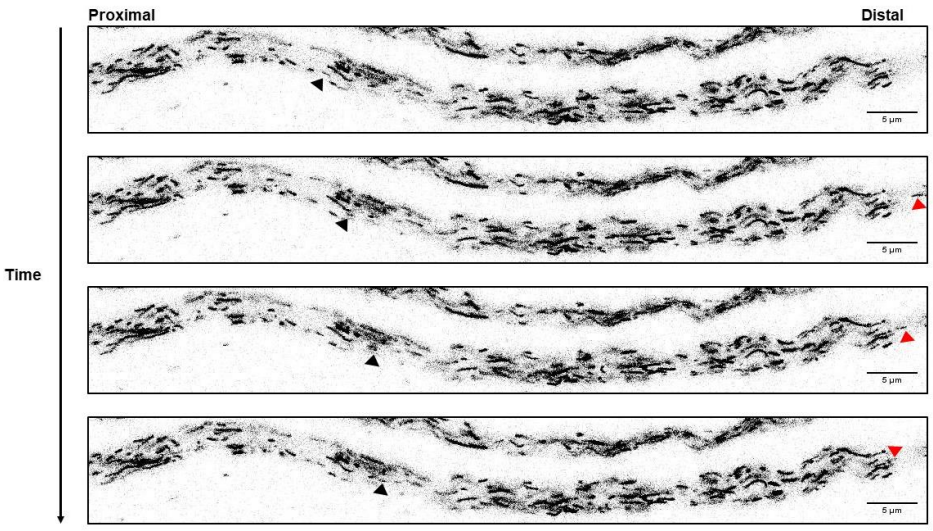


Figure 29. Representative still images of live-imaging of mitochondria in sural nerve axons from hTTR^{A97S}-Thy1-MitoCFP mouse. Black arrows and red arrows indicate anterograde and retrograde moving mitochondria, respectively.

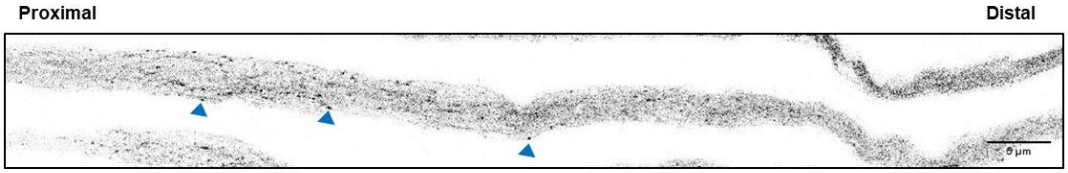


Figure 30. Representative still image of live-imaging of EB3 comets in sural nerve axons from hTTR^{A97S}-Thy1:EB3-YFP mouse. Blue arrows indicate EB3 comets.

To determine whether a possible defect on axonal transport and MT dynamics could derive from an alteration on MT density (number of MTs per axonal area), we performed the quantification of this parameter in cross section of sural nerves from 9-months old hTTR^{A97S} mice and hTTR^{WT} control mice. MT density is readout for alterations in the total number of MTs. An alteration in this parameter could indicate a defect on MT nucleation or MT fragmentation and loss.

In ATTR-PN loss of unmyelinated fibres happens first and is followed by a to loss of myelinated fibres, from smaller to bigger (Coimbra and Andrade 1971). Additionally, in hTTR^{A97S} mice both small fibre neuropathy and large fibre neuropathy were observed (Kan, Chiang et al. 2018). We saw no differences regarding MT density in both unmyelinated and myelinated fibres in the sural nerve of hTTR^{A97S} mice when compared to hTTR^{WT} control mice (Figure 31). These results demonstrate that there are no differences in the mass of MTs between hTTR^{A97S} and control mice, at least and 9 months of age. Nevertheless, although the number of MTs is similar, their dynamics might be altered.

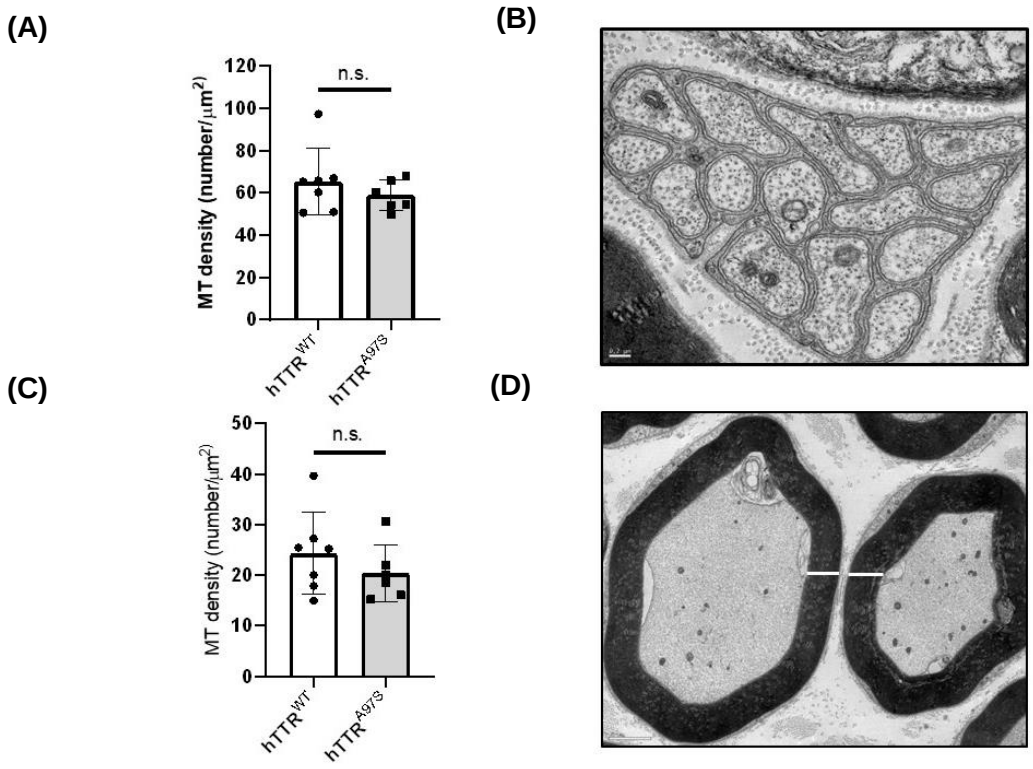


Figure 31. MT density in the sural nerve of hTTR^{A97S} is not altered. (A-B) MT density analysis in unmyelinated fibres: quantification of MT density (A). Data presented as mean ± SEM. n=6-7 animals/condition. Statistical significance determined by Student's t-test: n.s. non-significant; image of unmyelinated fibres (B) (C-D) Quantification of MT density in myelinated fibres: quantification of MT density (C). Data presented as mean ± SEM. n=6-7 animals/condition. Statistical significance determined by Student's t-test: n.s. non-significant; image of myelinated fibres (D).

In this part of the work, all the tools to assess axonal transport of mitochondria and MT dynamics in the sural nerve were established, what will allow the future quantification of these parameters in hTTR^{A97S} mice.

Discussion

As previously referred, the cytoskeleton has been implicated in many neurodegenerative diseases (Eira, Silva et al. 2016) but in ATTR-PN remained largely unaddressed. In our group the interaction of the cytoskeleton and TTR has been well studied. In a V30M *D. melanogaster* model the observed rough eye phenotype and axonal projections defects were related to actin dysfunction, and the dysregulation of the Rho GTPase family (M, Lopes et al. 2020). Moreover, TTR has been implicated physiologically to have multiple roles such as mediating nerve regeneration (Fleming, Saraiva et al. 2007) and acting as a metalloprotease (Liz, Faro et al. 2004). Interestingly, in a TTR KO mouse model it was reported that TTR remodels the MT cytoskeleton supporting the physiological link between this protein and this cell component (Eira, Magalhães et al. 2021). Moreover, these results suggest that a loss of function phenotype may be relevant for the development of ATTR-PN. In this work, as previously established, a mouse model of ATTR-PN was used, allowing for unequivocally identification of cytoskeleton alterations as hallmarks of neurodegeneration induced by mutant TTR.

We initially focused on axonal actin dysfunction by performing the with the analysis of actin trails, a form of F-actin dynamics recently identified in hippocampal neurons (Ganguly, Tang et al. 2015). Few to no work was done regarding actin trails in DRG neurons, but identification of such structure via stochastic optical reconstruction microscopy (STORM) has already been performed (Unsain, Bordenave et al. 2018). Our results showed no difference regarding actin trails length or rate of polymerization when comparing DRG neurons from $hTTR^{A97S}$ mice with control DRG neurons from $hTTR^{WT}$ mice. However, we observed a reduction in the number of actin trails in $hTTR^{A97S}$ DRG neurons, retrogradely and anterogradely, which may relate to insufficient transport of actin (Roy 2016) or/and presynaptic vesicles transport (Chenouard, Xuan et al. 2020). Due to the sheer polarization of neurons and the extreme distances that axons occupy *in vivo*, cell homeostasis is extremely reliant on the efficient transport of cargoes. So, we can speculate that the lack of actin trails may induce impairment in actin-dependent transport and, consequently, to neurodegeneration.

Our results supported that the reduction of actin trails in $hTTR^{A97S}$ DRG neurons was being mediated by the overactivity of Rac1, as its inhibition reverted the observed phenotype. Ganguly and colleagues showed that actin trails are formin-dependent, but

Arp2/3-independent in hippocampal neurons. For this, they used the drug SMIFH2, which inhibits all formins, so pinpointing which formin is more relevant to actin trails is impossible (Ganguly, Tang et al. 2015). We could speculate that a lack of actin trails would be related with a lack of activity of some formin induced by Rac1 signalling. Interestingly, the interaction of the Rho GTPase family with formins has been established over the years. For example, RhoA interacts with mDia1 and mDia2 and Rac1 interacts with both FH1/FH2 domain-containing protein 1 (FHOD 1) and formin-like protein 1 (FRL1), but the impact of such interactions is not clear (Higgs 2005). Parallelly, our data suggested that RAGE mediates actin dysfunction upstream and in the same signalling axis of Rac1. mDia1 can act as a downstream effector of RAGE and it has been reported that this signalling axis, RAGE-mDIA1, leads to activation of Rac1 during C6 glioma migration (Kim, Jeong et al. 2021). This may in part explain the overactivation of Rac1, and why antagonizing RAGE leads to a recovery phenotype in growth cone morphology experiments. Coupled with the previous actin trails data, we could say that experiments using a RAGE antagonist would be interesting to see if the actin dysfunction in the axon is also regulated by this receptor, upstream of Rac1. Interestingly, considering that mDIA1, a formin, is in fact activated by RAGE, the reduction of actin trails may seem unexplainable. However, mammalians encode 15 formins and their interactions with Rho GTPases are not fully understood (Higgs 2005, Breitsprecher and Goode 2013). This way, we can only safely affirm that Rac1 overactivation leads to both actin dysfunction in the growth cone and axon, and that RAGE plays a role in Rac1 activation. In the future measuring levels of mDia1 or activation state may be a good approach to further understand this signalling axis.

Downstream of Rac1 some effectors were found to be dysregulated in DRG neurons from $hTTR^{A97S}$ mice. The protein complex Arp2/3 was one of them, essential for the formation of branched actin (Pollard 2016). Although it is not clear the impact in cell physiology of the augmented presence, we can speculate that the excess of branching in actin would be deleterious to neuronal homeostasis. As previously referred, actin trails are not Arp2/3 dependent, being that those structures are linear events of polymerization (Ganguly, Tang et al. 2015), so relating this augment with the actin trails results is difficult. However, we can speculate that the excess of Arp2/3 with a limited G-actin pool would, in turn, inhibit formins, as few actin monomers would be free for polymerization. It has been reported that the activity of profilin, a G-actin binding protein that controls its availability, is important to give balance to Arp2/3 activity, namely, when competing with formins (Rotty, Wu et al. 2015, Suarez, Carroll et

al. 2015). This way, to assess profilin activity or presence in hTTR^{A97S} DRG neurons would be interesting. If profilin does not have an enlarged presence/activity, we could assume that the excess of Arp2/3 would have "free rein" over actin dynamics. Parallelly, cofilin was also found to be altered as its inactive form, p-cofilin, was reduced in neurites of DRG neurons from hTTR^{A97S} mice. This would suggest a larger severing activity of this enzyme, which should relate to more actin polymerization as more barbed ends become available (Møller, Klip et al. 2019). However, the phenotype that we observed in the axon, a reduction in the number of actin trails, would suggest less polymerization again being difficult to correlate such data, especially considering that the impact of cofilin in actin trails dynamics has not been dissected. To further clarify the impact of both cofilin and Arp2/3 further experiments should be done. For cofilin, the generation of a phosphomimetic mutant by transfection of hTTR^{A97S} DRG neurons, would allow to assess cofilin impact in the observed actin dysfunction. For Arp2/3, recapitulating actin trails experiments by treating hTTR^{A97S} DRG neurons with CK666, an Arp2/3 inhibitor, would relate the observed enlarged presence to the actin dysfunction phenotype in the axon.

Further, we addressed whether this actin dysfunction phenotype was being triggered by the extracellular or intracellular presence of human mutant TTR *in vitro*. We only found hTTR in hTTR^{WT} DRG neurons media via ELISA. The fact that we did not find TTR in hTTR^{A97S} DRG neurons media does not explain the observed actin dysfunction. However, we can say with this result that TTR is most probably in the extracellular media. In turn, this could lead to an overactivation of Rac1 via some receptors, most probably RAGE considering our results and the fact that this receptor has been reported to bind to TTR being activated (Sousa, Yan et al. 2000). We hypothesize that, since TTR A97S is probably in a monomeric and unfolded form, it could not be detected in the ELISA assay. Alternatively, cells may already come "primed" from hTTR^{A97S} mice, possibly being that the alterations in signalling cascades and its effects on cell physiology are persistent throughout the time of our cell cultures. Optionally, DRG neurons may uptake TTR and "carry" it to our cell cultures, as it has been reported that DRG neurons can uptake TTR in a clathrin-dependent megalin-mediated manner (Fleming, Mar et al. 2009). Future experiments should clarify this topic.

Preliminary data for this work showed that axonal transport of mitochondria was impaired in 9-months old hTTR^{A97S} DRG peripheral roots. We showed that levels of α-tubulin acetylation were reduced in hTTR^{A97S} DRG peripheral roots when compared

with the control group, $hTTR^{WT}$, what could explain transport alterations. Acetylation of α-tubulin is related to stable microtubules and is abundant in the axon, as MTs need to be stable to properly transport cargoes (Janke and Kneussel 2010). In line with our results, reduction of this tubulin PTM has been observed in other peripheral neuropathies namely Charcot-Marie Tooth disease (Eira, Silva et al. 2016). The upregulation of HDAC6, a protein that deacetylates MTs, has been related to multiple peripheral neuropathies (Prior, Van Helleputte et al. 2018), being that its inhibition and subsequent recuperation of levels of acetylated tubulin has been reported to hinder neurodegeneration in Charcot-Marie Tooth type 2A (CMT2A) (Benoy, Vanden Berghe et al. 2017, Picci, Wong et al. 2020) and chemotherapy-induced peripheral neuropathy (CIPN) (Krukowski, Ma et al. 2017). This way, inhibition of HDAC6 would be interesting in axonal transport experiments, possibly identifying this deacetylase as a new therapeutical target in ATTR-PN.

In ATTR-PN, neurodegeneration happens firstly in the PNS namely the nerves that emit to the lower limbs. One of these nerves, the sural nerve is a purely sensory nerve that arises from the sciatic nerve and suffers degeneration early, being associated with the early symptoms of ATTR-PN, such as loss of sensation in the feet (Planté-Bordeneuve and Said 2011, Miniato and Nedeff 2021). To dissect what leads to these events in the sural nerve and translate more adequately what happens in humans, we optimized a protocol for the live imaging of mitochondrial transport (Misgeld, Kerschensteiner et al. 2007) and MT dynamics (Kleele, Marinković et al. 2014). Additionally, at the sural nerve level we assessed MT density. MT density directly relates with the total mass of MTs and could explain an impairment in axonal transport or MT dynamics. In our experiments, we saw no reduction of MT density in unmyelinated fibres and myelinated fibres. We could speculate that it is too early in the onset of the disease to have an impact in the number of MTs and that axonal transport defects must relate to alterations at the level of “finer” alterations of MTs, namely, PTMs. The assessment of PTMs in the sural nerve, namely, levels of α-tubulin acetylation of tubulin, as their reductions has been related to multiple peripheral neuropathies, and we have shown it was reduced in DRG peripheral roots from $hTTR^{A97S}$ 9-months old mice, making this assessment of the upmost importance. Additionally, the application of a HDAC6 inhibitor and subsequent mitochondrial transport and MTs dynamics evaluation, could allow direct implication of such alterations in acetylation on neurodegeneration.

Although experiments and objectives were separate regarding actin and MTs, in neurons these cytoskeletal elements coexist and interact. In ATTR-PN, considering our results, most probably, actin and MTs interact and promote neurodegeneration in association. For example, in this work, the role of Rho GTPases was not explored regarding MTs, but it is known that these components interact. RhoA activates mDia1 which can lead to alterations in MT behaviour, namely their stabilization (Wojnacki, Quassollo et al. 2014, Møller, Klip et al. 2019). Alternatively, Rac1 has also been reported to promote MT growth and stabilization in multiple situations (Wojnacki, Quassollo et al. 2014). This would, in part, makes us think that Rac1 overactivation should lead to more stable MTs, something that our results do not corroborate. However, if we consider that Rac1 interacts with a myriad of proteins and even counteracts RhoA (Caron 2003), which activates mDia1 and promotes microtubule stabilization, the rationalization of this interplay is much harder. Further experiments focusing on the interconnection of Rac1 and MTs should be much more explored, being that Rac1 was overactivated in $hTTR^{A97S}$ DRG neurons and could be altering MTs and axonal transports. Besides this, MTs and actin have an extensive crosstalk: MTs and actin may crosslink, actin may guide and anchor MTs and MTs plus-end may serve as an harbour for actin polymerization (Dogterom and Koenderink 2019). So, we can speculate that an actin dysfunction may translate a dysfunction at the level of MTs and vice versa. Clearly, these cytoskeletal dysfunctions contribute to neurodegeneration, as our results *in vitro* and previous reports support this hypothesis (Eira, Silva et al. 2016), but many questions arise: do the actin dysfunction and MT impairment contribute equally? These components work in tandem to lead to neurodegeneration? Does one of these dysfunctions precedes the other? And if one precedes the other, do they have a causal relationship, where, for example, an actin dysfunction leads to further dysfunction on MTs level? Answering these questions would lead to an understanding of cytoskeleton involvement in neurodegeneration and allow for the rationalization of new therapies in tandem, both considering actin and MTs.

As previously stated, no current therapy for ATTR-PN acts directly at the level of neurodegeneration, focusing instead on the amyloidogenic potential of TTR. The identification of new therapeutical targets at the level of the cytoskeleton could bridge this gap and help patients. Regarding our results related with Rac1, we could speculate that inhibiting this GTPase would be advantageous, but the search of inhibitors is still ongoing, as Rac1 signalling is ubiquitous and targeting it specifically is difficult,

demanding further study (Marei and Malliri 2017). Upstream of Rac1, RAGE inhibition seems promising but due to the abundance of ligands and existence of different variants of this receptor, the creation of new specific antagonists is a serious challenge (Rojas, Morales et al. 2019). Our results also suggest Arp2/3 and cofilin as possible targets but due to their ubiquitous nature may not be appropriate. Therefore, the identification of upstream or downstream signalling proteins related to Rac1 and not so ubiquitous as this Rho GTPase is needed. At the level of MTs and axonal transport, our results suggest that maybe targeting HDAC6, as it had a positive effect in other peripheral neuropathies (d'Ydewalle, Krishnan et al. 2011, Krukowski, Ma et al. 2017), would restore acetylation levels and prevent neurodegeneration. However, further study is needed to identify more possible targets. Additionally, the validation of our results in neurons derived from induced pluripotent stem cells (iPSCs) from patients would facilitate the possible identification of therapeutical targets in humans and help with the serious challenge that ATTR-PN presents.

Conclusion

Our results suggest an overall cytoskeletal dysfunction, both at the levels of actin, MTs and axonal transport, preceding neurodegeneration in an ATTR-PN mouse model. This work sheds light on the pathophysiology and mechanisms of neurodegeneration in ATTR-PN and the possibility of identifying new therapeutical targets for the disease.

References

Adams, D., Y. Ando, J. M. Beirão, T. Coelho, M. A. Gertz, J. D. Gillmore, P. N. Hawkins, I. Lousada, O. B. Suhr and G. Merlini (2021). "Expert consensus recommendations to improve diagnosis of ATTR amyloidosis with polyneuropathy." J Neurol **268**(6): 2109-2122.

Adams, D., A. Gonzalez-Duarte, W. D. O'Riordan, C.-C. Yang, M. Ueda, A. V. Kristen, I. Tournev, H. H. Schmidt, T. Coelho and J. L. Berk (2018). "Patisiran, an RNAi therapeutic, for hereditary transthyretin amyloidosis." New England Journal of Medicine **379**(1): 11-21.

Aillaud, C., C. Bosc, L. Peris, A. Bosson, P. Heemeryck, J. Van Dijk, J. Le Friec, B. Boulan, F. Vossier and L. E. Sanman (2017). "Vasohibins/SVBP are tubulin carboxypeptidases (TCPs) that regulate neuron differentiation." Science **358**(6369): 1448-1453.

Aillaud, C., C. Bosc, Y. Saoudi, E. Denarier, L. Peris, L. Sago, N. Taulet, A. Cieren, O. Tort and M. M. Magiera (2016). "Evidence for new C-terminally truncated variants of α- and β-tubulins." Molecular biology of the cell **27**(4): 640-653.

Akhmanova, A. and M. O. Steinmetz (2015). "Control of microtubule organization and dynamics: two ends in the limelight." Nat Rev Mol Cell Biol **16**(12): 711-726.

Alberts, A. S., H. Qin, H. S. Carr and J. A. Frost (2005). "PAK1 negatively regulates the activity of the Rho exchange factor NET1." J Biol Chem **280**(13): 12152-12161.

Aleshire, S. L., C. A. Bradley, L. D. Richardson and F. F. Parl (1983). "Localization of human prealbumin in choroid plexus epithelium." Journal of Histochemistry & Cytochemistry **31**(5): 608-612.

Ando, Y. and M. Ueda (2012). "Diagnosis and therapeutic approaches to transthyretin amyloidosis." Curr Med Chem **19**(15): 2312-2323.

Andrade, C. (1952). "A peculiar form of peripheral neuropathy: familiar atypical generalized amyloidosis with special involvement of the peripheral nerves." Brain **75**(3): 408-427.

Arnold, D. B. and G. Gallo (2014). "Structure meets function: actin filaments and myosin motors in the axon." J Neurochem **129**(2): 213-220.

Bamburg, J. R., B. W. Bernstein, R. C. Davis, K. C. Flynn, C. Goldsbury, J. R. Jensen, M. T. Maloney, I. T. Marsden, L. S. Minamide, C. W. Pak, A. E. Shaw, I. Whiteman and O. Wiggan (2010). "ADF/Cofilin-actin rods in neurodegenerative diseases." Curr Alzheimer Res **7**(3): 241-250.

Benoy, V., P. Vanden Berghe, M. Jarpe, P. Van Damme, W. Robberecht and L. Van Den Bosch (2017). "Development of Improved HDAC6 Inhibitors as Pharmacological Therapy for Axonal Charcot-Marie-Tooth Disease." Neurotherapeutics **14**(2): 417-428.

Benson, M. D. (2013). "Liver transplantation and transthyretin amyloidosis." Muscle Nerve **47**(2): 157-162.

Benson, M. D., M. Waddington-Cruz, J. L. Berk, M. Polydefkis, P. J. Dyck, A. K. Wang, V. Planté-Bordeneuve, F. A. Barroso, G. Merlini and L. Obici (2018). "Inotersen treatment for patients with hereditary transthyretin amyloidosis." New England Journal of Medicine **379**(1): 22-31.

Bento-Abreu, A., A. Velasco, E. Polo-Hernández, P. L. Pérez-Reyes, A. Tabernero and J. M. Medina (2008). "Megalin is a receptor for albumin in astrocytes and is required for the synthesis of the neurotrophic factor oleic acid." J Neurochem **106**(3): 1149-1159.

Blake, C., M. Geisow, S. Oatley, B. Rerat and C. Rerat (1978). "Structure of prealbumin: secondary, tertiary and quaternary interactions determined by Fourier refinement at 1.8 Å." Journal of molecular biology **121**(3): 339-356.

Breitsprecher, D. and B. L. Goode (2013). "Formins at a glance." J Cell Sci **126**(Pt 1): 1-7.

Bretschneider, T., K. Anderson, M. Ecke, A. Müller-Taubenberger, B. Schroth-Diez, H. C. Ishikawa-Ankerhold and G. Gerisch (2009). "The three-dimensional dynamics of actin waves, a model of cytoskeletal self-organization." Biophysical journal **96**(7): 2888-2900.

Burkel, B. M., G. Von Dassow and W. M. Bement (2007). "Versatile fluorescent probes for actin filaments based on the actin-binding domain of utrophin." Cell motility and the cytoskeleton **64**(11): 822-832.

Caron, E. (2003). "Rac signalling: a radical view." Nat Cell Biol **5**(3): 185-187.

Chenouard, N., F. Xuan and R. W. Tsien (2020). "Synaptic vesicle traffic is supported by transient actin filaments and regulated by PKA and NO." Nature Communications **11**(1): 5318.

Coimbra, A. and C. Andrade (1971). "Familial amyloid polyneuropathy: an electron microscope study of the peripheral nerve in five cases. I. Interstitial changes." Brain **94**(2): 199-206.

Coles, C. H. and F. Bradke (2015). "Coordinating neuronal actin–microtubule dynamics." Current Biology **25**(15): R677-R691.

Conde, C. and A. Cáceres (2009). "Microtubule assembly, organization and dynamics in axons and dendrites." Nat Rev Neurosci **10**(5): 319-332.

Connelly, S., S. Choi, S. M. Johnson, J. W. Kelly and I. A. Wilson (2010). "Structure-based design of kinetic stabilizers that ameliorate the transthyretin amyloidoses." Current opinion in structural biology **20**(1): 54-62.

Connors, L. H., A. Lim, T. Prokaeva, V. A. Roskens and C. E. Costello (2003). "Tabulation of human transthyretin (TTR) variants, 2003." Amyloid **10**(3): 160-184.

Cornwell, G. G., 3rd, K. Sletten, B. Johansson and P. Westermark (1988). "Evidence that the amyloid fibril protein in senile systemic amyloidosis is derived from normal prealbumin." Biochem Biophys Res Commun **154**(2): 648-653.

d'Ydewalle, C., V. Benoy and L. Van Den Bosch (2012). "Charcot-Marie-Tooth disease: emerging mechanisms and therapies." Int J Biochem Cell Biol **44**(8): 1299-1304.

d'Ydewalle, C., J. Krishnan, D. M. Chiheb, P. Van Damme, J. Irobi, A. P. Kozikowski, P. Vanden Berghe, V. Timmerman, W. Robberecht and L. Van Den Bosch (2011). "HDAC6 inhibitors reverse axonal loss in a mouse model of mutant HSPB1-induced Charcot-Marie-Tooth disease." Nat Med **17**(8): 968-974.

Deane, R., I. Singh, A. P. Sagare, R. D. Bell, N. T. Ross, B. LaRue, R. Love, S. Perry, N. Paquette, R. J. Deane, M. Thiyagarajan, T. Zarcone, G. Fritz, A. E. Friedman, B. L. Miller and B. V. Zlokovic (2012). "A multimodal RAGE-specific inhibitor reduces amyloid β-mediated brain disorder in a mouse model of Alzheimer disease." J Clin Invest **122**(4): 1377-1392.

Dehmelt, L. and S. Halpain (2005). "The MAP2/Tau family of microtubule-associated proteins." Genome Biol **6**(1): 204.

Delague, V., A. Jacquier, T. Hamadouche, Y. Poitelon, C. Baudot, I. Boccaccio, E. Chouery, M. Chaouch, N. Kassouri, R. Jabbour, D. Grid, A. Mégarbané, G. Haase and N. Lévy (2007). "Mutations in FGD4 encoding the Rho GDP/GTP exchange factor FRABIN cause autosomal recessive Charcot-Marie-Tooth type 4H." Am J Hum Genet **81**(1): 1-16.

Dickson, B. J. (2001). "Rho GTPases in growth cone guidance." Curr Opin Neurobiol **11**(1): 103-110.

Diebold, B. A., B. Fowler, J. Lu, M. C. Dinauer and G. M. Bokoch (2004). "Antagonistic cross-talk between Rac and Cdc42 GTPases regulates generation of reactive oxygen species." J Biol Chem **279**(27): 28136-28142.

Dogterom, M. and G. H. Koenderink (2019). "Actin–microtubule crosstalk in cell biology." Nature Reviews Molecular Cell Biology **20**(1): 38-54.

Dominguez, R. and K. C. Holmes (2011). "Actin structure and function." Annu Rev Biophys **40**: 169-186.

Eaton, S. L., S. L. Roche, M. Llavero Hurtado, K. J. Oldknow, C. Farquharson, T. H. Gillingwater and T. M. Wishart (2013). "Total Protein Analysis as a Reliable Loading Control for Quantitative Fluorescent Western Blotting." PLOS ONE **8**(8): e72457.

Eden, S., R. Rohatgi, A. V. Podtelejnikov, M. Mann and M. W. Kirschner (2002). "Mechanism of regulation of WAVE1-induced actin nucleation by Rac1 and Nck." Nature **418**(6899): 790-793.

Eira, J., J. Magalhaes, N. Macedo, M. E. Pero, T. Misgeld, M. M. Sousa, F. Bartolini and M. A. Liz (2021). "Transthyretin promotes axon growth via regulation of microtubule dynamics and tubulin acetylation." bioRxiv.

Eira, J., J. Magalhães, N. Macedo, M. E. Pero, T. Misgeld, M. M. Sousa, F. Bartolini and M. A. Liz (2021). "Transthyretin Promotes Axon Growth via Regulation of Microtubule Dynamics and Tubulin Acetylation." Front Cell Dev Biol **9**: 747699.

Eira, J., C. S. Silva, M. M. Sousa and M. A. Liz (2016). "The cytoskeleton as a novel therapeutic target for old neurodegenerative disorders." Prog Neurobiol **141**: 61-82.

Etienne-Manneville, S. and A. Hall (2002). "Rho GTPases in cell biology." Nature **420**(6916): 629-635.

Fabrizi, G. M., F. Taioli, T. Cavallaro, S. Ferrari, L. Bertolasi, M. Casarotto, N. Rizzuto, T. Deconinck, V. Timmerman and P. De Jonghe (2009). "Further evidence that mutations in FGD4/frabin cause Charcot-Marie-Tooth disease type 4H." Neurology **72**(13): 1160-1164.

Felding, P. and G. Fex (1982). "Cellular origin of prealbumin in the rat." Biochimica et Biophysica Acta (BBA)-General Subjects **716**(3): 446-449.

Feltri, M. L., U. Suter and J. B. Relvas (2008). "The function of RhoGTPases in axon ensheathment and myelination." Glia **56**(14): 1508-1517.

Fernandes, A., T. Coelho, A. Rodrigues, H. Felgueiras, P. Oliveira, A. Guimarães, M. Melo-Pires and R. Taipa (2019). "Clinicopathological correlations of sural nerve biopsies in TTR Val30Met familial amyloid polyneuropathy." Brain Communications **1**(1): fcz032.

Fleming, C. E., F. M. Mar, F. Franquinho, M. J. Saraiva and M. M. Sousa (2009). "Transthyretin internalization by sensory neurons is megalin mediated and necessary for its neuritogenic activity." J Neurosci **29**(10): 3220-3232.

Fleming, C. E., F. M. Mar, F. Franquinho, M. J. Saraiva and M. M. Sousa (2009). "Transthyretin internalization by sensory neurons is megalin mediated and necessary for its neuritogenic activity." Journal of Neuroscience **29**(10): 3220-3232.

Fleming, C. E., M. J. Saraiva and M. M. Sousa (2007). "Transthyretin enhances nerve regeneration." J Neurochem **103**(2): 831-839.

Fukushima, N., D. Furuta, Y. Hidaka, R. Moriyama and T. Tsujiuchi (2009). "Post-translational modifications of tubulin in the nervous system." J Neurochem **109**(3): 683-693.

Ganguly, A., Y. Tang, L. Wang, K. Ladt, J. Loi, B. Dargent, C. Leterrier and S. Roy (2015). "A dynamic formin-dependent deep F-actin network in axons." Journal of Cell Biology **210**(3): 401-417.

Gao, Y., J. B. Dickerson, F. Guo, J. Zheng and Y. Zheng (2004). "Rational design and characterization of a Rac GTPase-specific small molecule inhibitor." Proc Natl Acad Sci U S A **101**(20): 7618-7623.

Goodson, H. V. and E. M. Jonasson (2018). "Microtubules and Microtubule-Associated Proteins." Cold Spring Harb Perspect Biol **10**(6).

Hazenberg, B. P. (2013). "Amyloidosis: a clinical overview." Rheum Dis Clin North Am **39**(2): 323-345.

Heasman, S. J. and A. J. Ridley (2008). "Mammalian Rho GTPases: new insights into their functions from in vivo studies." Nat Rev Mol Cell Biol **9**(9): 690-701.

Herrmann, H., S. V. Strelkov, P. Burkhard and U. Aebi (2009). "Intermediate filaments: primary determinants of cell architecture and plasticity." J Clin Invest **119**(7): 1772-1783.

Higgs, H. N. (2005). "Formin proteins: a domain-based approach." Trends Biochem Sci **30**(6): 342-353.

Hirano, A. (1994). "Hirano bodies and related neuronal inclusions." Neuropathol Appl Neurobiol **20**(1): 3-11.

Holmgren, G., L. Steen, J. Ekstedt, C. G. Groth, B. G. Ericzon, S. Eriksson, O. Andersen, I. Karlberg, G. Nordén, M. Nakazato and et al. (1991). "Biochemical effect of liver transplantation in two Swedish patients with familial amyloidotic polyneuropathy (FAP-met30)." Clin Genet **40**(3): 242-246.

Horio, T. and H. Hotani (1986). "Visualization of the dynamic instability of individual microtubules by dark-field microscopy." Nature **321**(6070): 605-607.

Hu, X., C. Viesselmann, S. Nam, E. Merriam and E. W. Dent (2008). "Activity-dependent dynamic microtubule invasion of dendritic spines." J Neurosci **28**(49): 13094-13105.

Huang, Y. A., C. H. Hsu, H. C. Chiu, P. Y. Hsi, C. T. Ho, W. L. Lo and E. Hwang (2020). "Actin waves transport RanGTP to the neurite tip to regulate non-centrosomal microtubules in neurons." J Cell Sci **133**(9).

Hudson, B. I., A. Z. Kalea, M. del Mar Arriero, E. Harja, E. Boulanger, V. D'Agati and A. M. Schmidt (2008). "Interaction of the RAGE cytoplasmic domain with diaphanous-1 is

required for ligand-stimulated cellular migration through activation of Rac1 and Cdc42." Journal of Biological Chemistry **283**(49): 34457-34468.

Hur, E. M. and F. Q. Zhou (2010). "GSK3 signalling in neural development." Nat Rev Neurosci **11**(8): 539-551.

Hyung, S. J., S. Deroo and C. V. Robinson (2010). "Retinol and retinol-binding protein stabilize transthyretin via formation of retinol transport complex." ACS Chem Biol **5**(12): 1137-1146.

I. Oliveira da Silva, M., C. S. Lopes and M. A. Liz (2020). "Transthyretin interacts with actin regulators in a Drosophila model of familial amyloid polyneuropathy." Scientific Reports **10**(1): 13596.

Jaffe, A. B. and A. Hall (2005). "Rho GTPases: biochemistry and biology." Annu Rev Cell Dev Biol **21**: 247-269.

Janke, C. and M. Kneussel (2010). "Tubulin post-translational modifications: encoding functions on the neuronal microtubule cytoskeleton." Trends Neurosci **33**(8): 362-372.

Jellinger, K. A. (2010). "Basic mechanisms of neurodegeneration: a critical update." Journal of cellular and molecular medicine **14**(3): 457-487.

Johnson, S. M., S. Connelly, C. Fearns, E. T. Powers and J. W. Kelly (2012). "The transthyretin amyloidoses: from delineating the molecular mechanism of aggregation linked to pathology to a regulatory-agency-approved drug." J Mol Biol **421**(2-3): 185-203.

Kalebic, N., C. Martinez, E. Perlas, P. Hublitz, D. Bilbao-Cortes, K. Fiedorczuk, A. Andolfo and P. A. Heppenstall (2013). "Tubulin acetyltransferase αTAT1 destabilizes microtubules independently of its acetylation activity." Mol Cell Biol **33**(6): 1114-1123.

Kalpachidou, T., L. Spiecker, M. Kress and S. Quarta (2019). "Rho GTPases in the Physiology and Pathophysiology of Peripheral Sensory Neurons." Cells **8**(6).

Kan, H. W., H. Chiang, W. M. Lin, I. S. Yu, S. W. Lin and S. T. Hsieh (2018). "Sensory nerve degeneration in a mouse model mimicking early manifestations of familial amyloid polyneuropathy due to transthyretin Ala97Ser." Neuropathol Appl Neurobiol **44**(7): 673-686.

Kanda, Y., D. S. Goodman, R. E. Canfield and F. J. Morgan (1974). "The amino acid sequence of human plasma prealbumin." Journal of Biological Chemistry **249**(21): 6796-6805.

Kapitein, L. C. and C. C. Hoogenraad (2011). "Which way to go? Cytoskeletal organization and polarized transport in neurons." Mol Cell Neurosci **46**(1): 9-20.

Kim, H. J., M. S. Jeong and S. B. Jang (2021). "Molecular Characteristics of RAGE and Advances in Small-Molecule Inhibitors." International Journal of Molecular Sciences **22**(13): 6904.

Kleele, T., P. Marinković, P. R. Williams, S. Stern, E. E. Weigand, P. Engerer, R. Naumann, J. Hartmann, R. M. Karl, F. Bradke, D. Bishop, J. Herms, A. Konnerth, M. Kerschensteiner, L. Godinho and T. Misgeld (2014). "An assay to image neuronal microtubule dynamics in mice." Nat Commun **5**: 4827.

Kohno, K., J. A. Palha, K. Miyakawa, M. J. Saraiva, S. Ito, T. Mabuchi, W. S. Blaner, H. Iijima, S. Tsukahara, V. Episkopou, M. E. Gottesman, K. Shimada, K. Takahashi, K. Yamamura and S. Maeda (1997). "Analysis of amyloid deposition in a transgenic mouse model of homozygous familial amyloidotic polyneuropathy." Am J Pathol **150**(4): 1497-1508.

Krukowski, K., J. Ma, O. Golonzhka, G. O. Laumet, T. Gutti, J. H. van Duzer, R. Mazitschek, M. B. Jarpe, C. J. Heijnen and A. Kavelaars (2017). "HDAC6 inhibition effectively reverses chemotherapy-induced peripheral neuropathy." Pain **158**(6): 1126-1137.

Kühn, S. and M. Geyer (2014). "Formins as effector proteins of Rho GTPases." Small GTPases **5**: e29513.

Lacroix, B., J. van Dijk, N. D. Gold, J. Guizetti, G. Aldrian-Herrada, K. Rogowski, D. W. Gerlich and C. Janke (2010). "Tubulin polyglutamylation stimulates spastin-mediated microtubule severing." J Cell Biol **189**(6): 945-954.

Lamb, Y. N. and E. D. Deeks (2019). "Tafamidis: A Review in Transthyretin Amyloidosis with Polyneuropathy." Drugs **79**(8): 863-874.

LaPointe, N. E., G. Morfini, S. T. Brady, S. C. Feinstein, L. Wilson and M. A. Jordan (2013). "Effects of eribulin, vincristine, paclitaxel and ixabepilone on fast axonal transport and kinesin-1 driven microtubule gliding: implications for chemotherapy-induced peripheral neuropathy." Neurotoxicology **37**: 231-239.

Ledford, H. (2018). "Gene-silencing technology gets first drug approval after 20-year wait." Nature **560**(7718): 291-293.

Lee, J. J. and S. M. Swain (2006). "Peripheral neuropathy induced by microtubule-stabilizing agents." Journal of Clinical Oncology **24**(10): 1633-1642.

Leite, S. C., R. Pinto-Costa and M. M. Sousa (2021). "Actin dynamics in the growth cone: a key player in axon regeneration." Curr Opin Neurobiol **69**: 11-18.

Leite, S. C. and M. M. Sousa (2016). "The neuronal and actin commitment: Why do neurons need rings?" Cytoskeleton (Hoboken) **73**(9): 424-434.

Liepnieks, J. J. and M. D. Benson (2007). "Progression of cardiac amyloid deposition in hereditary transthyretin amyloidosis patients after liver transplantation." Amyloid **14**(4): 277-282.

Liz, M. A., C. J. Faro, M. J. Saraiva and M. M. Sousa (2004). "Transthyretin, a new cryptic protease." J Biol Chem **279**(20): 21431-21438.

Loudon, R. P., L. D. Silver, H. F. Yee, Jr. and G. Gallo (2006). "RhoA-kinase and myosin II are required for the maintenance of growth cone polarity and guidance by nerve growth factor." J Neurobiol **66**(8): 847-867.

Lowery, L. A. and D. Van Vactor (2009). "The trip of the tip: understanding the growth cone machinery." Nat Rev Mol Cell Biol **10**(5): 332-343.

M, I. O. d. S., C. S. Lopes and M. A. Liz (2020). "Transthyretin interacts with actin regulators in a Drosophila model of familial amyloid polyneuropathy." Sci Rep **10**(1): 13596.

Macedo, B., A. R. Batista, J. B. do Amaral and M. J. Saraiva (2007). "Biomarkers in the assessment of therapies for familial amyloidotic polyneuropathy." Mol Med **13**(11-12): 584-591.

Magalhães, J., J. Eira and M. A. Liz (2021). "The role of transthyretin in cell biology: impact on human pathophysiology." Cell Mol Life Sci **78**(17-18): 6105-6117.

Makover, A., H. Moriwaki, R. Ramakrishnan, M. Saraiva, W. Blaner and D. Goodman (1988). "Plasma transthyretin. Tissue sites of degradation and turnover in the rat." Journal of Biological Chemistry **263**(18): 8598-8603.

Marei, H. and A. Malliri (2017). "Rac1 in human diseases: The therapeutic potential of targeting Rac1 signaling regulatory mechanisms." Small GTPases **8**(3): 139-163.

Merlini, G. and V. Bellotti (2003). "Molecular mechanisms of amyloidosis." New England Journal of Medicine **349**(6): 583-596.

Millecamps, S. and J.-P. Julien (2013). "Axonal transport deficits and neurodegenerative diseases." Nature Reviews Neuroscience **14**(3): 161-176.

Miniato, M. A. and N. Nedeff (2021). Anatomy, Bony Pelvis and Lower Limb, Sural Nerve, StatPearls Publishing, Treasure Island (FL).

Misgeld, T., M. Kerschensteiner, F. M. Bareyre, R. W. Burgess and J. W. Lichtman (2007). "Imaging axonal transport of mitochondria in vivo." Nat Methods **4**(7): 559-561.

Møller, L. L. V., A. Klip and L. Sylow (2019). "Rho GTPases—emerging regulators of glucose homeostasis and metabolic health." Cells **8**(5): 434.

Muñoz-Lasso, D. C., C. Romá-Mateo, F. V. Pallardó and P. Gonzalez-Cabo (2020). "Much More Than a Scaffold: Cytoskeletal Proteins in Neurological Disorders." Cells **9**(2).

Murakami, T., K. Sango, K. Watabe, N. Niimi, S. Takaku, Z. Li, K. i. Yamamura and Y. Sunada (2015). "Schwann cells contribute to neurodegeneration in transthyretin amyloidosis." Journal of Neurochemistry **134**(1): 66-74.

Murillo, B. and M. Mendes Sousa (2018). "Neuronal Intrinsic Regenerative Capacity: The Impact of Microtubule Organization and Axonal Transport." Dev Neurobiol **78**(10): 952-959.

Namme, J. N., A. K. Bepari and H. Takebayashi (2021). "Cofilin Signaling in the CNS Physiology and Neurodegeneration." Int J Mol Sci **22**(19).

Naylor, H. M. and M. E. Newcomer (1999). "The structure of human retinol-binding protein (RBP) with its carrier protein transthyretin reveals an interaction with the carboxy terminus of RBP." Biochemistry **38**(9): 2647-2653.

Nimnual, A. S., L. J. Taylor and D. Bar-Sagi (2003). "Redox-dependent downregulation of Rho by Rac." Nat Cell Biol **5**(3): 236-241.

Nobes, C. D. and A. Hall (1995). "Rho, rac, and cdc42 GTPases regulate the assembly of multimolecular focal complexes associated with actin stress fibers, lamellipodia, and filopodia." Cell **81**(1): 53-62.

Okabe, S. (2020). "Regulation of actin dynamics in dendritic spines: Nanostructure, molecular mobility, and signaling mechanisms." Mol Cell Neurosci **109**: 103564.

Pareyson, D. and C. Marchesi (2009). "Diagnosis, natural history, and management of Charcot-Marie-Tooth disease." Lancet Neurol **8**(7): 654-667.

Picci, C., V. S. C. Wong, C. J. Costa, M. C. McKinnon, D. C. Goldberg, M. Swift, N. M. Alam, G. T. Prusky, S. Shen, A. P. Kozikowski, D. E. Willis and B. Langley (2020). "HDAC6 inhibition promotes α-tubulin acetylation and ameliorates CMT2A peripheral neuropathy in mice." Exp Neurol **328**: 113281.

Planté-Bordeneuve, V. and G. Said (2011). "Familial amyloid polyneuropathy." Lancet Neurol **10**(12): 1086-1097.

Pollard, T. D. (2016). "Actin and Actin-Binding Proteins." Cold Spring Harb Perspect Biol **8**(8).

Prior, R., L. Van Helleputte, V. Benoy and L. Van Den Bosch (2017). "Defective axonal transport: A common pathological mechanism in inherited and acquired peripheral neuropathies." Neurobiol Dis **105**: 300-320.

Prior, R., L. Van Helleputte, Y. E. Klingl and L. Van Den Bosch (2018). "HDAC6 as a potential therapeutic target for peripheral nerve disorders." Expert Opinion on Therapeutic Targets **22**(12): 993-1007.

Ramasamy, R., S. J. Vannucci, S. S. D. Yan, K. Herold, S. F. Yan and A. M. Schmidt (2005). "Advanced glycation end products and RAGE: a common thread in aging, diabetes, neurodegeneration, and inflammation." Glycobiology **15**(7): 16R-28R.

Raz, A. and D. S. Goodman (1969). "The interaction of thyroxine with human plasma prealbumin and with the prealbumin-retinol-binding protein complex." Journal of Biological Chemistry **244**(12): 3230-3237.

Reixach, N., S. Deechongkit, X. Jiang, J. W. Kelly and J. N. Buxbaum (2004). "Tissue damage in the amyloidoses: Transthyretin monomers and nonnative oligomers are the major cytotoxic species in tissue culture." Proceedings of the National Academy of Sciences **101**(9): 2817-2822.

Ridley, A. J. and A. Hall (1992). "The small GTP-binding protein rho regulates the assembly of focal adhesions and actin stress fibers in response to growth factors." Cell **70**(3): 389-399.

Ridley, A. J., H. F. Paterson, C. L. Johnston, D. Diekmann and A. Hall (1992). "The small GTP-binding protein rac regulates growth factor-induced membrane ruffling." Cell **70**(3): 401-410.

Rojas, A., M. Morales, I. Gonzalez and P. Araya (2019). "Inhibition of RAGE axis signaling: A pharmacological challenge." Current drug targets **20**(3): 340-346.

Roll-Mecak, A. (2020). "The Tubulin Code in Microtubule Dynamics and Information Encoding." Dev Cell **54**(1): 7-20.

Roll-Mecak, A. and F. J. McNally (2010). "Microtubule-severing enzymes." Curr Opin Cell Biol **22**(1): 96-103.

Rotty, J. D., C. Wu, E. M. Haynes, C. Suarez, J. D. Winkelman, H. E. Johnson, J. M. Haugh, D. R. Kovar and J. E. Bear (2015). "Profilin-1 serves as a gatekeeper for actin assembly by Arp2/3-dependent and -independent pathways." Dev Cell **32**(1): 54-67.

Roy, S. (2016). "Waves, rings, and trails: The scenic landscape of axonal actin." Journal of Cell Biology **212**(2): 131-134.

Roy, S. (2016). "Waves, rings, and trails: The scenic landscape of axonal actin." J Cell Biol **212**(2): 131-134.

Rozenbaum, M. H., S. Large, R. Bhambri, M. Stewart, J. Whelan, A. van Doornewaard, N. Dasgupta, A. Masri and J. Nativi-Nicolau (2021). "Impact of Delayed Diagnosis and Misdiagnosis for Patients with Transthyretin Amyloid Cardiomyopathy (ATTR-CM): A Targeted Literature Review." Cardiol Ther **10**(1): 141-159.

Ruberg, F. L., M. Grogan, M. Hanna, J. W. Kelly and M. S. Maurer (2019). "Transthyretin Amyloid Cardiomyopathy: JACC State-of-the-Art Review." J Am Coll Cardiol **73**(22): 2872-2891.

Ruggiero, C. and E. Lalli (2021). "Targeting the cytoskeleton against metastatic dissemination." Cancer Metastasis Rev **40**(1): 89-140.

Ruthel, G. and G. Banker (1998). "Actin-dependent anterograde movement of growth-cone-like structures along growing hippocampal axons: a novel form of axonal transport?" Cell Motil Cytoskeleton **40**(2): 160-173.

Sanchez, A. D. and J. L. Feldman (2017). "Microtubule-organizing centers: from the centrosome to non-centrosomal sites." Current opinion in cell biology **44**: 93-101.

Santos, S. D., R. Fernandes and M. J. Saraiva (2010). "The heat shock response modulates transthyretin deposition in the peripheral and autonomic nervous systems." Neurobiol Aging **31**(2): 280-289.

Saraiva, M. J., S. Birken, P. P. Costa and D. Goodman (1984). "Amyloid fibril protein in familial amyloidotic polyneuropathy, Portuguese type. Definition of molecular abnormality in transthyretin (prealbumin)." The Journal of clinical investigation **74**(1): 104-119.

Saraiva, M. J., J. Magalhaes, N. Ferreira and M. R. Almeida (2012). "Transthyretin deposition in familial amyloidotic polyneuropathy." Curr Med Chem **19**(15): 2304-2311.

Saraiva, M. J. M. (2002). "Hereditary transthyretin amyloidosis: molecular basis and therapeutical strategies." Expert reviews in molecular medicine **4**(12): 1-11.

Sasaki, H., S. Tone, M. Nakazato, K. Yoshioka, H. Matsuo, Y. Kato and Y. Sakaki (1986). "Generation of transgenic mice producing a human transthyretin variant: a possible mouse model for familial amyloidotic polyneuropathy." Biochem Biophys Res Commun **139**(2): 794-799.

Sasaki, H., N. Yoshioka, Y. Takagi and Y. Sakaki (1985). "Structure of the chromosomal gene for human serum prealbumin." Gene **37**(1-3): 191-197.

Seibert, F. B. and J. W. Nelson (1942). "Electrophoretic study of the blood protein response in tuberculosis." Journal of Biological Chemistry **143**(1): 29-38.

Sekijima, Y. (2015). "Transthyretin (ATTR) amyloidosis: clinical spectrum, molecular pathogenesis and disease-modifying treatments." J Neurol Neurosurg Psychiatry **86**(9): 1036-1043.

Shimada, K., S. Maeda, T. Murakami, S. Nishiguchi, F. Tashiro, S. Yi, S. Wakasugi, K. Takahashi and K. Yamamura (1989). "Transgenic mouse model of familial amyloidotic polyneuropathy." Mol Biol Med **6**(4): 333-343.

Silva, C. S., J. Eira, C. A. Ribeiro, Â. Oliveira, M. M. Sousa, I. Cardoso and M. A. Liz (2017). "Transthyretin neuroprotection in Alzheimer's disease is dependent on proteolysis." Neurobiol Aging **59**: 10-14.

Sipe, J. D., M. D. Benson, J. N. Buxbaum, S. Ikeda, G. Merlini, M. J. Saraiva and P. Westermark (2012). "Amyloid fibril protein nomenclature: 2012 recommendations from the Nomenclature Committee of the International Society of Amyloidosis." Amyloid **19**(4): 167-170.

Socolow, E. L., K. A. Woeber, R. H. Purdy, M. Holloway and S. Ingbar (1965). "Preparation of I-131-labeled human serum prealbumin and its metabolism in normal and sick patients." The Journal of Clinical Investigation **44**(10): 1600-1609.

Sousa, M. M., I. Cardoso, R. Fernandes, A. Guimarães and M. J. Saraiva (2001). "Deposition of transthyretin in early stages of familial amyloidotic polyneuropathy: evidence for toxicity of nonfibrillar aggregates." Am J Pathol **159**(6): 1993-2000.

Sousa, M. M., S. Du Yan, R. Fernandes, A. Guimaraes, D. Stern and M. J. Saraiva (2001). "Familial amyloid polyneuropathy: receptor for advanced glycation end products-dependent triggering of neuronal inflammatory and apoptotic pathways." J Neurosci **21**(19): 7576-7586.

Sousa, M. M., A. G. Norden, C. Jacobsen, T. E. Willnow, E. I. Christensen, R. V. Thakker, P. J. Verroust, S. K. Moestrup and M. J. Saraiva (2000). "Evidence for the role of megalin in renal uptake of transthyretin." Journal of Biological Chemistry **275**(49): 38176-38181.

Sousa, M. M. and M. J. Saraiva (2001). "Internalization of transthyretin: evidence of a novel yet unidentified receptor-associated protein (RAP)-sensitive receptor." Journal of Biological Chemistry **276**(17): 14420-14425.

Sousa, M. M., S. D. Yan, D. Stern and M. J. Saraiva (2000). "Interaction of the receptor for advanced glycation end products (RAGE) with transthyretin triggers nuclear transcription factor kB (NF-kB) activation." Laboratory investigation **80**(7): 1101-1110.

Stiess, M. and F. Bradke (2011). "Neuronal polarization: the cytoskeleton leads the way." Dev Neurobiol **71**(6): 430-444.

Suarez, C., R. T. Carroll, T. A. Burke, J. R. Christensen, A. J. Bestul, J. A. Sees, M. L. James, V. Sirotkin and D. R. Kovar (2015). "Profilin regulates F-actin network homeostasis by favoring formin over Arp2/3 complex." Dev Cell **32**(1): 43-53.

Tahirovic, S., F. Hellal, D. Neukirchen, R. Hindges, B. K. Garvalov, K. C. Flynn, T. E. Stradal, A. Chrostek-Grashoff, C. Brakebusch and F. Bradke (2010). "Rac1 regulates neuronal polarization through the WAVE complex." J Neurosci **30**(20): 6930-6943.

Tanskanen, M., T. Peuralinna, T. Polvikoski, I. L. Notkola, R. Sulkava, J. Hardy, A. Singleton, S. Kiuru-Enari, A. Paetau, P. J. Tienari and L. Myllykangas (2008). "Senile systemic amyloidosis affects 25% of the very aged and associates with genetic

variation in alpha2-macroglobulin and tau: a population-based autopsy study." Ann Med **40**(3): 232-239.

Tu, P. H., P. Raju, K. A. Robinson, M. E. Gurney, J. Q. Trojanowski and V. M. Lee (1996). "Transgenic mice carrying a human mutant superoxide dismutase transgene develop neuronal cytoskeletal pathology resembling human amyotrophic lateral sclerosis lesions." Proc Natl Acad Sci U S A **93**(7): 3155-3160.

Ueda, M. and Y. Ando (2014). "Recent advances in transthyretin amyloidosis therapy." Transl Neurodegener **3**: 19.

Unsain, N., M. D. Bordenave, G. F. Martinez, S. Jalil, C. Von Bilderling, F. M. Barabas, L. A. Masullo, A. D. Johnstone, P. A. Barker and M. Bisbal (2018). "Remodeling of the actin/spectrin membrane-associated periodic skeleton, growth cone collapse and F-actin decrease during axonal degeneration." Scientific reports **8**(1): 1-16.

Van Helleputte, L., M. Kater, D. P. Cook, C. Eykens, E. Rossaert, W. Haeck, T. Jaspers, N. Geens, P. Vanden Berghe, C. Gysemans, C. Mathieu, W. Robberecht, P. Van Damme, G. Cavaletti, M. Jarpe and L. Van Den Bosch (2018). "Inhibition of histone deacetylase 6 (HDAC6) protects against vincristine-induced peripheral neuropathies and inhibits tumor growth." Neurobiol Dis **111**: 59-69.

Vatassery, G. T., H. T. Quach, W. E. Smith, B. A. Benson and J. H. Eckfeldt (1991). "A sensitive assay of transthyretin (prealbumin) in human cerebrospinal fluid in nanogram amounts by ELISA." Clin Chim Acta **197**(1): 19-25.

Vieira, M. and M. J. Saraiva (2014). "Transthyretin: a multifaceted protein." Biomol Concepts **5**(1): 45-54.

Wallace, M. R., S. L. Naylor, B. Kluve-Beckerman, G. L. Long, L. McDonald, T. B. Shows and M. D. Benson (1985). "Localization of the human prealbumin gene to chromosome 18." Biochem Biophys Res Commun **129**(3): 753-758.

Watanabe, K., S. Al-Bassam, Y. Miyazaki, T. J. Wandless, P. Webster and D. B. Arnold (2012). "Networks of polarized actin filaments in the axon initial segment provide a mechanism for sorting axonal and dendritic proteins." Cell Rep **2**(6): 1546-1553.

Wechalekar, A. D., J. D. Gillmore and P. N. Hawkins (2016). "Systemic amyloidosis." Lancet **387**(10038): 2641-2654.

Westermark, P., K. Sletten, B. Johansson and G. G. Cornwell, 3rd (1990). "Fibril in senile systemic amyloidosis is derived from normal transthyretin." Proc Natl Acad Sci U S A **87**(7): 2843-2845.

Wicher, G., M. Larsson, A. Fex Svenningsen, E. Gyllencreutz, L. Rask and H. Aldskogius (2006). "Low density lipoprotein receptor-related protein-2/megalin is

expressed in oligodendrocytes in the mouse spinal cord white matter." J Neurosci Res **83**(5): 864-873.

Wilczek, H. E., M. Larsson and B. G. Ericzon (2011). "Long-term data from the Familial Amyloidotic Polyneuropathy World Transplant Registry (FAPWTR)." Amyloid **18 Suppl 1**: 193-195.

Winder, S. J. and K. R. Ayscough (2005). "Actin-binding proteins." J Cell Sci **118**(Pt 4): 651-654.

Wojnacki, J., G. Quassollo, M.-P. Marzolo and A. Cáceres (2014). "Rho GTPases at the crossroad of signaling networks in mammals: impact of Rho-GTPases on microtubule organization and dynamics." Small GTPases **5**(1): e28430.

Woo, D., Y. Seo, H. Jung, S. Kim, N. Kim, S. M. Park, H. Lee, S. Lee, K. H. Cho and W. D. Heo (2019). "Locally Activating TrkB Receptor Generates Actin Waves and Specifies Axonal Fate." Cell Chem Biol **26**(12): 1652-1663.e1654.

Xu, K., G. Zhong and X. Zhuang (2013). "Actin, spectrin, and associated proteins form a periodic cytoskeletal structure in axons." Science **339**(6118): 452-456.

Yang, M., B. Yordanov, Y. Levy, R. Brüschweiler and S. Huo (2006). "The sequence-dependent unfolding pathway plays a critical role in the amyloidogenicity of transthyretin." Biochemistry **45**(39): 11992-12002.

Yi, S., K. Takahashi, M. Naito, F. Tashiro, S. Wakasugi, S. Maeda, K. Shimada, K. Yamamura and S. Araki (1991). "Systemic amyloidosis in transgenic mice carrying the human mutant transthyretin (Met30) gene. Pathologic similarity to human familial amyloidotic polyneuropathy, type I." Am J Pathol **138**(2): 403-412.

Yokoyama, T., M. Mizuguchi, Y. Nabeshima, K. Kusaka, T. Yamada, T. Hosoya, T. Ohhara, K. Kurihara, K. Tomoyori and I. Tanaka (2012). "Hydrogen-bond network and pH sensitivity in transthyretin: Neutron crystal structure of human transthyretin." Journal of structural biology **177**(2): 283-290.

Yu, I., C. P. Garnham and A. Roll-Mecak (2015). "Writing and Reading the Tubulin Code." J Biol Chem **290**(28): 17163-17172.

Yuan, A., M. V. Rao, Veeranna and R. A. Nixon (2017). "Neurofilaments and Neurofilament Proteins in Health and Disease." Cold Spring Harb Perspect Biol **9**(4).

Zajączkowska, R., M. Kocot-Kępska, W. Leppert, A. Wrzosek, J. Mika and J. Wordliczek (2019). "Mechanisms of Chemotherapy-Induced Peripheral Neuropathy." Int J Mol Sci **20**(6).

Zenke, F. T., M. Krendel, C. DerMardirossian, C. C. King, B. P. Bohl and G. M. Bokoch (2004). "p21-activated kinase 1 phosphorylates and regulates 14-3-3 binding to GEF-H1, a microtubule-localized Rho exchange factor." J Biol Chem **279**(18): 18392-18400.

Supplementary information

Sural mitochondrial transport live imaging optimization

The imaging of explants is challenging as tissue integrity and consequent cellular processes die down relatively quickly. The sciatic nerve (a large and robust nerve) is composed of the combination of 3 DRG peripheral roots (L3-L5) in mice and trifurcates in three other nerves: the tibial nerve, the peroneal nerve, and the sural nerve. Preservation of the ganglia would be the best strategy has it promotes maintenance of cell processes, being that it contains the cells bodies of neurons. The sural nerve is very thin and distant from the ganglia, being specially challenging as explant viability is short, not compatible with a complete flow-through of live imaging. So, to ensure tissue viability instead of removing just the sural nerve we tried the removal of this nerve in association with the sciatic nerve (Figure 32). This method allowed the acquisition of good images of mitochondria movement and EB3 dynamics in a Leica SP8 (Leica, Germany) confocal fluorescence microscope.

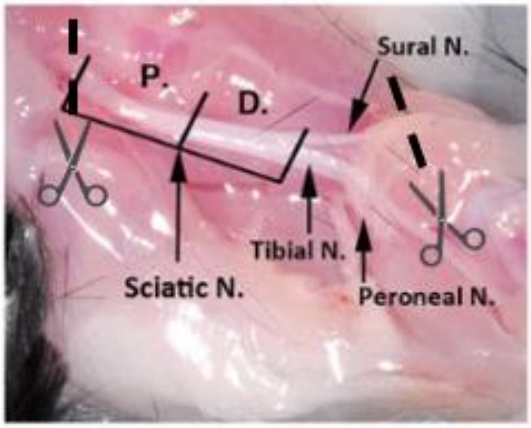


Figure 32. Scissors plus dashed lines denote the zone where incisions were made to obtain the explant. The tibial and peroneal nerves were discarded. Adapted from (Eaton, Roche et al. 2013).

FRAP EGFP-actin optimization

DRG neurons were transfected has previously described with 0,5ug of EGFP-actin+pEGFP-C1 (Figure 33). Cells were then platted in glass bottom µ-dishes at a density of 20000 cells/dish. After 24hours medium was changed to fully supplemented (1%P/S, 50ng/mL NGF, 1x B27 2mM L-Glu) DMEM:F12 without phenol red. A confocal microscope Leica SP8 was used to perform photo bleaching and live imaging, results seemed satisfactory although recovery was apparently to fast which would demand further optimization, maybe by reducing transfection levels and recording videos with more temporal resolution, but no further experiences were performed. When a

determined area is photobleached the EGFP-actin is reincluded in filaments, so recovery of fluorescence correlates with actin polymerization.

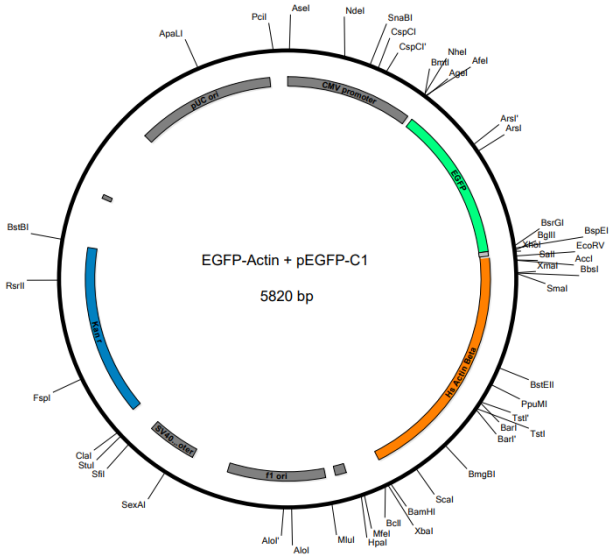


Figure 33. EGFP-Actin + pEGFP-C1 plasmid construct used in FRAP.

Polymerase chain reaction

Cells for PCR were platted in a 12-well plate or a 24-well plate: one animal per well or half the cells from one animal per well, respectively. For the RNA extraction a NZY Total RNA Extraction Kit (NZYTech, Portugal) was used. Cells were lysed chemically using the provided buffer with β-mercaptoethanol (Sigma-Aldrich, EUA). The provided protocol was followed and resulting RNA was stored at -80ºC. A small aliquot was taken to evaluate RNA quality in Experion™ Automated Eletrophoresis Station (Bio-Rad, USA). After concentration determination in a NanoDrop1000 (Thermo Fisher Scientific, EUA) the same amount of RNA for all samples was converted in cDNA using a NZY First-Strand cDNA Synthesis Kit (NZYTech, Portugal), the provided protocol was followed. For PCR reaction in a 384-well plate the following was added: 1µL of cDNA, 5µL of SYBR® Green Master Mix (Bio-Rad, USA), 0,5µl of primers (stock at 10uM; Table 4) and 3µl of DEPC water. Technical duplicates and blank for each condition were performed (mix without cDNA). A series dilution to evaluate reaction efficiency was also performed. PCR was run in a CFX384 Touch Real-Time PCR Detection System (Bio-Rad, USA). The amplification protocol included an initial denaturation and enzyme activation at 95°C for 5 minutes followed by 30 cycles of denaturation at 95°C for 30 seconds, annealing at 61°C for 90 seconds, extension at 72°C for 30 seconds and a final extension at 60°C for 10 minutes. Primer efficacy was

evaluated using positive controls. All primers were designed in Beacon Designer™ (Premier Biosoft, USA).

Table 4. List of the primers used for PCR and respective sequences.

Gene/Primer	Sequence
hTTR (foward)	5' TCT TAC TGG AAG GCA CTT 3'
hTTR (reverse)	5' TGG TGG AAT AGG AGT AGG 3'
moRAGE (foward)	5' ATC CTG CCT CTG AAC TCA 3'
Mo RAGE (reverse)	5' GTC TCC TGG TCT CTT CCT 3'
Mo β-actin	5' GCT GTG CTA TGT TGC TCT A 3'
Mo β-actin	5' CTC GTT GCC AAT AGT GAT GA 3'

TTR ICC

DRG neurons were platted at a density of 5000 cells per well in a multi-well 24-well plate and fixed at DIV1 with 4% PFA in PBS for 15 minutes at RT. After washing with PBS, cells were permeabilized with 0,2% Triton X-100 in PBS for 10 minutes at RT and then autofluorescence was quenched using 200mM NH_4CL for 5 minutes at RT (washing with PBS was performed in between steps). Coverslips were transferred to a humid chamber and cells were blocked using 2,5%NDS in PBS for 1 hour at RT. Primary antibodies were then added in blocking buffer: anti-TTR and anti-β3-tubulin (Table 1) at 4ºC O/N. After washing, cells were incubated with secondary antibodies 1 hour at RT and mounted using Fluoromount.